UNIVERSITA' POLITECNICA DELLE MARCHE

FACOLTA' DI INGEGNERIA

Corso di Laurea magistrale **Biomedical Engineering**

Muscle Co-contractions estimated during walking in Parkinson's disease by analyzing the surface EMG signal in time-frequency domain

Relatore: Chiar.mo/a

Prof. **Sandro Fioretti**

Tesi di Laurea di:

Carlotta Biagini

Correlatore:

Prof. **Francesco Di Nardo**

A.A. **2021** / **2022**

INDEX

Introduction

Parkinson's disease (PD) is a diffused and the second most frequent neurodegenerative disorder after Alzheimer's disease (AD), that is estimated to affect almost 0.5–1% of the population over 65 years and increasing to 1–3% in older age population in the world [1,2]. PD is characterized by the progressive degradation of dopaminergic neurons located in the substantia nigra of the brain. Consequently, the reduced uptake of dopamine in the basal ganglia leads to a lack of communication between the brain and the muscles, giving rise to the dysfunctional motor symptoms that define the disease. Even though the actual cause of this pathology is still unknown, it definitely compromises the quality of life of people affected by it, since it involves serious motor and cognitive disorders. The most debilitating motor symptoms that impact people with Parkinson are bradykinesia, tremor, rigidity, postural instability and gait difficulties [3,4]. These symptoms can be followed by cognitive problems (memory loss and concentration difficulties), sleep disturbances, autonomic dysfunction, depression, psychiatric changes, and sensory symptoms. As a consequence, the ability to maintain balance while performing simple tasks of daily living, like walking, is generally impaired in parkinsonian subjects. Although rehabilitation activities or dopaminergic treatment may reduce some of the signs of the pathology, the main symptom, highlighted through gait dysfunction, leads to the demand for the development of new rehabilitation technologies. Stereophotogrammetry, dynamometric force platforms, and electromyography are the gold standard techniques frequently adopted in gait analysis, allowing the estimation of kinematic, dynamic and electromyographic parameters related to human motion. Differently from kinematic and kinetic features, electromyography signals are directly linked to the nervous system and can provide information on the muscular recruitment strategies adopted by the central and peripheral nervous system.

In particular, surface electromyography (sEMG) is a reliable tool which allows to measure over the skin surface the electrical potential produced by the underlying muscle during contractions. sEMG is considered specifically suitable for monitoring the dynamic activity of muscles during walking. In clinical gait analysis, sEMG is frequently used to evaluate muscular coordination, but it can be also employed for functional diagnosis or for the monitoring of the disease progress and clinical outcomes. Furthermore, it results to be a useful tool to examine the variability related to muscle activation among healthy and pathological conditions during free walking [5,6].

Several studies reported a different behavior in muscle recruitment between PD patients and healthy subjects during limb movements [7,8]. In particular, these studies, examining amplitude-based information on the envelope of sEMG signals during gait analysis in Parkinson's disease, have been focused mainly in the more distal muscles of the lower limbs. It was found that tibialis anterior muscle

peaked later in PD compared to healthy adults during loading phase, and tibialis anterior and gastrocnemius medialis displayed greater variability in amplitude in individuals with PD compared to healthy older adults. However, the latter muscle displayed lower timing variability during unloading in PD. Moreover, the studies [9,10] evaluated differences in muscular activity at slow walking speed between healthy and parkinsonian subjects, with a greater tibialis anterior muscle's activity bilaterally during the swing phase, compared to healthy groups, whilst a decreased amplitude of the plantarflexor muscle during stance in parkinsonian groups. On the contrary, Cioni et al. [11] reported the tibialis anterior displaying similar activity patterns in the two groups of healthy and patients.

As for muscle activation detection, sEMG shows to be a reliable tool also for the estimation of co-contraction between two muscles. The concept of co-contraction (or co-activation) implies the simultaneous activation of the two antagonist muscles or muscle groups crossing the same targeted joint [12], contributing significantly to motion control during physiological processes connected to motor learning. It has recently been shown that muscle co-contraction is a very frequent phenomenon in normal walking and its main purpose is to maintain control of muscle action and ensure the stability of the joint in the performance of certain motor tasks [13,14].

Nevertheless, numerous studies have found that the increased or decreased capacity to co-contract muscles is a sign of dysfunction in elderly people and people with neuromotor diseases. Furthermore, a higher incidence of the co-contraction phenomenon has been adopted by the neuromotor system to develop compensatory strategies in order to obtain greater stability in movement [15,16]. In sight of these considerations, the understanding of the influence of pathological conditions on muscle recruitment and muscle co-contraction mechanisms would allow the development of reliable methodologies and implementation of new therapeutic and rehabilitative strategies. There are several methods of investigation which allow to define muscle co-contraction: advanced mathematical models based on the evaluation of muscle momentum [17]; simpler indices derived from the analysis of electromyographic signals suitable in clinical settings [18,19]; the employment of various techniques such as statistical gait analysis (SGA) [20]. Some of these studies evaluated time-domain characterization of muscular co-contraction, based on the overlapping period between activation intervals of agonist and antagonist muscles [20,21] and the relevance of the phenomenon in children's pathologies [22]. Further studies focused on the quantification of muscle co-contraction in patients with PD. In the studies reported in [23,24], a greater coactivation of dorsiflexor and plantarflexor muscles was observed in people with Parkinson during treadmill walking compared to healthy adults, mainly during the stance phase. Higher simultaneous activation of ankle muscles for parkinsonian patients has been identified by [25] making a comparison with healthy ones, and evaluating in

addition, a high co-contraction index for older controls with respect to young controls. Although there are many studies that highlight changes in the pattern of co-contraction, some do not achieve this [26].

Most of these approaches mainly allow to collect data on muscle co-contraction in the time domain, thus neglecting information on the frequency content of the signal. To fill this gap, further literature focused on the use of wavelet analysis to analyze cross-correlation time-frequency for multiple sEMG signals in Parkinson's disease in upper limb monitoring [27], or for muscle fatigue assessing [28].

To the best of our knowledge, there are no quantitative studies reported in literature investigating the co-contraction intervals and the consequent frequency content of the sEMG signal measured on the analyzed muscles. Recently, algorithms based on the wavelet transform have been developed, which successfully allowed to characterize the sEMG signal in both time and frequency domain [29,30]. In particular, the algorithm in [29] introduces a time-frequency representation called scalogram allowing the simultaneous identification of muscle activation intervals and the corresponding frequency range of the signal. The product of the matrices of Wavelet coefficients associated with two sEMG signals provided the so-called coscalogram function, which allows to locate the cross-energy density between the signals. In the approach used in the latter study, the co-scalogram function has been interpreted as an estimate in the time-frequency domain of muscle co-contraction.

The aim of this work is to analyze the sEMG signals measured over tibialis anterior and gastrocnemius lateralis in order to characterize the co-contraction activity of two antagonistic ankle-joint muscles in time-frequency domain, during walking of subjects suffering from PD. For this purpose, kinematic and sEMG data were acquired from a population of 19 parkinsonian patients and a control population of 10 healthy subjects at the Movement Analysis Laboratory (BioMovLab) of the Department of Information Engineering of the University of Padua.

Chapter 1. Muscle contraction and co-contraction

Muscle contraction is the result of a series of coordinated intracellular modifications that leads to the movement of the muscle fiber and, consequently, of the muscle itself. Contraction occurs in all muscle types; It is best represented in skeletal muscle, where there is a metameric structure (the sarcomere) endowed with morphological and functional peculiarities. The mechanism involves the interaction of the contractile proteins actin and myosin in the presence of calcium, by which the contraction occurs as a result of a chemical, electrical or mechanical stimulus producing an action potential that propagates along the membrane of the muscle fiber. The source of energy for this contraction is supplied by adenosine triphosphate (ATP), which is produced in the mitochondria. ATP is stored as two products, adenosine diphosphate (ADP) and phosphate, at specific binding sites on the myosin heads [31]. On the other hand, posture maintenance and movement management can be accomplished with a motor strategy called co-contraction, which consists in the simultaneous activation of antagonist and agonist muscles. This is an important mechanism used by the central nervous system to improve joint stability and accuracy during motor execution [32].

1.1 Structure of the skeletal muscle

In the muscular system, muscle tissue is categorized into three distinct types: skeletal, cardiac, and smooth muscle. Each type of muscle tissue in the human body has a unique structure and a specific role. Skeletal muscle is found throughout the body and functions to contract in response to a stimulus. Skeletal muscle serves many purposes, including producing movement, sustaining body posture and position, maintaining body temperature, storing nutrients, and stabilizing joints [33]. The best-known feature of skeletal muscle is its ability to contract and cause movement [34]. In contrast to smooth and cardiac muscle contraction, the majority of skeletal muscle contraction is under voluntary control, receiving neural inputs allowing conscious control of muscles. Skeletal muscle comprises approximately 40% of total body weight in humans and contains 50 to 75% of all body proteins [35]. Skeletal muscle is a highly organized tissue composed of bundles of muscle fibres called myofibers which contain several myofibrils. The myofibrils are composed of two types of myofilaments (proteins) known as *actin* (thin filaments), *myosin* (thick filaments). The arrangement of actin and myosin gives skeletal muscle its microscopic, striated appearance and creates the functional units called sarcomeres. When viewed under electron microscopy, sarcomeres are oriented longitudinally and comprise several distinct regions. The Z line, or Z disk, is the terminal boundary of the sarcomere where α-actinin acts as an anchor for the actin filaments. The M line is the central-most line of the

sarcomere, where myosin filaments are anchored together through binding sites within the myosin filament. The H band contains the M line and it is the central region of the sarcomere that contains only myosin filaments. A band (dark band) is a larger portion of the sarcomere that contains myosin fibres and includes regions of actin and myosin overlap. The I band (light band) covers the terminal regions of two adjacent sarcomeres and contains only actin filaments (Figure 1.1) [33].

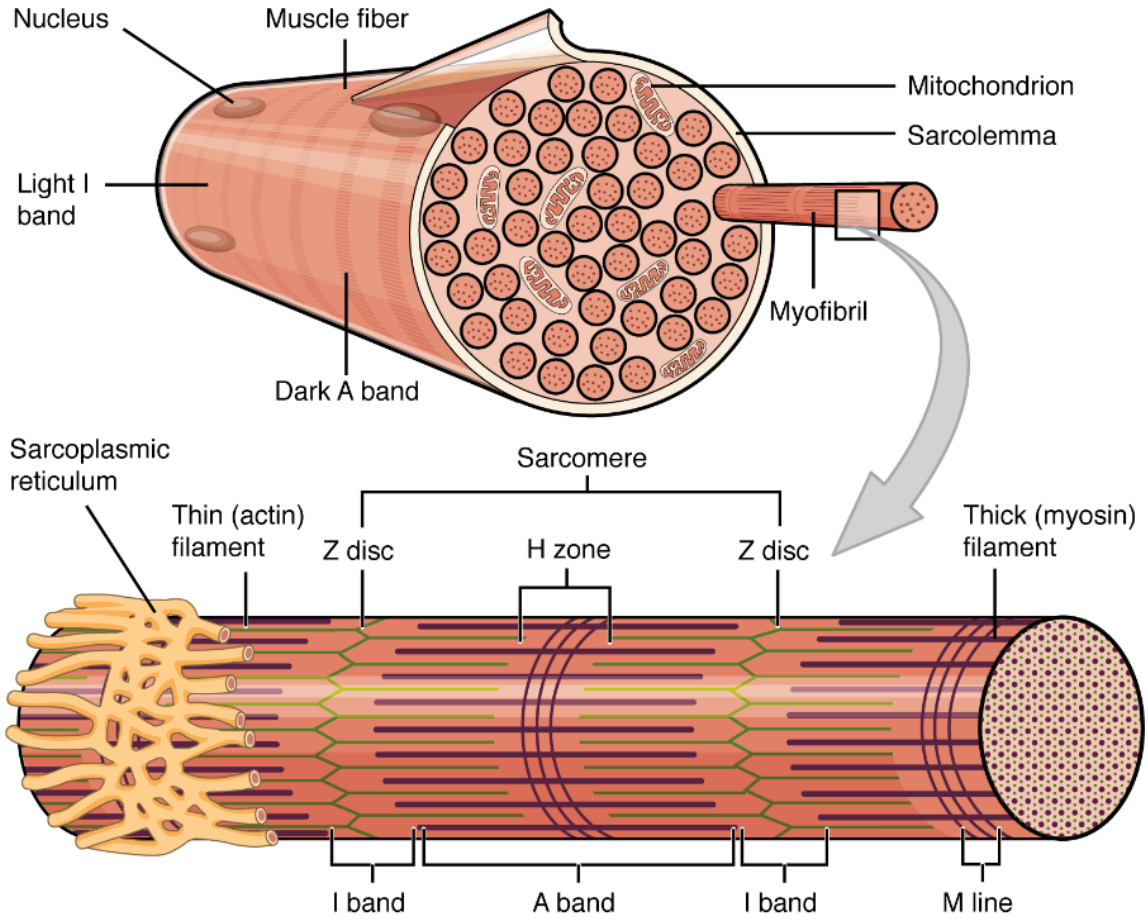

Figure 1.1 *Structure of the skeletal muscle: A skeletal muscle fibre is surrounded by a plasma membrane called the sarcolemma, which contains sarcoplasm, the cytoplasm of muscle cells. A muscle fibre is composed of many myofibrils, which are bundles of actin and myosin filaments organized into a chain of repeating units called sarcomeres with light and dark regions that give the cell its striated appearance [34].*

The thin actin filaments are mainly composed of two proteins that play a fundamental role in the process of muscle contraction that are tropomyosin, responsible for opening and closing the actin site and troponin. The latter is characterized by three units including troponin T that combines troponin

with tropomyosin, troponin C with a binding site with calcium ions and troponin I which inhibits the binding between actin and myosin. The function of tropomyosin is to prevent actin and myosin from interacting when the muscle is at rest, consequently preventing muscle contraction. When the muscle is stimulated to contract, calcium, binding to troponin C determines a change in the conformation of the entire molecule that modifies the position of tropomyosin exposing the sites of actin-myosin interaction [36].

1.2 Muscle contraction mechanism

The basis for understanding muscle contraction is the sliding filament model (Figure 1.2) [36]. Muscle contraction results from the arrangement and interactions between the thin and thick filaments, allowing for the sarcomeres to generate force. When signalled by a motor neuron, a skeletal muscle fibre is activated. During muscle contraction, the myofilaments themselves do not change length, but actually slide across each other so the distance between the Z-discs decreases resulting in the shortening of the sarcomere. The length of the A band does not change (the thick myosin filament remains at a constant length), but the H zone and I band regions reduce and the myofilaments sliding makes the actin filaments move into the A band and H zone.

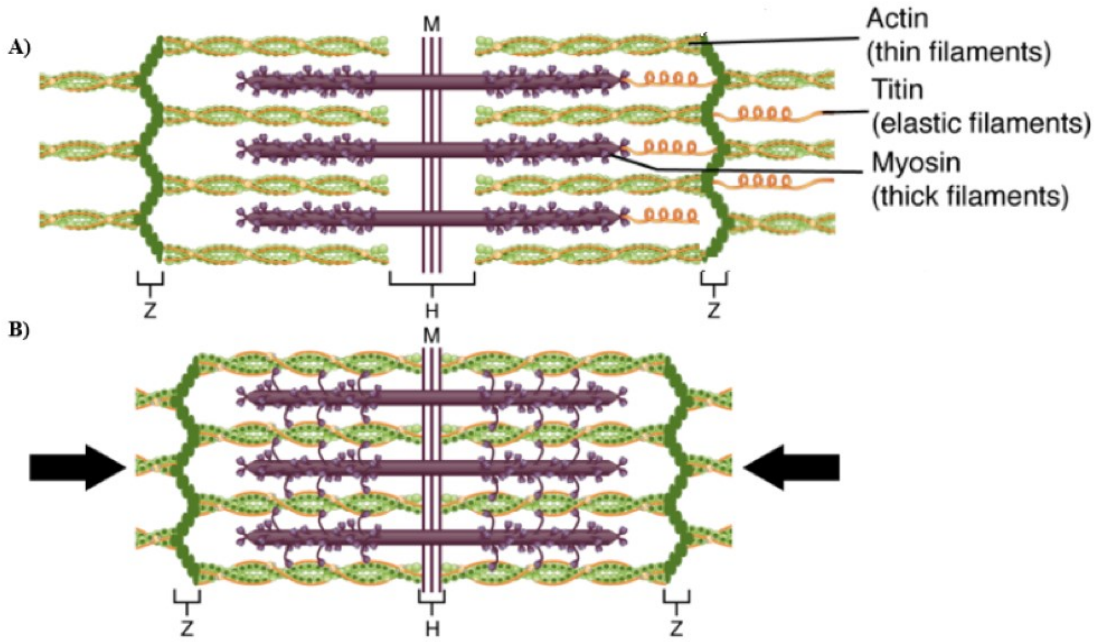

Figure 1.2 *Sliding Filament Model of Muscle Contraction: A) Relaxed sarcomere, B) contracted sarcomere. When a sarcomere reduces, the Z-discs move closer together, and the I band becomes smaller. The A band stays the same width. At full contraction, the thin and thick filaments have the most amount of overlap [34].*

The process of skeletal muscle contraction begins first at the neuromuscular junction (NMJ), which is the synapse between a motoneuron, the cell responsible for innervating muscle fibres, and a muscle fibre. A single motoneuron and the muscle fibres it innervates are collectively called a motor unit [36]. The action potentials travel along the axon of the motor neuron to the axon terminals at the NMJ and subsequent depolarization results in the opening of chemically-gated calcium (Ca) channels of the presynaptic membrane causing the release of acetylcholine (ACh) at the neuromuscular junction. The ACh molecules diffuse to the postsynaptic membrane at the muscle fibre, also known as the motor endplate, where they bind to the nicotinic receptors. The resulting depolarization of motor endplate initiates the action potentials in the muscle fibre [36].

1.2.1 Excitation-contraction coupling

The signalling process leading to calcium release and muscle contraction is known as Excitation-Contraction Coupling [37]. The excitation-contraction is the mechanism that converts the action potentials mentioned above in the muscle fibres into muscle fibre contraction. The action potential that arrives to the muscle fibre membrane is conducted to the interior of the muscle cell through the transverse tubular (T-tubule) system. T-tubules contain dihydropyridine receptors adjacent to the terminal cisternae of the sarcoplasmic reticulum that stores calcium. When T-tubules become depolarized, their dihydropyridine receptors undergo a conformational change that mechanically interacts with the ryanodine receptors on the sarcoplasmic reticulum [36]. The interaction causes the opening of the ryanodine receptors on the sarcoplasmic reticulum and the release of Ca from the sarcoplasmic reticulum. The calcium released then binds to the regulatory protein troponin C on the actin thin myofilament. This initiates a series of molecular events causing the displacement of tropomyosin blocking the active site of the actin filament.

1.2.2 Cross-bridge cycling

As said previously, muscle contraction is generated by the myosin heads of the thick filament that bind to actin and pull the thin filament which shortens the sarcomere and produces force. Cross-bridge cycling is the mechanism by which skeletal muscle contracts (Figure 1.3). At the beginning of this cycle, myosin is bound tightly to actin in a step termed “rigor”. In the absence of basic physiologic energy, such as death, this is a semi-permanent state called rigor mortis. The series of events that result in the generation of force begins when adenosine triphosphate (ATP) is made available to an existing actin–myosin cross-bridge [35]. The binding of ATP to the myosin head, induces a

conformational change of the myosin head that causes the release of the actin-myosin cross-link [33]. After ATP is bound and the cross-link is released, ATP is hydrolysed to adenosine diphosphate (ADP) and inorganic phosphate (Pi), “re-cocking” and moving the myosin head toward the positive end of actin (closer to the ends of the sarcomere). As long as there is adequate Ca2+ to maintain an uncovered actin-binding site, the myosin head will form a cross-bridge with actin. The release of ADP and inorganic phosphate causes the power stroke where the myosin head moves toward the negative end of actin (toward the centre of the sarcomere), displacing the actin filament and shortening the sarcomere. To complete the cycle, ADP is released, and the sarcomere returns to a state of rigor. This cycle repeats as long as Ca2+ is bound to troponin C [33].

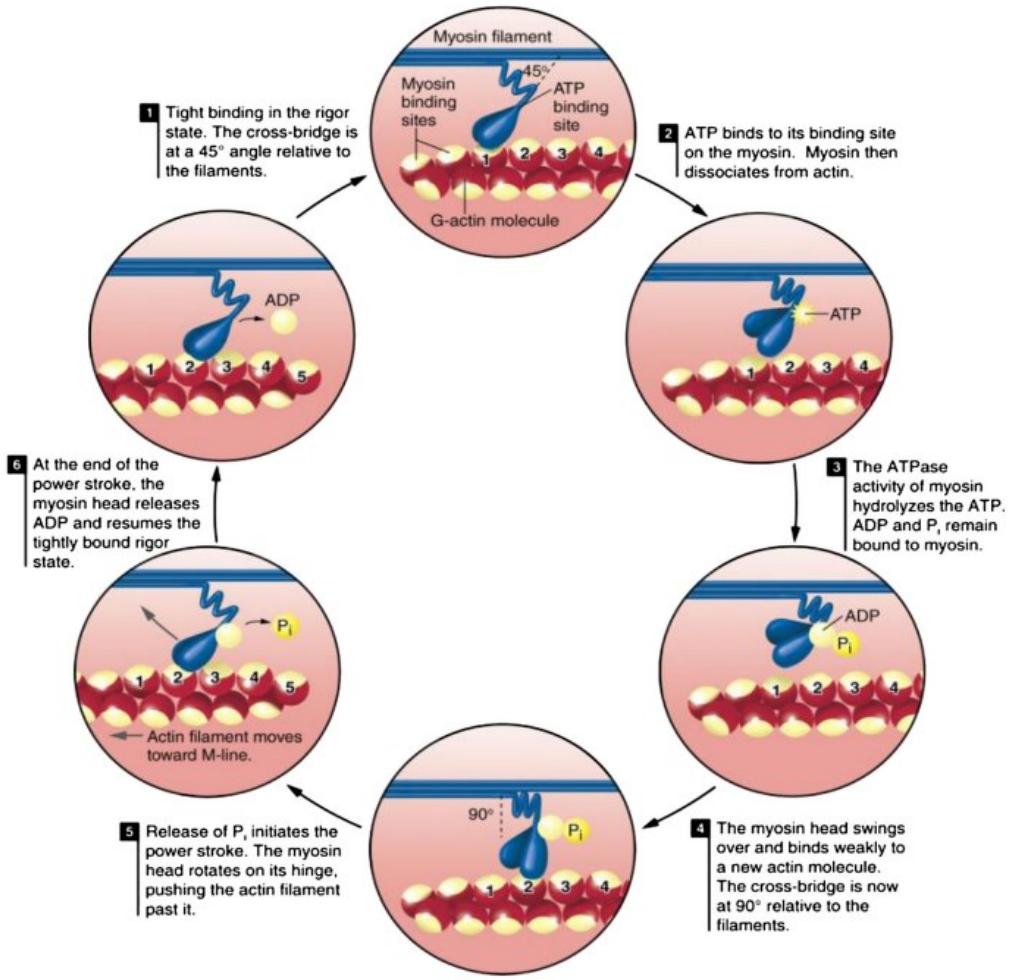

Figure 1.3 *Cross-bridge cycle: sequence of events by which the thick and thin filaments slide past one another for the generation of force and power. There are two states of cross-bridges, weak-binding and strong-binding state. As the name implies, the latter is a more important contributor to force generation and more cross-bridges exist in this state during maximal muscle activation. The repeated movement is dependent on ATP, which provides energy needed for the myosin head to reposition or re-cock [35].*

1.3 Electromiography

Electromyography is the discipline that deals with the detection, analysis, and use of the electrical signal that emanates from contracting muscles [38]. The EMG signal is a biomedical signal that measures electrical currents generated by muscle's motor units during its contraction representing neuromuscular activities. The nervous system always controls the muscle activity (contraction/relaxation). Hence, it is a complicated signal, controlled by the nervous system and dependent on the anatomical and physiological properties of muscles [39].

There are mainly two types of electromyography depending on the type of electrode used: the needle or wire electromyography is an invasive technique in which the potential value is acquired by positioning the electrode inside the muscle. This technique provides localized information that allows the identification and separation of contributions due to different motor units. The surface electromyography (sEMG) with sensors placed on the skin, is instead a procedure with less invasiveness; the surface signal is the result of the overlapping of the action potentials of all the motor units below the electrode. Although it is a technique subjected to greater disturbances, is still the cheapest; these days surface-detections are preferably used to obtain information about the time or intensity of superficial muscle activation [40]. Electromyography signals are considered most useful as electrophysiological signals in both medical and engineering fields and it is considered a valuable tool for understanding the human body's behaviours under normal and pathological conditions and to evaluate treatment outcomes [41]. The most prevalent areas of application are for the detection of muscle disorders, neurological impairments, playing an important role in neurorehabilitation, to investigate the associations between EMG and muscle damage, fatigue and mental stress [42]. sEMG is also suitable for the detection of coactivation of agonist and antagonist muscles, so that physiological activation patters could be distinguished from pathological one.

1.3.1 Acquisition system

The building block of the sEMG (Figure 1.4) starts with an electrode that serves as a transducer to convert ion current in the body into an electrical signal. The function of the amplifier is to convert the measured signal to an appropriate level for an analogue storage (e.g., tape recorder) and/or signal processing. In addition to amplification, signal conditioning and processing include filtering and analogue-to-digital (A/D) conversion respectively. The signal could be momentarily stored on tape for later digitization or may be modified by the analogue processing to provide the desired display.

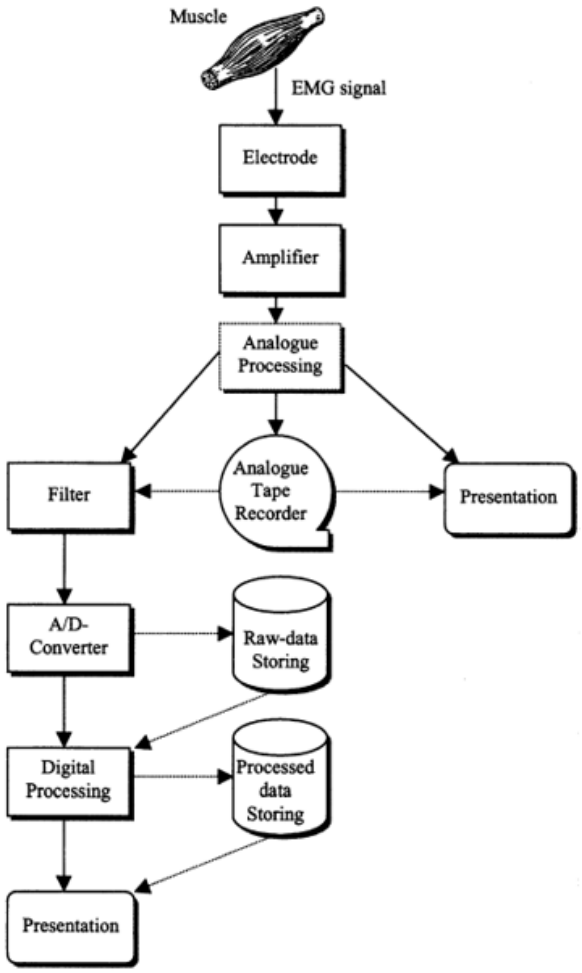

***Figure* 1.4** *Block scheme of the electromyograph.*

1.3.2 Surface electrodes

The surface electrode is an essential part of the measurement equipment. For instance, when using appropriate amplifiers and A/D-converters, the signal-to-noise ratio (SNR) is almost entirely controlled by the electrodes [43], which perform a transduction function between the ionic current generated by the human body and the electronic current transferred to the electronic equipment. SEMG electrodes typically used are made of a metallic part in silver-silver chloride (Ag-AgCl) covered by an adhesive conductive gel (which is the electrolyte) and surrounded by a plastic cap. Modern electrodes are disposable adhesive instruments in which the electrolyte gel is already incorporated (Figure 1.5).The electrodes have to be attached properly to the subject's skin, properly exfoliated, in combination with an electrolyte gel to prevent skin reaction, motion artifacts and further

reduce contact impedance. Inappropriate fixation due to movement artifacts can cause common mode disturbance in amplifiers and effectively reduce the SNR of the recorded EMG. The lower this impedance, the better is the signal propagation from the skin to the amplifier and this will improve signal detection. The best treatment to reduce electrode-skin impedance, is to mildly rubbing the skin with medical abrasive paste leading to a reduction of about -90% [44].

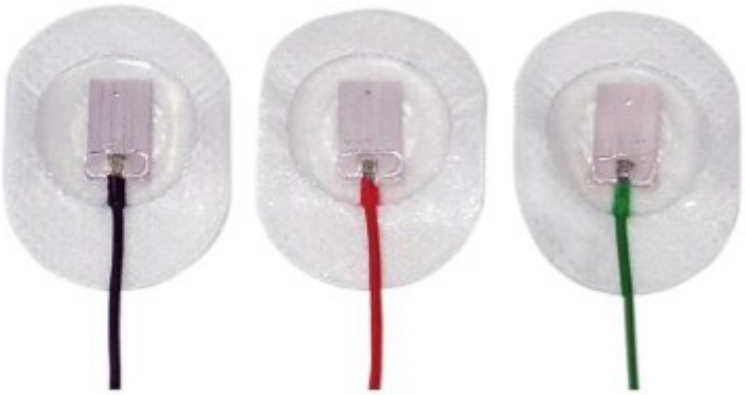

Figure 1.5 *Surface electrodes.*

There are many possible configurations of surface electrodes that can be used to record the EMG signal. Surface electrodes can be arranged in different configurations: in the *monopolar configuration* a single electrode is positioned with respect to a reference electrode which must be located on an electrically neutral tissue away from the active electrode. Bipolar surface electrodes are simple to apply but the SNR and spatial resolution of the recorded EMG are less compared to EMG records generated by using differential amplification such as the *bipolar configuration*. The latter is the most common used configuration based on two electrodes each with respect to a reference electrode and placed in relatively proximity to the active fibres. A differential amplifier is employed in order to reduce signals common to both electrodes and to amplify the potential difference between the two; therefore, they provide the advantage of increased spatial resolution and improved SNR. It is recommended to place the electrodes aligned longitudinally with the muscle fibres direction between the zone of muscle fibre innervation (motor point) and the tendon insertion or between two motor points. Using bipolar configuration, the optimal outcome is obtained orienting the two detection

surfaces of the electrodes in the direction (parallel) of the muscle fibres, otherwise less amplitude and frequency content of the signal will be recorded. Information on recommended electrode placement procedures for different muscles and muscle areas can also be found in the SENIAM guidelines. In general, in addition to the measures to be taken to reduce the skin impedance, it is necessary to space the electrodes at least 2 cm apart, and place them as much as possible at the centre of the belly of the muscle which activity wants to be evaluated and absolutely avoid the "motor points", or those areas where even the slightest electric current can cause a perceptible spasm on the surface of the muscle fibres [45]. These precautions, combined with a correct adhesion of the electrodes, allow to avoid noise due to crosstalk, that is to say, EMG signal from other muscles. Other typical interferences are interference line, due to the electrical network, movement artifacts and artifacts from ECG due to the possibility that the EMG also can collect electrical signals of cardiac activity.

1.3.3 EMG signal acquisition

The EMG signal is based on action potentials collection at the muscle fibre membrane resulting from depolarization and repolarization processes [45]. The cellular membrane presents an electric potential difference between the intracellular and the extracellular environment due to the different ionic concentration between the inner and outer compartments, known as resting potential. In muscle and nerve cells, the application of appropriate stimuli determines a sudden and momentary upheaval of the resting potential; this change in the electrical state of the membrane represents the action potential, which consists of a rapid reversal of the rest potential, which goes from -70 mV to +30 mV (depolarization phase), immediately followed by an equally rapid return to the original value (repolarization phase). When the contraction occurs, a stimulus coming from the Central Nervous System (CNS), in the case of voluntary contraction, or coming from an external electrical stimulator, in the case of induced contraction, propagates along the axon of a motor neuron and then reaches the fibers of the motor unit. Starting from the innervation point of each fiber, two depolarization zones are generated (having an area between 1 and 3 mm^2) which, after the initial excitation, propagate towards the end of the fiber at a speed of 3-5 m / s. The action potential in moving along the fiber, generates an electric field that diffuses in the surrounding conductive medium producing electrical activity that can be acquired from the electrodes placed on the skin. The resulting signal is given by the spatial-temporal summation of the individual action potentials produced by the depolarizations of the muscle fibers of a motor unit, and it is called MUAPT (motor unit action potential train). Therefore, the surface EMG signal is given by the superposition of the MUAPs of the various motor units (Figure 1.6). There are two mechanisms that influence amplitude and density of the observed

signal that are the recruitment of MUAPs and the Firing frequency (frequency of activation of motor units) that allow to control muscle activity in terms of strength and frequency of contraction. The overlapping of the MUAPs of the different motor units gives rise to the sEMG signal called Raw EMG, which will be later processed. By their nature, EMG peaks are randomly shaped, which means that a "raw" recording cannot be accurately reproduced in exact form. This is because the set of constantly recruited motor units change continuously within the examined surface and they may produce an overlapping peak.

By applying a smoothing algorithm or selecting a parameter of suitable amplitude, the random contents of the signal are eliminated or at least reduced. The raw sEMG signal can vary between ±5000 μV (at the limit) and typically the frequency content varies between 6 and 500 Hz, although it shows the highest frequency power between about 20-150 Hz [45].

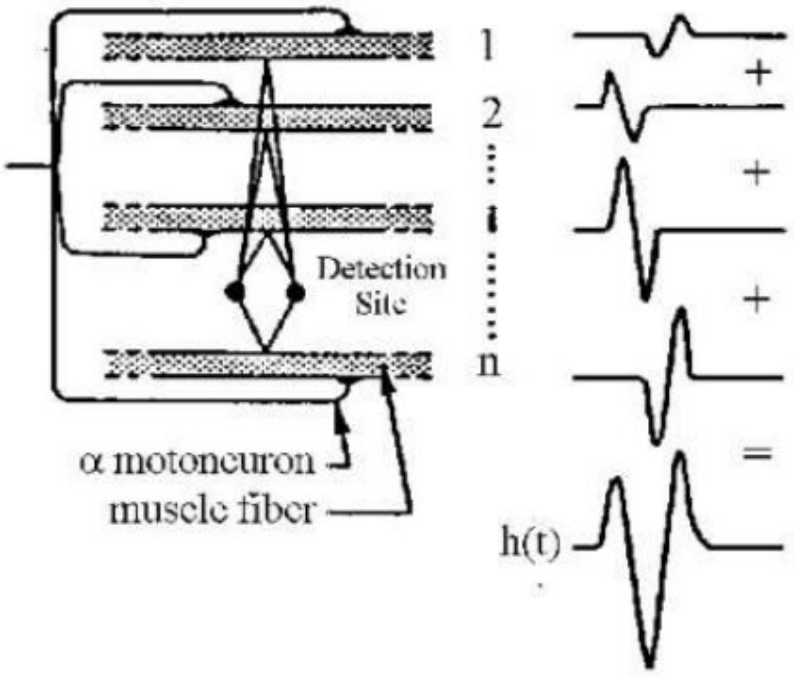

Figure 1.6 *Schematic representation of the MUAP generation: sEMG signal is a summation of action potentials generated by motor units lying within the detection volume of the electrodes [46].*

1.3.4 Amplifiers

A differential detecting setup is used in order to reduce the considerably higher noise signal coming from power line source. The signal is detected at two sites and the differential amplifiers amplify the voltage difference (V_d) between two points (electrodes) by a factor of A_d (the amplifier differential

gain) to obtain the output voltage, V_{out}, (Figure 1.7) [41]. Signals appearing identically at both inputs sites at the same time will be removed and not amplified. An example of an undesired signal that could emerge simultaneously at both amplifier inputs would be electrical interference from power lines, which occurs at a frequency of 50 Hz or 60 Hz [41]. Amplifiers also suppress EMG signals from distant muscles, which appear at the amplifier as common-mode signals, whereas signals close to the detection surfaces will be different and consequently will be amplified. Ideally noise or interference signals would be completely rejected by the amplifier, however, in practice these unwanted common-mode voltages will receive some small amplification and the output voltage of the amplifier will contain some unwanted common-mode signals.

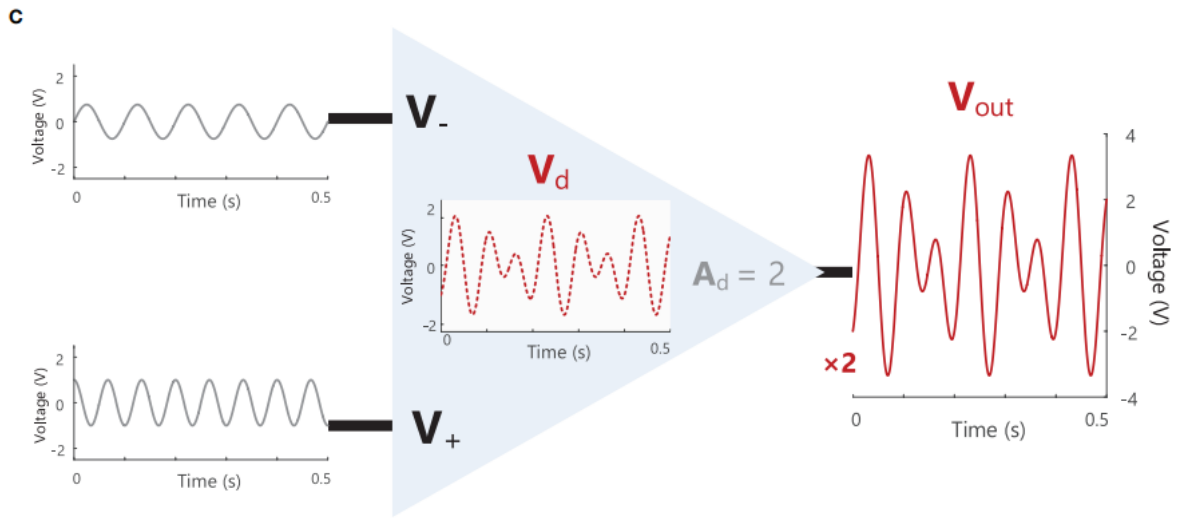

Figure 1.7 *A schematic illustration the function of a differential amplifier, which receives two input signals at V− and V+. The amplifier calculates the difference between these signals (V_d) and multiplies (amplifies) V_d by the gain of the amplifier, A_d (in this example the signal is increased by a factor of 2) [41].*

The essential components of an amplifier are the differential gain, input impedance, common mode rejection ratio (CMRR), and frequency response of the amplifier relative to the acquired signals [47]:

- Usually, the amplifiers have a linear amplification range of ±10V or greater and the ratio between input and output voltage (differential gain =A_d) ranges between from 10,000:1 to 100,000:1 [47].

- Common-mode rejection ratio (CMRR): The accuracy by which the differential amplifier can subtract common-mode signals (e.g., noise or interference) is quantified by the CMRR. The CMRR is the ratio of the differential gain to the common mode gain and the minimum specifications for EMG amplifiers range from 80-100 dB [47]. A differential amplifier should have a high differential gain and low common mode gain.
- *Input impedance*: the source impedance is present at each of the two input terminals and it acts as an obstacle to current flow between the input terminal and ground (reference) [41]. It may range from several thousand ohms (kΩ) to several megohms (MΩ), and in order to prevent attenuation and distortion of the detected signal due to the effects of input loading, the input impedance of the differential amplifier should be as large as possible, without causing secondary complications to the workings of the differential amplifier.
- *Frequency response*: it has to be in line with the EMG signal characteristics; it can have a lower cut-off frequency (10Hz) to remove the artifacts due to subject movements and higher cut-off frequency (500Hz) that depends on the type of electrodes used. The band of the sEMG signal is up to 500Hz.The sampling frequency to use to avoid loss of information must be at least 1000Hz (twice the band of the signal).

1.3.5 Filter

Hardware filters are used to remove unwanted components from the signal before the A/D conversion. Typically, a high pass filter at a very low frequency, with a cut-off frequency of 10–30 Hz, and it is used to remove the baseline drift and, in part, motion artifacts [44]. A low pass filter removes higher frequency contributions that are produced by electronic components with a cut-off frequency of 350–400 Hz [44].

1.3.6 A/D converter

In order to be stored and processed as a digital signal, the analog signal must be first sampled to preserve the full range of frequency components in the EMG signal. The analog-to-digital (A/D) converter is responsible for converting the analog signal into bits through sampling and quantization processes. Sampling consists of transforming the signal from the continuous-time domain to the discrete-time domain. According to the Nyquist sampling theorem, digital sampling should be conducted at an adequate sampling rate: the minimum sampling rate should be twice the signal bandwidth [41]. Generally, from 1000-1500Hz is commonly accepted as a sufficient rate for most surface EMG applications. If the sampled signal (including noise) contains frequency components

that are higher than half the sampling rate, aliasing will occur, such that high-frequency components are reflected onto the lower frequencies. To avoid aliasing problems, an analogue low- pass filter, also called anti-aliasing filter, must be used. In addition, the signal amplitude should be set by the amplifier to an appropriate level to minimize the quantization error, that is due to the difference between the original signal value and the digitized value [43].

As regards the quantization, this divides the sampled analog signal into levels that identify a different voltage range, where each level corresponds to a very specific binary encoding. The number of bits used for an EMG is 12 (2^{12} levels) [45].

1.3.7 Time and frequency domain analysis

The acquired raw signal allows to establish the relationship between its signal amplitude and the force exerted by the muscle under isometric conditions. To quantify the amplitude of the raw sEMG signal, analysis methods are needed for correct interpretation of the time-varying muscle activities. One of these methods is the *linear envelope* approach provides a fast and simple detection of the muscular activity and it requires two-step process: the first step is the "full wave rectification" step essential for getting the shape or "envelope" of the EMG signal. Since the EMG signal is naturally nearly zero mean, with fast oscillations, the full rectification of the signal is an important step to calculate the absolute value of the signal inverting the negative values into positives and therefore preserving the signal energy [48]. A low pass filter (2nd order low-pass Butterworth filter) at a 5 Hz cut-off frequency is applied then to the rectified signal. The amplitude of the signal can be estimated as the average value of the rectified signal (ARV Average Rectified Value) in which a moving average of the signal is performed by taking a time window shifted over the rectified signal [43]. As result, the linear envelope is obtained, following the trend of the original signal and it is regularized so as to highlight its trend. The envelope quite closely resembles the shape of the muscle tension curve. This process reduces the frequency content of the EMG signal, but it is easy to interpret and to detect the onset activity (time instant when the muscle activates). Alternatively, the amplitude of the signal can also be defined as RMS (Root Mean Square) and therefore it provides more information than the previously described methods, since it gives an estimate of the standard deviation and variance and reflects the electrical strength of the signal (Figure 1.8) [43].

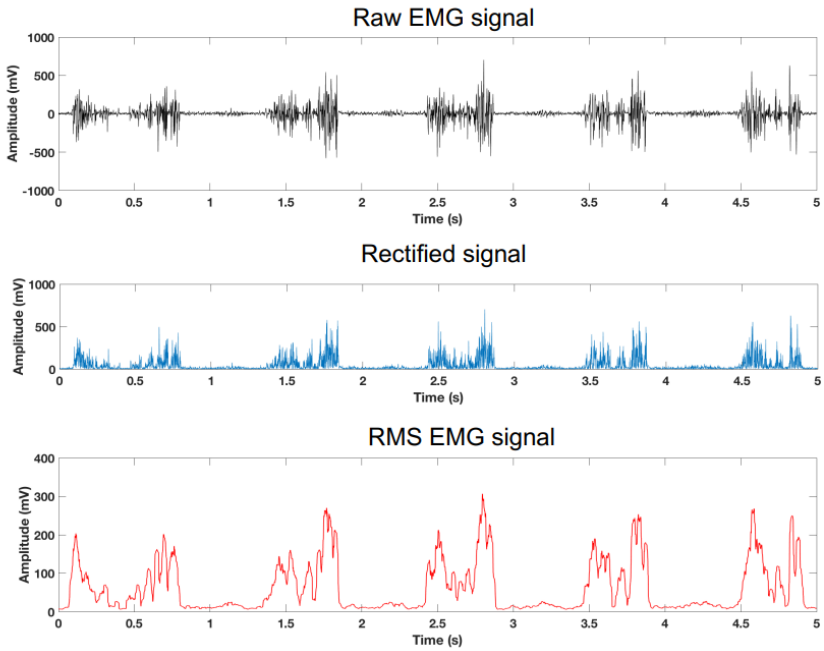

Figure 1.8 *RMS of the EMG signal.*

In the time domain, ON-OFF activation intervals on the raw signal of a muscle can be extracted. The ON instant is estimated by calculating the intersection of the linear regression of the RMS noise and EMG signal. When the activity exceeds the reference threshold the muscle is defined as being active (ON), otherwise it is OFF. Double threshold methods are considered better in comparison to single threshold methods [39]. In the double-threshold method there are an amplitude and a temporal threshold. When the signal exceeds the first threshold (amplitude) and remains above it for at least the second threshold (temporal), this sample is acknowledged as the ON-instant of the muscle activity. In the same way, the first sample after the ON instant, from which the signal remains below the first threshold for at least 30 ms, is acknowledged as the OFF-instant [49]. As reported in literature [50,51,52], other techniques as TKEO are used to detect muscular onset detecting instantaneous changes in frequency and amplitude of sEMG sign where amplitude and frequency increase considerable faster and it is relatively easy to separate muscle activity from background activity. Additionally, the Wavelet transform approach is taken into account and will be covered in the later chapter 2.

Regarding the frequency domain analysis, this is based on the estimation of the power spectral density function (PSD) of the signal. Examining sEMG signals in the frequency domain can provide information on changes in the frequency content of the signal, manifesting as alterations in the shape

of the EMG amplitude/power spectrum. Frequency domain features such as median and mean frequency (MNF and MDF respectively) are extracted from the power spectrum of the signal, by proving useful information about the muscle fatigue index inability [53].

When a muscle contraction occurs, a progressive change in the shape of the amplitude and frequency of the power spectrum occurs; there is a compression towards the lower frequencies and an increase in amplitude and a consequent decrease in the values of average frequency and median. The more rapid and marked is this compression, the greater is the level of contraction and it allows to define muscle fatigue not as the inability to further sustain a certain level of contraction, but as the set of phenomena that lead to this inability [53]. The most widely used method for estimating the frequency spectrum of the surface EMG signal is the Fourier transform (FT). Nevertheless, no information can be retrieved from FT about the time instances when these frequencies occur, and this kind of approach is insufficient to give a complete and exhaustive representation of the electrophysiological phenomena behind neuromuscular activations. Therefore, the requirement that a signal's frequency does not change over time (stationarity) is a crucial prerequisite for the use of an FT analysis. However, this is not the case for dynamic muscle activity. In order to overcome this limitation, new methodologies have been introduced, such as the wavelet transform, that will be discussed in the chapter 2. This technique results to be a reliable tool to characterize the EMG signal in both time-frequency domain without the stationarity requirement of the signal.

1.4 Muscle co-contraction

The moveable end of the muscle that attaches to the bone being pulled is called the muscle's insertion, and the end of the muscle attached to a fixed (stabilized) bone is called the origin [34]**.** Skeletal muscles, which are responsible for posture and movement as said previously, are attached to bones and arranged in opposing groups around joints, that provide stability to the skeleton, and allow movement. A joint will have at least two muscles crossing it to be able to move in either direction. Upon activation, the muscle pulls the insertion toward the origin. Although a number of muscles may be involved in an action, the principal muscle involved is called the prime mover, or agonist**.** A muscle with the opposite action of the prime mover is called an antagonist**.** Antagonists play two important roles in muscle function: they maintain body or limb position, and they control rapid movement [34]. The stimulation of proprioceptive end organs in the contracting muscle is thought to cause cessation or diminution of excitatory impulses along the motor neuron to the antagonist muscle [54]. This type of neuro-muscular activation pattern is possible thanks to a nervous mechanism that is defined with the term "reciprocal innervation", by which refers to the mutual collaborative strategy

that, within the movement, the agonist and antagonist muscles adopt. From the above, the concept of "coactivation" or "co-contraction" arises, which implies the simultaneous activation of the two opposite muscle groups, agonist and antagonist and in order for muscle coactivation to occur, reciprocal innervation must inhibited [55].

However, the general mechanism of it is still not fully understood, but over the years, researchers have begun to study in depth the phenomenon, considering the degree of muscle activation is one of the most useful parameters for the qualitative assessment of the neuromuscular function [56]. Firstly, muscle co-contraction was defined as the phenomenon of 'agonist-antagonist co-activation', by referring to the activity of two muscles within the same joint, each producing a force and/or a moment and effect that opposes this force [57]. This is due to the fact that muscles are unidirectional actuators [57]. In other words, all degrees of freedom in a joint are provided by at least two muscles with opposite effects. Although the mechanism of coactivation is still widely discussed, studies suggest that its main purpose is to maintain control of muscle action and ensure, in the performance of certain motor tasks, the stability of the joint [58,59]. Finding the ideal balance between the degree of muscle activation and the movement made is a challenging work for the central nervous system; since the stiffness of a joint is caused by a greater antagonist activation, increasing stiffness is crucial in preventing joint instability [26]. An excessive muscle activation may result in a reduction in the muscular system's performance leading to an overuse of the joint surfaces, otherwise a lower level of muscle activation will result in decreased joint stability, increasing the risk of damage for the individual [26].

Moreover, there is evidence that the co-contraction mechanism has different incidences depending on the population examined. In healthy subjects, coactivation occurs to maintain a uniform pressure on the joint considered when performing static or dynamic motor tasks. This is done to allow better motor control, but there is a greater incidence of the phenomenon in the performance of demanding motor tasks, which provide greater unpredictability in external conditions, postural perturbations, resulting in a higher need for corrective actions to cope with stronger destabilizers effects [57,60]. Furthermore, in populations with impaired motor function, elevated levels of muscles coactivation are typically observed, and comprehending the causes and the functional significance is crucial in movement disorders and motor rehabilitation areas [57]. In pathologies, the incidence of co-contraction is also higher in the performance of daily motor tasks, suggesting that coactivation is the response of the nervous system to the need to develop compensatory strategies to increase joint stability [6]. In particular, the normal activation of muscles is highly compromised in Parkinson’s disease in which increased coactivation has been described as typical of Parkinsonian rigidity [11]. Overall, the two major circuits, corticocerebellar-thalamo-cortical and corticobasal-thalamo-cortical,

seem to play a major role in defining coactivation patterns and these will be described later in the chapter 2 related to Parkinson's disease.

In the current study will be considered co-contraction signals elaborated from the sEMG signals of the tibialis anterior and gastrocnemius lateralis muscles, which play an antagonistic role in the ankle joint and whose coactivation plays a fundamental role during different phases of the gait: in fact, the coactivation of the agonist-antagonist muscles on the ankle is a phenomenon widely described in the literature, which allowed to reveal how, during the performance of crucial tasks such as weight loading or the transition from the support phase to the oscillation phase, the incidence and intensity of co-contractions in the ankle joint increases significantly [9,10,12,16,23,24,25,26]. Although there is a lack of uniformity in the quantification of coactivation, numerous methods of investigation have been developed that allow to define muscle co-contraction, from more advanced mathematical models based on the evaluation of muscle momentum to simpler indices derived from the analysis of electromyographic signals [18,19].

A typical technique for measuring muscular co-contraction during human motion is the Co-Contraction Index (CCI), of which two standards forms enable clinicians for a simple evaluation of muscle co-contraction using surface electromyography (EMG) data [12,61]. The use of the traditional CCI index described by Falconer and Winter represents a ratio of agonist/ antagonist overlap to total muscle activation and the total antagonist activity is calculated as the area under the curve formed by EMG envelope [60]. The study by [17] calculated CCI based on a formulation by Rudolph et al. (2000) using normalized joint moments from an antagonistic pair of muscles to describe the temporal and magnitude components of the EMG signals; however, the technique calculated from simulated muscle moments during gait. was significantly lower than CCI. On the other hand, in the study [62] the calculation of the CCI based on agonist and antagonist muscle moment may offer a more accurate description of muscle action compared to co-activation indexes, resulting in various CCI outcomes. A different approach has been employed for the time-domain characterization of muscular co-contraction, based on the overlapping period between activation intervals of agonist and antagonist muscles (Figure 1.9), in terms of variability of onset-offset muscular activation and occurrence frequency [20,21]. The same method has been used in the study where muscle co-contractions are particularly relevant in analysing children pathologies aimed to evaluate the asymmetric behaviour of lower-limb-muscle recruitment during walking in mild-hemiplegic children [22].

Nevertheless, as far as frequency analysis is concerned, this is used to quantify the process of muscle fatigue in stationary isometric contraction using traditional techniques, such as the Fourier transform [53]. For this purpose, more recent methods such as the Wavelet Transform have been introduced to characterize muscle fatigue and muscle co-contraction in the time-frequency domain [27,28,29].

These methods consist of using the continuous wavelet transform (CWT) to evaluate a single co-contraction signal, quantifying it in terms of time intervals, frequency range and amplitude. The approach using CWT technique, whose application in the analysis of the EMG signal will be deepened later, allows to statistically evaluate the crossed energy density in time-frequency between two signals, or the function of the CWT coscalogram, which allows to verify the cross-correlation between the two different signals obtained by the individual muscles [29].

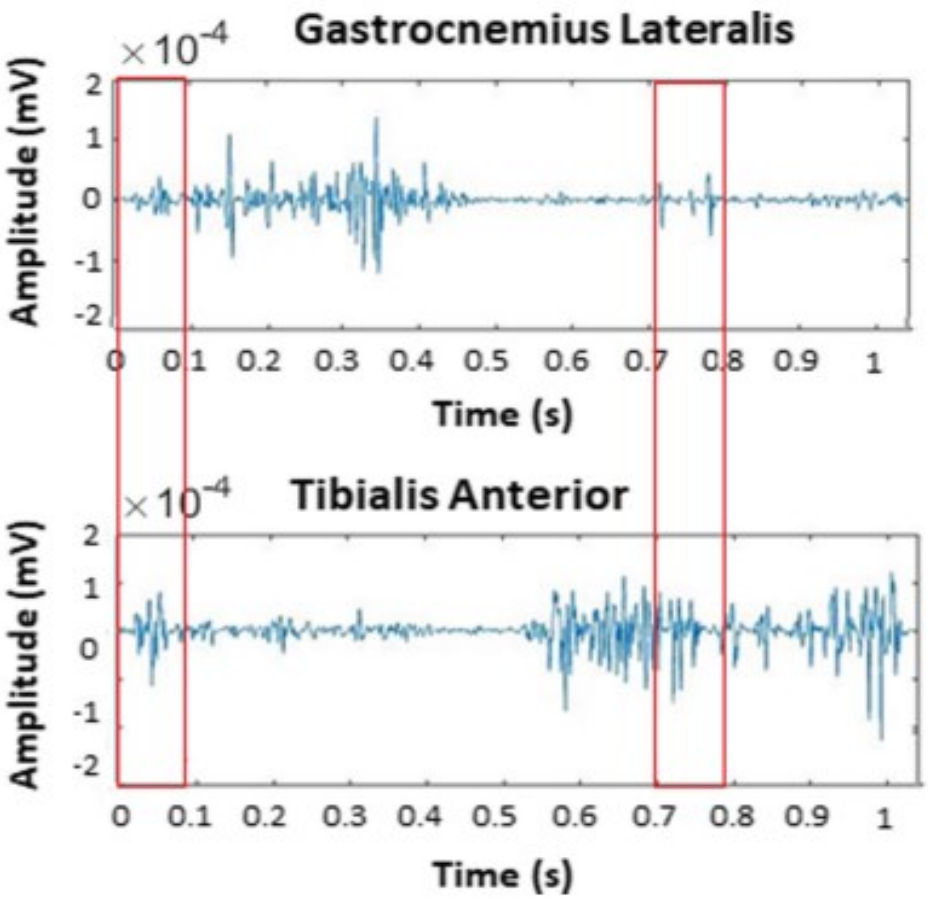

Figure 1.9 *Muscle co-contraction between two sEMG signals (Gastrocnemius lateralis and Tibialis Anterior) highlighted by a red box activation. Muscular co-contraction is identified as the overlapping periods among activation intervals of the considered muscles in the same strides.*

Chapter 2. Parkinson's disease

2.1 Neuropathology

Parkinson's disease (PD) is a complex and the second most frequent neurodegenerative disease after Alzheimer's disease (AD) [1], affecting 0.5–1% of 65–69 years of age population, rising to 1–3% among 80 years of age and older people [2]. It is also estimated that both the prevalence and incidence of PD case burden are expected to increase up to more than one million people by 2030 [63]. The most noticeable signs and symptoms of PD arise when nerve cells in the basal ganglia (BG), a region of the brain responsible for movement control, and the substantia nigra (SN) become impaired and/or die. These nerve cells, or neurons, normally generate an important chemical messenger, known as dopamine. Loss of dopaminergic (DA) neurons in the SN leads to a significant decrease of dopamine levels in synaptic terminals of the dorsal striatum (Figures 2.1-2.2), ultimately results in loss of the nigrostriatal pathway, that connects the substantia nigra pars compacta (SNpc) in the midbrain with the dorsal striatum (i.e., the caudate nucleus and putamen) in the forebrain [64].

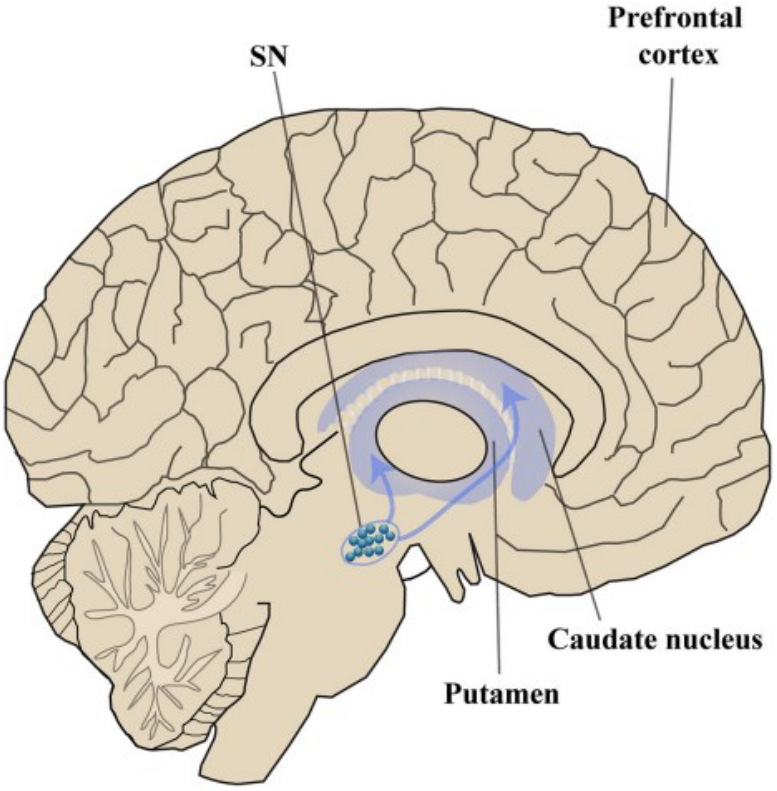

Figure 2.1 *Midbrain dopaminergic neurons (DA) are particularly sensitive in Parkinson's disease. (A) Loss of dopaminergic (DA) neurons occurs in the substantia nigra (SN). The degeneration of DA neurons is anticipated by dysfunction and in turn degeneration of the nigrostriatal pathway, which innervates the caudate nucleus and the putamen, form together the striatum.*

The decrease in the dopamine production triggers a variety of motor symptoms, such as tremor, slowness of movement, stiffness, and balance problems, which together characterize PD as movement disorder. A pathological hallmark of Parkinson's disease is microscopically represented by the presence of Lewy bodies (LB) (named after the neurologist F.H. Lewy who identified them in 1912, which accumulate in the subtantia nigra. Lewy bodies are spherical inclusions, found on histological examination, mainly formed by aggregates of alpha-synuclein, a protein in an insoluble form. The size of an LB can vary from 5 to 30 μm in diameter, and many LBs can be found within a single neuron. The composition of the dense granular material in LBs is unknown but possibly related to other components that immunohistochemical studies have found to be existent in LBs. [63].

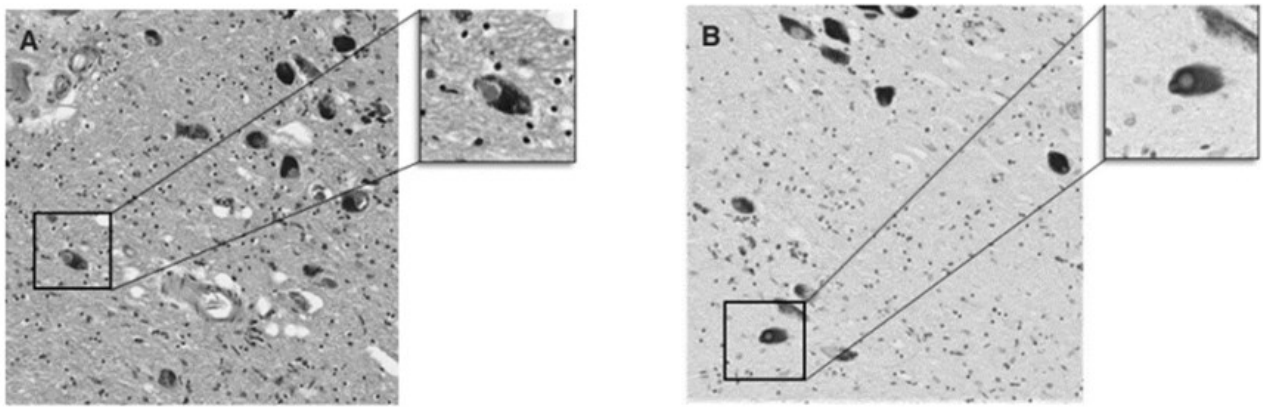

Figure 2.2*: Examples of LBs distribution with a surrounding halo in Lewy pathology in the substantia nigra pars compacta (SNpc) (A-B) and the corresponding enlarged view of the boxed region [65].*

2.1.1 Circuit models of the Basal Ganglia

The accurate sensory-motor processing in the brain is necessary for the proper execution of voluntary movements. This task is performed by a complex neural network, which includes the cerebral cortex, the motor thalamus and the basal ganglia nuclei. The thalamus and the cortex are functionally separated by the basal ganglia circuit, which function is to regulate movement execution by processing the signals flowing from the cortex and producing an output signal that returns back to the cortex through the thalamus. The basal ganglia circuit consist of a group of subcortical nuclei including the striatum, the globus pallidus, with the pars externa (GPe) and interna (GPi), the

subthalamic nucleus (STN), the substantia nigra pars compacta (SNc) and pars reticulata (SNr). The BG nuclei's connectivity to the cerebral-cortical regions provides a complex network of sensorimotor, limbic, and associative information, conferring on the BG an essential role in the control of movement as well as in associative learning, emotion and reward-related behaviour [66]. The striatum and STN represent the main entry points for cortical, brainstem and thalamic inputs into the BG circuitry. The inputs come from motor areas, including the somatosensory, motor and premotor cortices and terminate in the putamen where glutamatergic projections (excitatory) are received. From the input nuclei, the information is conveyed over multiple pathways to the two output nuclei, GPi and SNr. From these two output structures, the basal ganglia outflow is projected to the frontal areas of the cerebral cortex (via the thalamus) and at various brainstem structures such as superior colliculus (SC) and pedunculopontine nucleus (PPN). The output nuclei send GABAergic (inhibitory) projections to the thalamus, which in turn projects glutamatergic neurons back to cortical motor regions. The connections between the striatum and the output nuclei of the basal ganglia are thought to be organized into two distinct pathways, the so-called direct and indirect pathways, implying the facilitation or inhibition of voluntary movements (Figure 2.3). The net effects of these two pathways are facilitation (direct) and inhibition (indirect) of thalamic, and cortical activity. The direct pathway is formed through a monosynaptic connection between inhibitory neurons of the striatum and the GPi -SNr structure. These neurons are GABAergic striatal projection neurons (SPNs) that compose almost 95% of the striatum and they convey inhibitory efferent transmission. The neurons are identified by their expression of neuropeptide Dynorphin (Dyn) as a co-transmitter and by the dopamine D1 excitatory receptors they carry, projecting directly to the GPi-SNpr. On the other hand, the indirect pathway arises from a different set of striatal GABAergic neurons containing Enkephaline (Enk) and expressing D2 inhibitory receptors that project primarily to GPe which sends GABAergic projections to the subthalamic nucleus and then reaching the GPi/SNr outputs. In a healthy condition (Figure 2.3A), the activation of the direct pathway facilitates movement execution by reducing the GABAergic neural firing of the GPi/SNpr output and with subsequent disinhibition of thalamic nuclei and glutamatergic thalamocortical transmission (excitatory). This net effect will lead to an increased activity in appropriate cortical neurons. Neurons in the SNc travel to the striatum via the nigrostriatal pathway and release dopamine in the striatum to facilitate the activity of the direct pathway. In parallel, the activation of the indirect pathway reduces movement initiation, by inhibiting the GPe with subsequent disinhibition of the STN. Glutamatergic projections coming from the cortex activate the STN and an increased activity of GABA neurons of the output nuclei GPi/SNr occurs. Consequently, their inhibitory control over the motor thalamus results enhanced. The concurrent activation of both pathways preserves a balance between the direct and indirect pathways, activating

specific and voluntary actions via the direct pathway and inhibiting involuntary movements via the indirect pathway. The SNc project through the dopaminergic nigrostriatal pathway to the striatum where dopamine neurotransmitter is released. Dopamine can both excite the direct pathway by binding to D1 receptors and can inactivate the indirect pathway by binding to D2 receptors. In a parkinsonian condition (Figure 2.3B), a significant loss of dopaminergic neurons in the SNc and their projections to the striatum result to be the cause of the classical PD motor symptoms. Moreover, dopamine depletion causes a functional imbalance between the two pathways, leading to hypoactivity of the direct pathway and hyperactivity of the indirect pathway. As result the Gpe firing is suppressed and STN increases its activity overstimulating the GPi/SNpr which subsequently decreases thalamic projections to motor cortical areas, resulting in reduced movement.

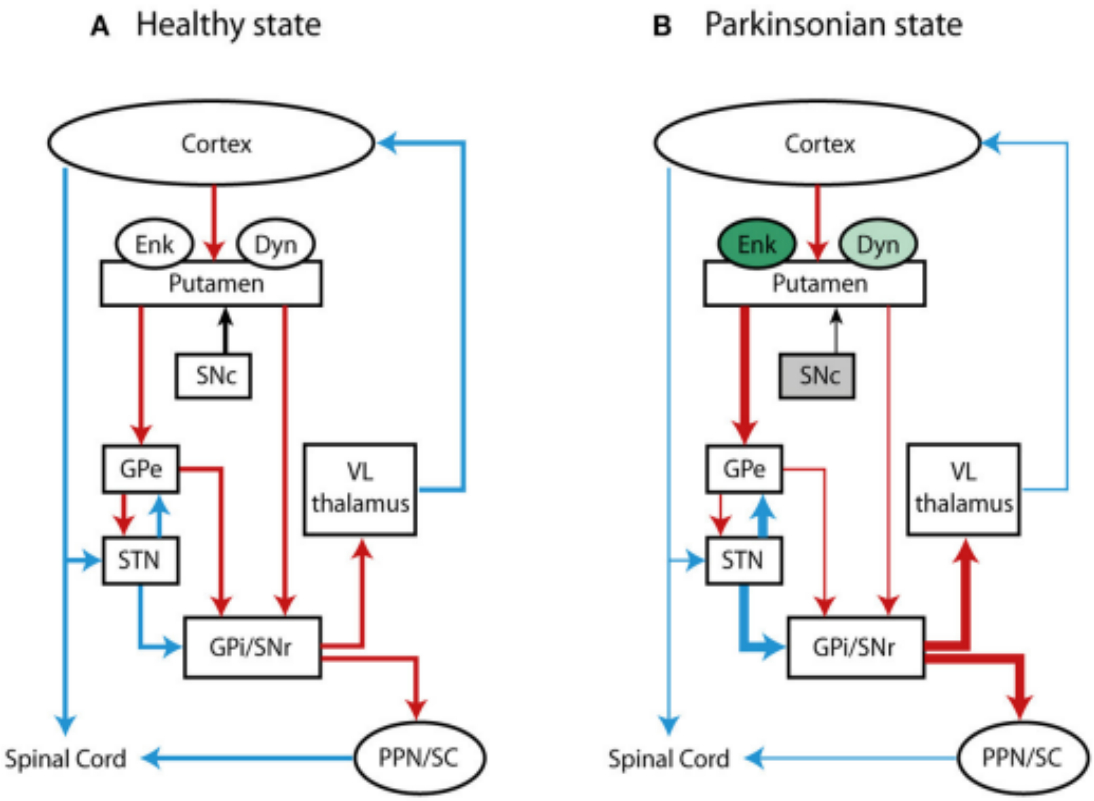

Figure 2.3 *Basal ganglia circuitry in normal condition (A) and PD condition (B). Red, blue and black lines indicate GABA-ergic, glutamatergic and dopaminergic projections, respectively. Blue arrows denote excitatory connections, red arrows identify inhibitory connections. Thick and thin lines represent increased activity and decreased activity of neural transmission. Green and light green colours represent increased and decreased levels of Enk and Dyn neuropeptides. The loss of dopaminergic cells in substantia nigra pars compact (SNc) represents PD condition and it is indicated with the grey colour [66].*

2.2 Diagnosis

The diagnosis of PD is a very delicate stage since it is not based on diagnostic tests that certify its presence, but it includes a clinical investigation during which the expert analyses mainly the symptoms, the patient's medical history and response to treatment. The first step is to identify the patient's "parkinsonism": the key elements of this clinical diagnosis are bradykinesia, tremor, and rigidity. In order to diagnose the pathology, it is also fundamental to prevent other causes of the disease, once the occurrence of parkinsonism has been determined. Moreover, there are also additional characteristics that support a conclusive clinical diagnosis of PD along with the presence of parkinsonism. The presence of nonmotor features also plays an important role, as these may be prominent even early in the disease course.

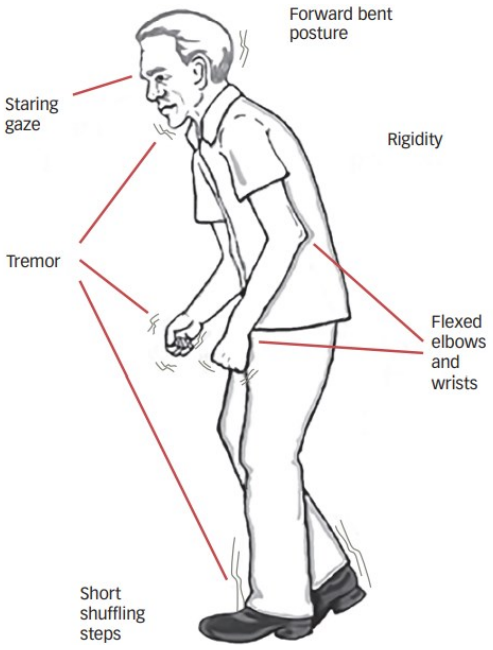

Figure 2.4 *movement symptoms associated with Parkinson's disease [67].*

The clinical diagnosis of PD can be supported by neuroimaging techniques that are primarily used to preclude other neurological disorders; for example dopamine transporter single-photon emission computed tomography (DaT SPECT) identifies the presynaptic dopamine neuronal dysfunction by demonstrating reduced uptake of a radioactive tracer that binds to dopamine transporters in the basal ganglia and it is highly accurate in differentiating PD from other parkinsonism's including multiple

system atrophy, progressive supranuclear palsy, that also involve DaT transporter [68]. Conventional brain imaging with MRI or CT is usually not necessary on condition that an alternative diagnosis is presumed such as normal pressure hydrocephalus or vascular parkinsonism.

2.2.1 Symptomatology

The main symptoms of PD are classified as motor-symptoms due to the constant and progressive loss of dopamine within the neurons; the most frequent motor features are commonly grouped under the parkinsonism term, which includes bradykinesia, rest tremor, rigidity and postural instability [3]. However, in several cases there is a series of non-motor symptoms (i.e., cognitive impairment, fatigue, constipation, sleep problems etc.) that often precede the diagnosis and may represent a fundamental element for its development, whose severity increases with the prolongation of the disease; these non-motor symptoms also contribute to increase the level of disability and reduce the quality of patient's life.

2.2.2. Motor-Symptoms

***Bradykinesia*:** it is identified as primary motor symptom of PD and it is typically demonstrated by slow movement, reduced or mask-like expression of the face (hypomimia), a decreased blink rate of the eyes, and problems with fine motor coordination. Initial clinical signs include also the slowness of reaction times and difficulties with performing simultaneous tasks and loss of hand movements [4]. By observing the gait, when entering the clinic room, patients may exhibit a reduced arm swing, shuffling steps and also a stooped posture.

***Tremor*:** it is generally described as “pill-rolling” (pronation/supination) and low frequency (4–6 Hz). It should start unilaterally but can progress to involve both sides, although it should remain asymmetric. It is apparent in the most distal part of a limb, that is, the hand if the upper limb is involved. It can occur at rest and improve or even disappear on activity. In the early stage of the disease, it is typically intermittent, and patients often notice it in relaxed state. When the patient is performing another activity, like walking or counting backwards, the tremor also becomes more evident. [4].

***Rigidity*:** it consists of an increase in muscle tone and resistance to passive movements; it can affect the neck, shoulders, wrists and hips and causes physical tension within the patient. Rigidity is one of

the symptoms principals of the disease, found in most patients, and it is often associated with pain in the involved areas [69].

***Postural instability*:** it is a common sign especially occurring in the advanced stages of the disease with an associated falls risk, together with freezing of gait. Instability is mainly due to loss of postural reflexes in the patient; this sign leads to an impairment of balance, reflecting problems in walking and in daily-life activities, leading to assume a stooped position. The walk of the patient affected by Parkinson's disease becomes slow and limited, movements are lost swinging the arms and changing direction. Additionally, in some cases, the normal walk can be interrupted by events such as festination, in which the patient undergoes an acceleration of the gait by performing a quick succession of small steps, or freezing of gait *(*FOG), during which the patient displays motorial block, especially in the presence of directional changes or obstacles [70].

Freezing of gait (FOG): it is one of the most disturbing and least understood symptoms in PD in which patients are unable to initiate or continue locomotion. When a patient tries to lift a foot to step forward, the foot is “stuck” to the ground, making the patient feel as if his or her foot is glued to the ground [71]. It is estimated to be one of the largest causes of falls in people with Parkinson’s and can lead to serious damage and injury, drastically reducing the quality of life of the patient.

2.2.3 Non-motor Symptoms

Non-motor symptoms are not only detectable in the disease progression, but also sometimes they precede the motor symptoms. They can be classified in neuropsychiatric dysfunction, cognitive dysfunction, olfactory dysfunction, autonomic dysfunction related to orthostatic hypotension, constipation, and sleep abnormalities:

***Neuropsychiatric dysfunction*:** the most widespread disorder is *depression*, of which it is estimated to be affected 40% of patients. Anxiety and panic attacks are also frequently encountered, as is loss of interest and initiative, fatigue, indecisiveness, and anhedonia [66]. Other disorder, such as psychosis is a characteristic of the advanced stages of the pathology, which occurs in the form of visual hallucinations and paranoia, usually linked to suspicion of infidelity or abandonment; psychosis may be linked to the progressive degeneration of the disease itself but in most cases, it is caused by the side effects of dopaminergic agonists anhedonia [72].

***Cognitive dysfunction*:** it is related to psychomotor retardation, memory disorders, mood changes and personality, attention deficit and apathy. 30-40% of patients are likely to develop forms of

dementia which is associated with a more rapid progression of the disease leading to deterioration in the quality of life and increased mortality [68].

Olfactory dysfunction: it is considered one of the first indicators of diagnosis as it occurs in the early stages of the disease and afflicts 90% of the patients; the cause of such dysfunction is to be found in a defect of the system central nervous rather than a peripheral olfactory system problem [73].

Orthostatic hypotension**:** when the patient assumes upright position**,** a rapid decrease in blood pressure occurs, resulting in weakness, dizziness, confusion and blurred vision, up to falls and syncope in the most serious cases. It is estimated to be present in symptomatic form in 30% of patients; the severity of such a condition depends heavily on treatments dopaminergic, which can worsen the patient's situation [74].

Constipation: it may occur many years before the onset of motor symptoms and it produces less frequent and/or more difficult bowel motions, affecting more than 60% of PD patients. The disorder can be caused by the degeneration of Lewy bodies in the autonomic nervous system, physical weakness, insufficient fluid intake and medication side-effects [4].

Sleep disorders: these are the most frequent non-motor problems of PD with an incidence ranging from 60% to 98% of patients and correlate with disease severity and levodopa intake. They include difficulties falling asleep, frequent awakenings, nocturnal cramping, painful dystonia, or motor restlessness. In particular, the sleep behaviour disorder (RBD) is a type of parasomnia characterized by the loss of normal skeletal muscle atonia during REM sleep accompanied by jerkings and sometimes very violent limb and body movements during dreams. In individuals with RBD, the estimated probability of developing PD is much higher than in the general population, and compared to other early symptoms, RBD has the highest specificity and predictive value for the disease diagnosis. [4,74].

2.3 Treatment

Pharmacologic treatments for PD are primarily based on a dopamine replacement strategy using the dopamine precursor levodopa (L-DOPA) resulting to be particularly effective in the early stages of the disease [75]. L-dopa remains the single most effective drug in PD treatment, and it is often combined with a peripheral decarboxylase inhibitor, which increases its effectiveness and reduces side-effects such as nausea, vomiting and orthostatic hypotension, when using levodopa alone [75]. However, long-term levodopa treatment frequently can cause debilitating motor complications

including dyskinesia in younger onset patients. For this reason, dopamine agonists such as ropinirole or pramipexole may be used in earlier stages of treatment in an attempt to delay prescription of levodopa and the resulting motor complications. These drugs work by stimulation of the post-synaptic dopamine receptors by trying to replace the lost dopaminergic tone in the PD basal ganglia. Almost all patients with advancing PD will necessitate levodopa due to the ineffectiveness of dopamine agonists in symptomatic relief [76], but their longer half-life and more stable receptor stimulation will reduce dyskinesia. Nevertheless, more than 40% of individuals treated with oral dopamine agonists experience impulse control disorders dopamine agonists increase the risk of other side effects such as hallucinations, somnolence and impulse control disorders [75]. Other enzymes which metabolise levodopa and dopamine, such as catechol-O-methyltransferase (COMT) and monoamine oxidase-B (MAO-B) are effective monotherapies able to block enzymes that break down dopamine in order to prolong the levodopa benefits. Surgical interventions have also been shown to be effective in the symptomatic treatment of PD. Since levodopa, a deep brain stimulation (DBS) neurosurgical procedure is perhaps the most significant development in symptomatic PD therapy, normally performed at advanced stages of the disease, when complications led to a reduced quality of life. The procedure is based on the insertion of an electrode through the skull to reach and stimulate the globus pallidus, subthalamic nucleus, or thalamus. A pacemaker-like device is implanted and connected to the electrode through wires under the skin. The therapy is effective in reducing “off” periods, when symptoms recur and increasing “on” periods during which the patient experiences a good response to medication without dyskinesias, as well as in decreasing the levodopa dose, and improving tremor [77].

2.4 Unified Parkinson’s Disease Rating Scale

Unified Parkinson’s Disease Rating Scale, also known as the UPDRS scale, is a rating system used to assess the progression of Parkinson's disease in patients. Several medical organizations have modified the UPDRS scale over time, and it continues to serve as a foundation for research and treatment in PD clinics. The scale was originally developed in the 1980s and it assesses both motor and motor symptoms. Later, it was reviewed by Movement Disorder Society, which underlines some weaknesses and consequently led to draft a new version of the scale, called “MDS sponsored UPDRS revision” (MDS-UPDRS) [78]. It retained the strengths of the original scale, but resolved identified problems and especially incorporated a number of clinical PD-related problems poorly underlined in the original version. The MDS-UPDRS is structured according to 42 items grouped in four subscales:

- Section I: Non-motor experiences of daily living;
- Section II: Motor experiences of daily living;
- Section III: Motor examination for different body parts;
- Section IV: Motor complexities;

The first half part of Section I examines a number of behavioural aspects that are assessed by the investigator with all pertinent information from patients. The second part of Section I and the entire Section II are designed to be adapted to a questionnaire format and therefore can be completed by the patient, independently from the investigator. Additionally, these two sections can be reviewed by the investigator to ensure completeness and clarity, and also possible ambiguities can be explained. Section III is completed by the examiner, and it preserves the objective assessments of parkinsonism and all the tasks with specific instructions to give to the patient. Finally, for Section IV the investigator is required to conduct the interview. Each question is followed by five responses that are related to clinical terms, with a rating scale scores (0-4) and severity levels associated to the disease:

- 0: normal;
- 1: minimal, symptoms/signs with low intensity such that functionalities could not be affected.
- 2: mild, symptoms/signs with sufficient intensity to cause modest impact on functionality.
- 3: moderate, symptoms/signs with such intensity so that they have a considerable impact on the functionalities, without however preventing them.
- 4: Severe, symptoms/signs that prevent functionality.

Due to the aforementioned factors, these scales are typically used as evaluation tools rather than diagnostic instruments to identify the general clinical signs of parkinsonian patients without taking the pathophysiology of the condition into particular consideration.

Indeed, stereophotogrammetry, electromyography, and dynamometric force plates represent the gold standard techniques for the quantitative evaluation of human balance and to assess the balance-related deficits caused by PD. Stereophotogrammetry calculates the three-dimensional coordinates of points to reconstruct its position in the space by means of some cameras that acquire simultaneous images from different locations and this requires a specific motion laboratory to be applied. The use of force platforms is based on the reconstruction of the COP trajectory when the subject stands quietly or while executing a specific motor task and as for the remaining methods, the accelerometer and

gyroscope are two motion detection devices commonly used in modern technological equipment. Their operation is based on the concept of inertia, which is the resistance of masses to change their state of motion, hence called inertial units of measurement in engineering applications. However, Despite the contribution that these technologies have poured into the field of human gait analysis, they have numerous limitations. Stereophotogrammetric systems and pressure mats are affected by several significant problems, such as high instrumentation costs, limited number of cycles observed and/or invasiveness. The use of wearable sensors eases the impact of costs and allows gait events to be identified in an appropriate number of cycles. Despite this, the problems of size and experimental set-up in terms of time-consuming, are still relevant, especially for applications in pathology. In addition, wearable sensors may require special attention for correct positioning and the need for specific calibration procedures, which are not consistent with the timing of clinical practice. Therefore, it was considered necessary to develop new techniques designed to overcome these limitations and able to detect and classify gait events from the sEMG signal alone [79].

Chapter 3. Gait analysis

Gait Analysis is a fundamental aspect which is based on the evaluation of the characteristics of posture, body movement, muscle activity, as well as their variations compared to a normal situation, that can be very useful in the clinical field for the diagnosis of pathologies affecting one of the systems involved. Walking uses a repetitive sequence of limb movements to advance the body while maintaining the stability of the support. There are three basic approaches: the simplest of these is divided according to the variations in mutual contact with the ground by the two feet; the second considers the characteristics of time and space of the step; the third identifies the functional significance of events in the gait cycle and periods as functional phases of the gait. Regarding the pattern of reciprocal contact with the ground during the advancement of the body, one limb acts as a support, while the other advances until the next support; later, the two limbs exchange roles and both feet are in contact with the ground during the transfer of body weight from one limb to the other. This series of events is repeated alternately until the destination is reached.

This study will focus on the analysis of the ankle joint kinematics, in particular of the two antagonist muscles, the tibialis anterior and gastrocnemius lateralis, that attach to this joint.

3.1 Gait cycle subdivisions

Each gait cycle is divided into two periods, 'stance' and 'swing', called gait phases (Figure 3.1). The stance phase identifies the entire period during which the foot is in contact with the ground: it begins with the initial contact. The swing phase refers to the time in which the foot is raised for the advancement of the limb: the swing begins when the foot detaches from the ground ("toe off").

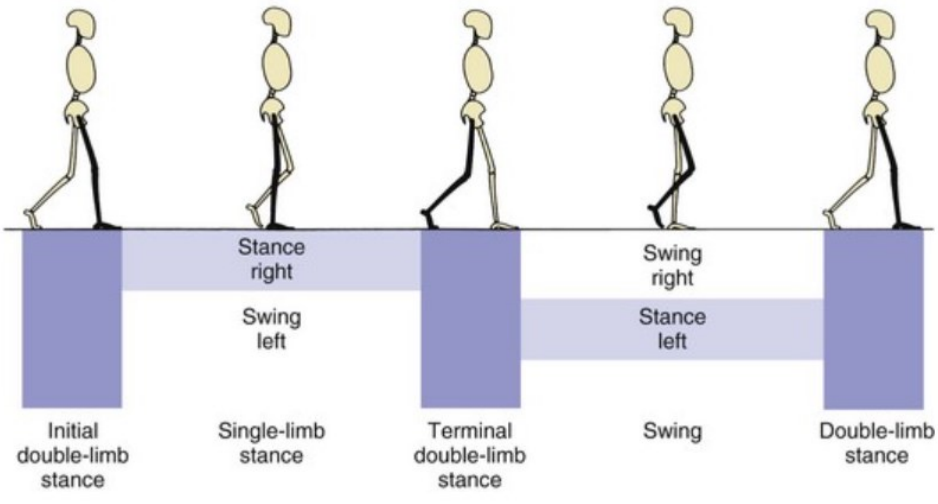

Figure 3.1 *Subdivision of gait cycle in stance and swing phases.*

The stance is divided into three intervals according to the sequence of contact with the ground by the two feet. The beginning and end of the stance include a period of bilateral contact (double support), while in the intermediate part the contact is only one foot.
The initial double stance is the beginning of the gait cycle; it is the time in which both feet are in contact with the ground; the single stance begins when the foot detaches for the oscillation and constitutes the best index to evaluate the support ability of the limb in that extremity; the double terminal stance begins with the contact to the ground by the other foot (initial contralateral contact) and continues until the limb that was in stance detaches for oscillation (ipsilateral detachment of the fingers) [80]. The normal distribution of periods of contact with the ground is approximately 60% for stance and 40% for swing. It is important to remember that the single stance on one limb is equivalent to the swing of the other limb since these occur at the same time. The duration of these gait cycle intervals depends on the speed of advancement of the person. Two concepts that are often confused must be distinguished: the *stride* the functional unit of reference in gait analysis. It is defined as the period between two successive initial contacts of the same foot and represents the temporal reference in which all other biomechanical events and muscular activity are described. The *step* is instead distance between initial swing and initial contact of the same limb.

3.1.2 Gait phases

The phases of the gait make possible to identify the functional meaning of the different movements at the level of the individual joints. The sequential combination of phases is also able to make the limb perform three basic tasks: weight acceptance, single support, and limb advancement (Figure 3.2). *Weight acceptance* is the beginning of the stance period and uses the first two phases of the step (initial contact and loading response). The single stance includes the next two phases (mid stance and terminal stance). The advancement of the limb begins in the final phase of stance (pre-swing) and continues through the three phases of the swing (initial swing, mid swing, and terminal swing) [80].

Weight Acceptance (Task A)

This task is characterized by the highest functional demands within the gait cycle. In fact, three functional schemes are necessary: impact absorption, initial stability of the limb and preservation of progression [80]. The difficulty lies in the immediate transfer of the weight of the body on a limb that has just finished the swing and represents an unstable alignment. Two steps of the gait are involved: initial contact and load response.

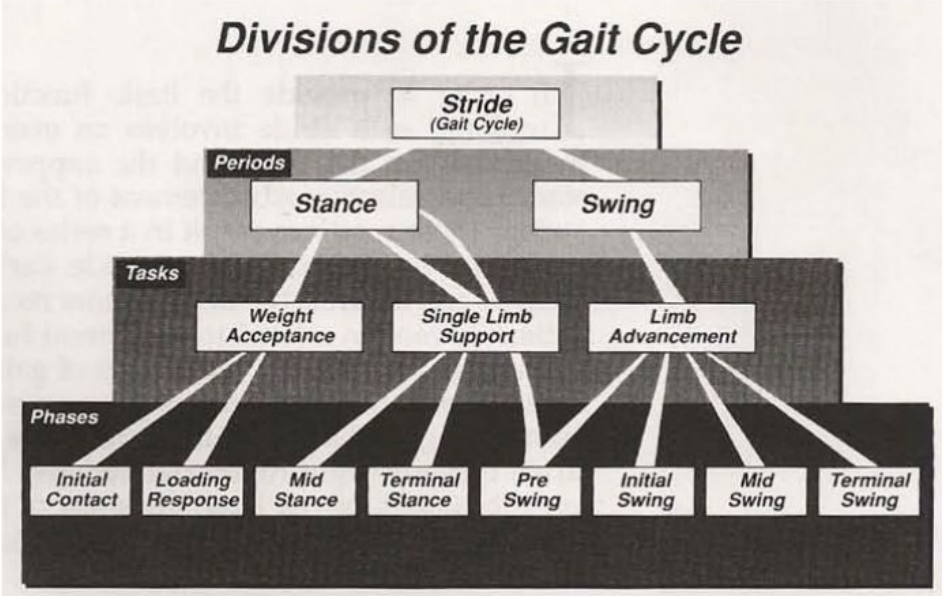

Figure 3.2 *Sub-phases of the gait cycle.*

Step 1-Initial contact

Range: 0-2% of the gait cycle.

The moment when the foot (heel) comes into contact with the ground. Joint positions at this time determine how to respond to the load of the limb. The alignment of the line of force with the joints introduces instability to the tibiotarsal joint and hip, while the knee is stable.

Objective: The limb is positioned to begin the stance with the rolling of the calcaneus (Figure 3.3).

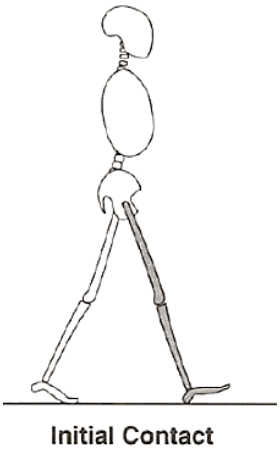

Figure 3.3 *Initial contact: there is a dorsiflexion of the ankle, an extension of the knee and a flexion of the hip.*

Step 2-Loading response

Range - 3-10% of the gait cycle.

It is the initial period of double stance. The phase begins with the initial contact to the ground and continues until the other foot is raised for the swing. The weight of the body is transferred to the advancing limb, the flexion of the tibiotarsal contributes to the absorption of the impact, while the flexion of the knee, introduced by the action of the pretibial muscles, is sufficient to maintain the stability required for load safety (Figure 3.4).

Objectives:

- Impact absorption.
- Stability under load.
- Preservation of progression.

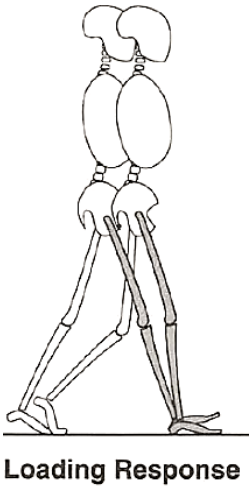

Figure 3.4 *Loading response: in this portion, the knee flexes slightly in order to absorb shock as the foot falls flat on the ground, stabilizing in advance of single limb stance.*

Single support (Task B)

The detachment of the contralateral foot for the swing determines the beginning of the single support interval for the supporting limb. This continues until the contralateral foot touches the ground again. In this interval, a limb has the responsibility to support the entire weight of the body both on the sagittal and frontal plane, allowing the simultaneous progression. These phases are included in the single support and are called *mid stance* and *terminal stance*. They differ in the mechanisms of progression [80].

Phase 3-Mid stance

Range - 10-30% of the gait cycle.

It begins when the contralateral foot is raised and continues until the weight of the body is aligned with the forefoot. The limb advances beyond the foot in stance through the dorsal flexion of the tibiotarsal (rotation of the tibiotarsal), while the knee and hip extend and the critical point for dynamic stability moves from the knee to the tibiotarsal (Figure 3.5).

Objectives:

- Progression over the stance limb.
- Stability of the limb and trunk.

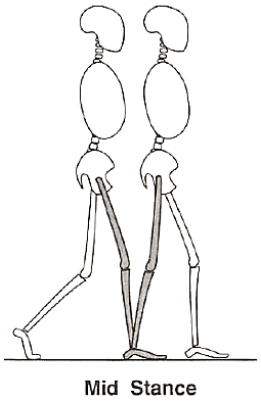

Figu*re 3.5* *Mid stance: there is an extension of the hip and knee.*

Step 4- Terminal stance

Range - 30-50% of the gait cycle.

This phase concludes the single support. It starts with the heel rise and continues until the other foot remains on the ground. During this phase the weight of the body is transferred beyond the forefoot. The knee continues to extend and then flexes slightly. The increased extension of the hip places the limb in a position of greater advance (Figure 3.6).

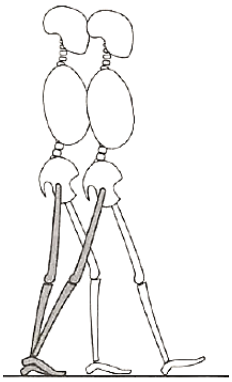

Figure 3.6 *Terminal stance: the extension of the knee and hip increases. The heel rises and the limb advances over the forefoot.*

Limb Advancement (Task C)

To ensure this task, during stance it is necessary the correct positioning of the limb which subsequently oscillates through three movements of rising, advancing, and preparing for subsequent support. Four gait phases are defined: p*re-swing, initial swing, mid swing and terminal swing.*

Step 5-Pre-swing

Range - 50-60% of the gait cycle.

It is the final phase of the stance that represents the second period of double stance (terminal). It ranges from the initial contact of the contralateral limb to the detachment of the ipsilateral fingers. There is an increase in plantar flexion of the tibiotarsal and knee, but a decrease in hip extension (Figure 3.7).

Objective:

- Positioning of the limb for the swing.

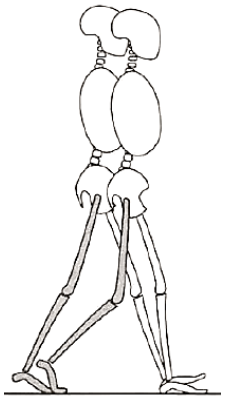

Figure 3.7 *Pre-swing: Thre is an increase in ankle plantar flexion, greater knee flexion and loss of hip extension.*

Step 6-Initial swing

Range - 60-73% of the gait cycle.

This phase accounts for one third of the swing period. It begins with the lifting of the foot from the ground and ends when the swinging limb is parallel to the support foot. The limb advances through hip flexion and there is an accentuated knee flexion. The tibiotarsal is only partially dorsiflexed (Figure 3.8).

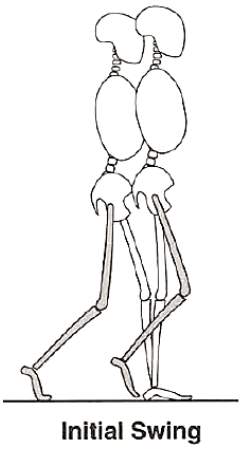

Figure 3.8 *Initial swing: the foot leaves the ground, and the limb advances due to hip flexion and increased knee flexion.*

Phase 7-Mid swing

Range - 73-87% of the gait cycle.

It is the second phase of the swing phase. It begins when the swinging limb is opposite to the loaded limb. The tibiotarsal flexes dorsally to the neutral position, the hip continues his flexion as the knee begins to extend. This phase ends when the oscillating limb advances and the tibia is vertical (Figure 3.9).

Objectives:

- Advancement of the limb.
- Lifting of the foot off the ground.

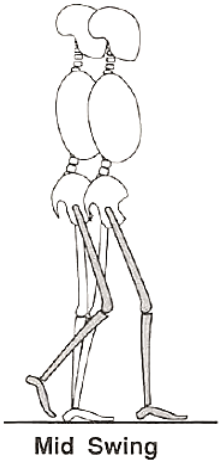

Figure 3.9 *Mid swing: there is a continuous dorsiflexion of the ankle reaching the neutral position, an extension of the knee and hip flexion that makes the limb to advance .*

Step 8- Terminal swing

Range - 87-100% of the gait cycle.

Final stage that begins with the vertical tibia and ends when the foot contacts with the ground. The advancement of the limb is complete with the extension of the knee. The hip maintains its initial flexion and the tibiotarsal remains dorsiflexion until the neutral position (Figure 3.10).

Objectives:

- Complete advancement of the limb.
- Preparation of the limb for stance.

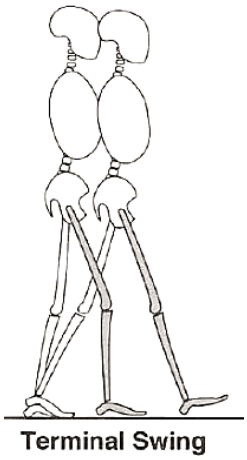

Figure 3.10 *Terminal swing: the ankle reaches the neutral position. There is an extension of the knee that completes the limb advancement and the hip maintains its earlier flexion.*

3.2 Energy conservation

During walking, which aims to allow the movement of the subject, the main functions performed by the musculoskeletal apparatus are the improvement of a propulsive force, the anticipation of postural stability, the absorption of shock due to impact with the ground and the conservation of energy during previous functions, in order to minimize the effort on the part of the of muscles. Therefore, the task that must be performed is the maintenance of stability in support through the control of the fall of the center of gravity and the advancement of the oscillating limb as the body progresses. The amount of work required during these actions determines the energy cost. Normal gait includes two mechanisms for conserving energy: modulation of gravity line alignment and selective muscle control [80]. Both serve to reduce the intensity and duration of the muscle action involved. The reduction of the distance between the center of gravity of the body and the line of progression represents the main mechanism to decrease the muscular work of the gait and, consequently, to conserve energy. The reduction of the oscillations of the center of mass (COM) of the body refers to the adjustments that are made on the three planes of space to reduce as much as possible the displacements in the sagittal plane and in the horizontal plane of it. These movements are defined "*determinants of gait*" [81]. Therefore, movements like pelvic rotations and knee flexion during the stance phase are synchronised to decrease COM displacements. Human gait has six determinants responsible for minimizing the gait energy expenditure and to reduce the displacement of the centre of mass that are the pelvic rotation (1st determinant), pelvic obliquity (2nd determinant), stance knee flexion (3rd determinant), foot and ankle mechanisms (4th and 5th determinants), and lateral displacement of the body (6th determinant):

- ***Pelvic rotation***

It occurs around a vertical axis during the gait cycle (Figure 3.11). The rotation is needed to reduce the angle of hip flexion and extension and to minimize the excursion of COM (vertical movement of the hip). Pelvic rotation occurs anteriorly on the swinging limb and posteriorly during midstance. It is maximal just before heel strike with a total motion of pelvic rotation of 3–5° to each side and it allows for longer steps without changing the COM displacement significantly [82].

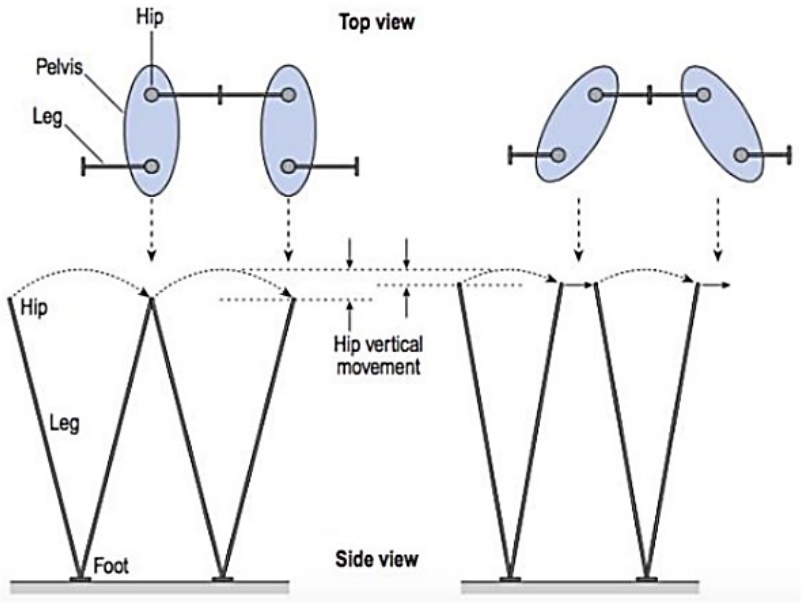

Figure 3.11 *Pelvic rotation.*

- ***Pelvic tilt***

The pelvis tilts about an anteroposterior axis, raising first one side and then the other. During walking, the hip of the swing leg decreases, and the pelvic rotation is about a horizontal axis, lowering the vertical displacement of the COM (Figure 3.12). When the pelvic is lowered, the hip abductors of the stance hip control pelvic tilt. During normal gait, the pelvis decreases 4–5° away from the stance leg and toward the swing leg. This pelvic dip decreases horizontal displacement of the COM during single limb support [82].

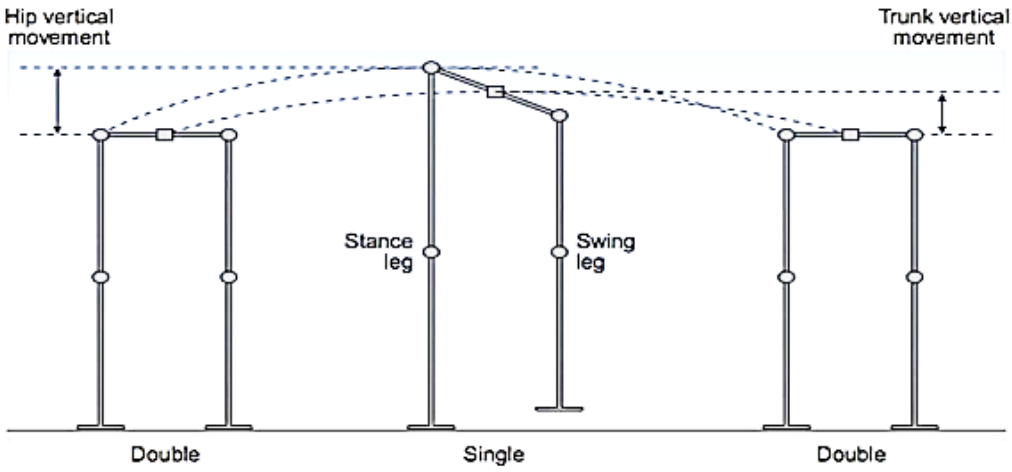

Figure 3.12 *Pelvic tilt.*

- ***Stance knee flexion***

Knee flexion acts to decrease vertical displacement of the COM. This occurs during midstance, as knee flexion to approximately 15° occurs and remains flexed until the foot is flat on the ground. However, flexion of the knee shortens the leg in the middle of the flexion and extension movement of the hip, reducing the height of centre of gravity (Figure 3.13).

- ***Ankle and foot mechanisms***

These are the fourth and fifth determinants that involve the control of the knee-ankle-foot motion. By lengthening the leg at the start of the stance phase (initial contact), the hip is flexed, and the knee is extended (Figure 3.13). Because the heel sticks out behind the ankle joint, it effectively lengthens the leg during the loading response with a dorsiflexion of the ankle and the height of the centre of mass is maintained constant. In the same way that the heel lengthens the leg, the forefoot lengthens it at the end of stance with a plantarflexion.

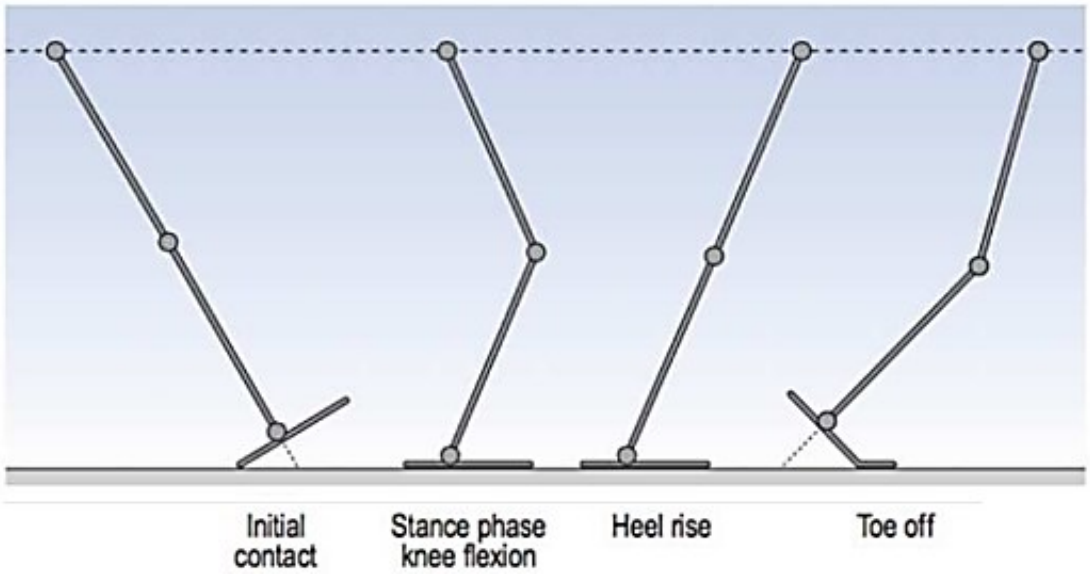

Figure 3.13 *The third, fourth and fifth determinants of gait are all concerned with adjusting the effective length of the leg, by lengthening it at the beginning and end of the stance phase and shortening it in the middle, to keep the hip height as constant as possible.*

- ***Lateral displacement of the body***

This is the lateral sway that occurs with each step, by determining the motion of the COM in the horizontal plane. The shifting of the pelvis occurs over the supporting foot to allow stability during the stance phase. The extent of sway depends on the base of support: if the feet are far apart, large lateral movements of the centre of gravity would be necessary to maintain balance; having them closer together reduces the size of these movements. Therefore, keeping the base narrow, little lateral movement is needed to maintain balance (Figure 3.14). The reduction in lateral acceleration and deceleration leads to reduce the use of muscular energy (ab/adductors are active to control lateral movement of the leg).

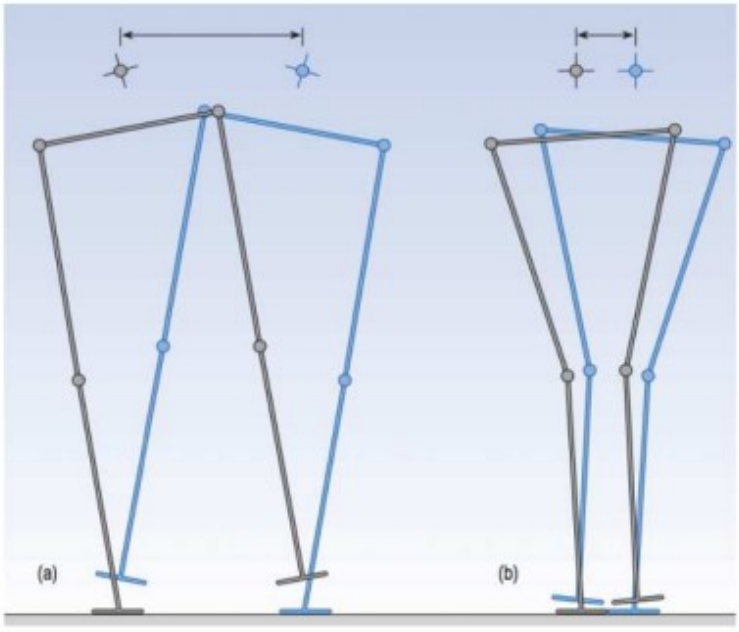

Figure 3.14 *Lateral displacement of the body: (a) larger lateral displacements due to a wider base of support; (b) smaller lateral displacements.*

3.3 Ankle joint

The ankle joint complex is composed of the lower leg and the foot, and it plays a fundamental role in the gait cycle, allowing any interaction between the lower limb and the ground. Although these joint experiences significant stress in terms of compression and shear forces, it seems to be less affected from degenerative processes compared to other joints, such as the hip and the knee [83]. The ankle joint consists of the meeting of the distal epiphysis (lower part) of the tibia and the fibula, and of the first bone of the foot which takes the name of astragalus. Various sub-joints are thus formed (Figure 3.15): the talocalcaneal (subtalar) composed of the calcaneus, the largest bone in the foot, and the talus, allows inversion and eversion of the ankle; the tibiotalar (talocrural) consisting of the junction between the distal ends of the tibia, fibula and the talus, enables plantarflexion and dorsiflexion motion of the foot, and the transverse-tarsal (talocalcaneonavicular) joint, which allows eversion-inversion motion of the foot.The tibiotarsal joint is an anatomical region of particular importance because it represents the node where vertical load forces are transmitted to a horizontal support complex.

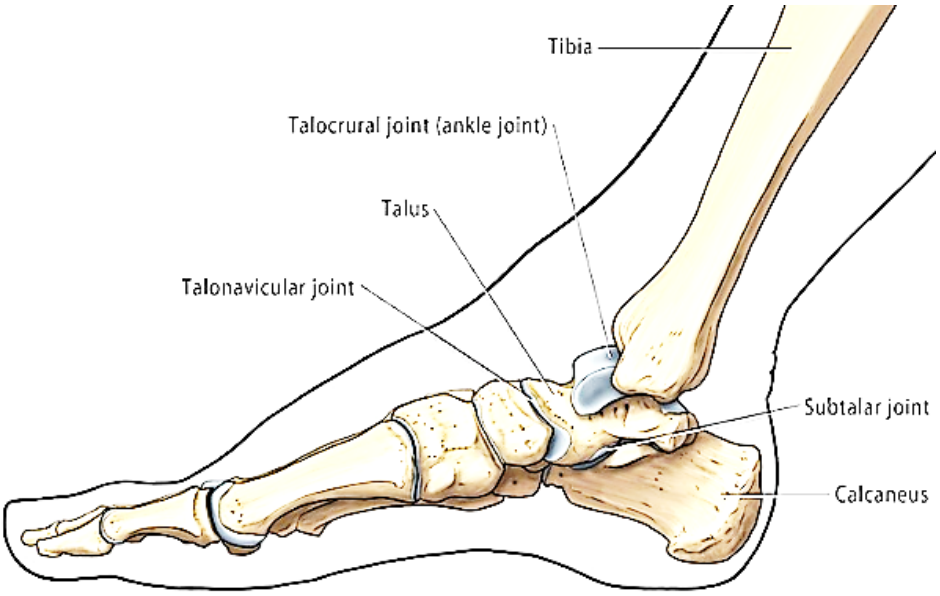

Figure 3.15 *Composition of the ankle joint.*

3.3.1 Ankle joint motion

Motion of the ankle occurs primarily in the sagittal plane, with plantar- and dorsiflexion occurring predominantly at the tibiotalar joint [83]. In each gait cycle, the ankle alternately twice plantarflexes and then dorsiflexes and so the entire joint excursion is about 30° (Figure 3.16). The first three movements occur in the stance phase, while the last one in the swing phase. In the initial contact of the heel, the angle of the ankle is neutral or may have a slight plantar flexion of some degrees; then, the first plantar flexion occurs as a response to the initial application of the load. This step is followed by another change of the angle direction (dorsiflexion) that occurs with the forefoot support. The dorsiflexion remains during the stance phase, reaching a maximum of about 10°, till the end of the single support phase. In the terminal stance phase, there is a rapid plantar flexion that reaches a maximum of 30°at the end of the stance. The detachment of the fingers begins the last moment of dorsal flexion. During the mid-swing phase, the angle returns to its initial neutral position of 0° and is maintained until the end [80].

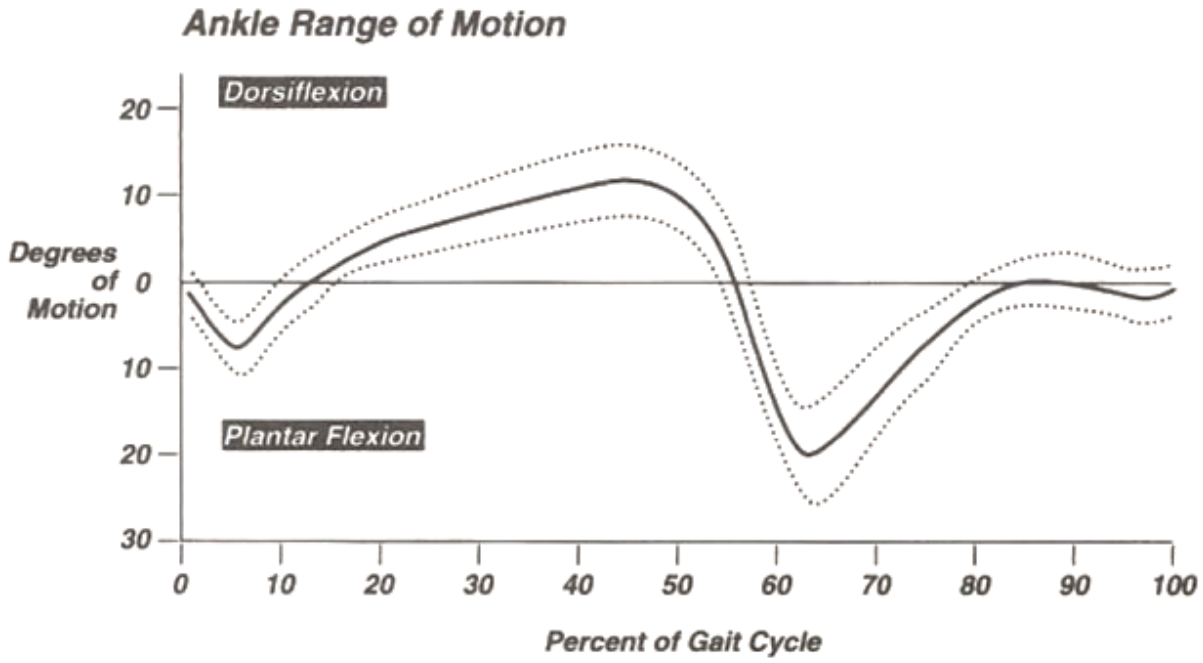

Figure 3.16 *Ankle joint range of motion (ROM).*

3.3.2 Recruitment of ankle muscles

The movement of the tibiotarsal is controlled by the action of the plantarflexors or dorsiflexors muscles (Figure 3.17). The scheme of activation of the tibiotarsal muscles is very phasic, it depends on the type of electrodes used to record muscle activity with EMG. Among the dorsiflexors muscles there are those that are located anterior to the tibiotarsal joint: tibialis anterior, extensor digitorum longus and the extensor hallucis longus. The extensor digitorum longus is flanked by the action of the third peroneal as they are joined and share the same tendon. The first dorsiflexion, during the single support, is an interval of high demand since the soleus and gastrocnemius decelerate the speed of advancement of the tibia on the foot against the progressive forces of the body. On the contrary, the second dorsiflexion action occurs during swing, when the weight alone must be controlled by the tibialis anterior and the long extensor of the fingers. Among the plantarflexors muscles there are those that are behind the tibiotarsal: soleus, gastrocnemius and perimalleolar muscles. Compared to dorsiflexors, plantarflexors are active during stance. The initial interval of plantar flexion, which occurs in response to the load, requires considerable effort of the pretibial muscles. In contrast, the second movement in plantar flexion, which occurs during pre-swing, represents a period of low

muscle demand even if the amplitude is greater [80]. The study will be conducted on the analysis of the two muscles tibialis anterior and gastrocnemius lateralis.

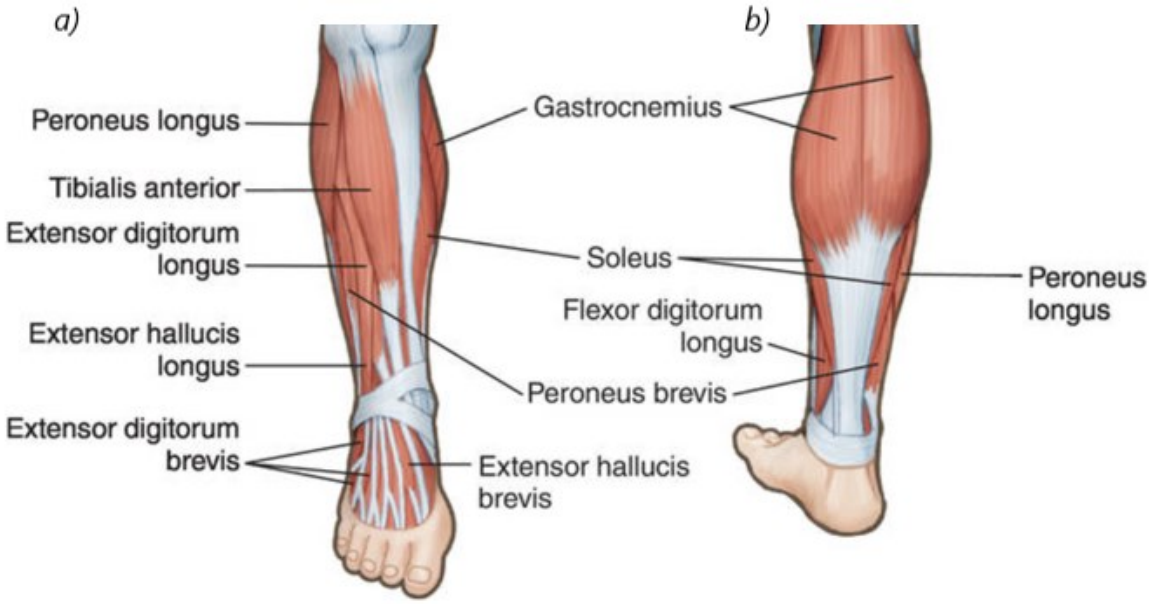

Figure 3.17 *Muscles involved in the ankle and foot joint: a) dorsiflexor muscles of the ankle joint, b) plantarflexor muscles of the ankle joint.*

The activity of the dorsiflexors muscles begins during the pre-swing: the first muscle to contract is the extensor digitorum longus, active throughout the pre-swing, and immediately after, during the mid-swing, the tibialis anterior and the extensor hallucis longus intervene. At initial contact all pretibial muscles are significantly active and terminate their action by the end of the loading response. Analyzing the tibialis anterior, its contraction intensity (expressed as a percentage) increases rapidly during the initial swing reaching 35% MMT (% Manual Muscle Test) and decreasing up to 10% in the mid-swing phase (Figure 3.18). In the initial contact, the tibialis anterior activation reaches the 45% MMT to stabilize the tibiotarsal joint by slowing the speed of plantarflexion and allowing progression during the loading response. The typical pattern of action is biphasic with two peaks of intensity in the initial swing phase and in the phase of loading response [80].

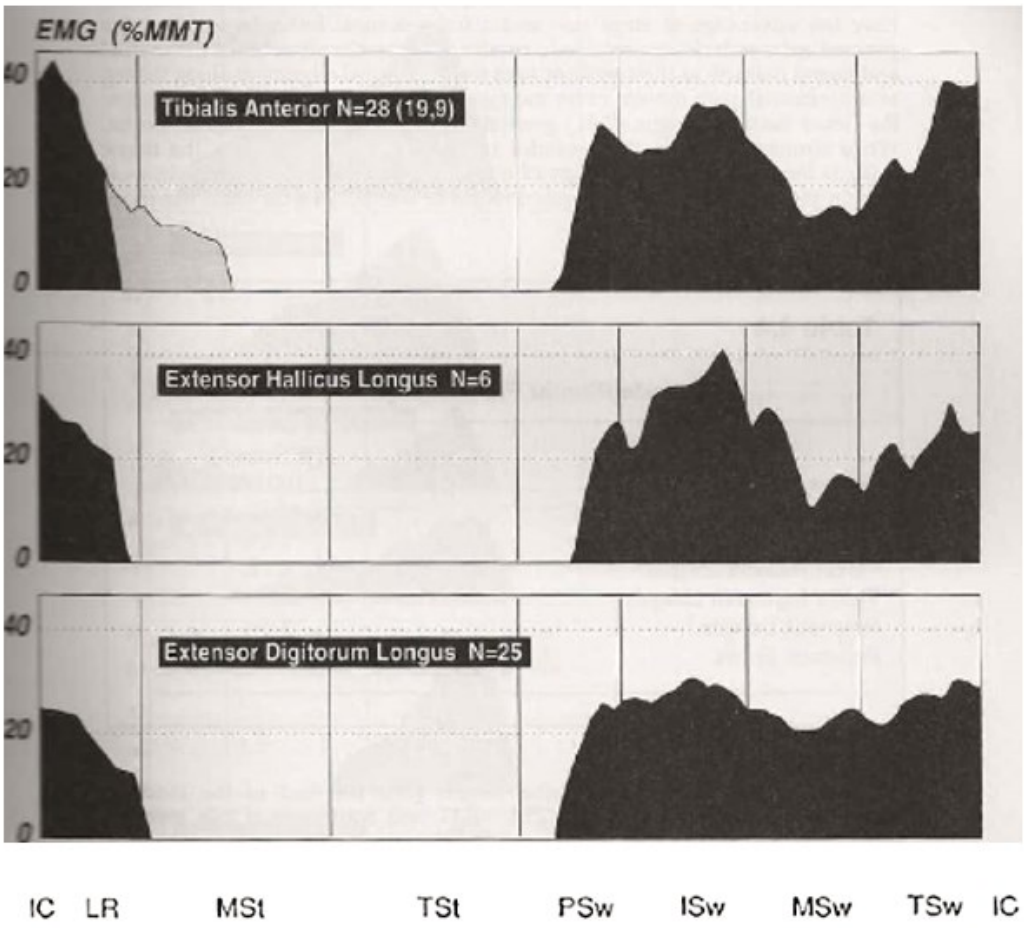

Figure 3.18 *Mean normal intensity of manual muscle test (%MMT) and activation time of the dorsiflexors muscles of the tibiotarsal during free walking quantified by electromyography (Perry 1992 [80]).*

On the other hand, the gastrocnemius lateralis is placed in the back of the leg that originates above the medial condyle and the lateral condyle of the femur. The two heads join and insert into the calcaneal tuberosity with the tendon of the soleus muscle. The gastrocnemius allows plantar flexion together with other muscles such as the soleus and helps knee flexion [80]. The gastrocnemius lateralis together with the soleus provide 93% of the internal moment in plantar flexion. These have a large size and a lever arm equal to the entire length of the calcaneus. The action of the soleus muscle begins at the end of the loading response phase, reaches 25% MMT and continues with this intensity until the mid-stance (Figure 3.19). With the beginning of the terminal stance (30% of the step cycle) there is an increase in amplitude up to 75% MMT from 45% of the gait cycle. Subsequently, the intensity of the action of the soleus decreases until it ceases at the beginning of the stance phase (pre-swing). The medial head of the gastrocnemius is activated parallel to the soleus while the onset of action of the lateral head may be delayed until mid-stance. The activation of the gastrocnemius

quickly follows that of the soleus (12% against 8% of GC) but during mid stance its increase reduces and is slower. The activation increases until to reach 25% MMT, persisting until the mid-stance. With the onset of the terminal stance its intensity increases to a peak around 60% MMT at 40% of GC and then decreases rapidly until the cessation after the start of the pre-swing. A brief contraction of the gastrocnemius in the mid swing is a frequent, but still unexplained, finding [80].

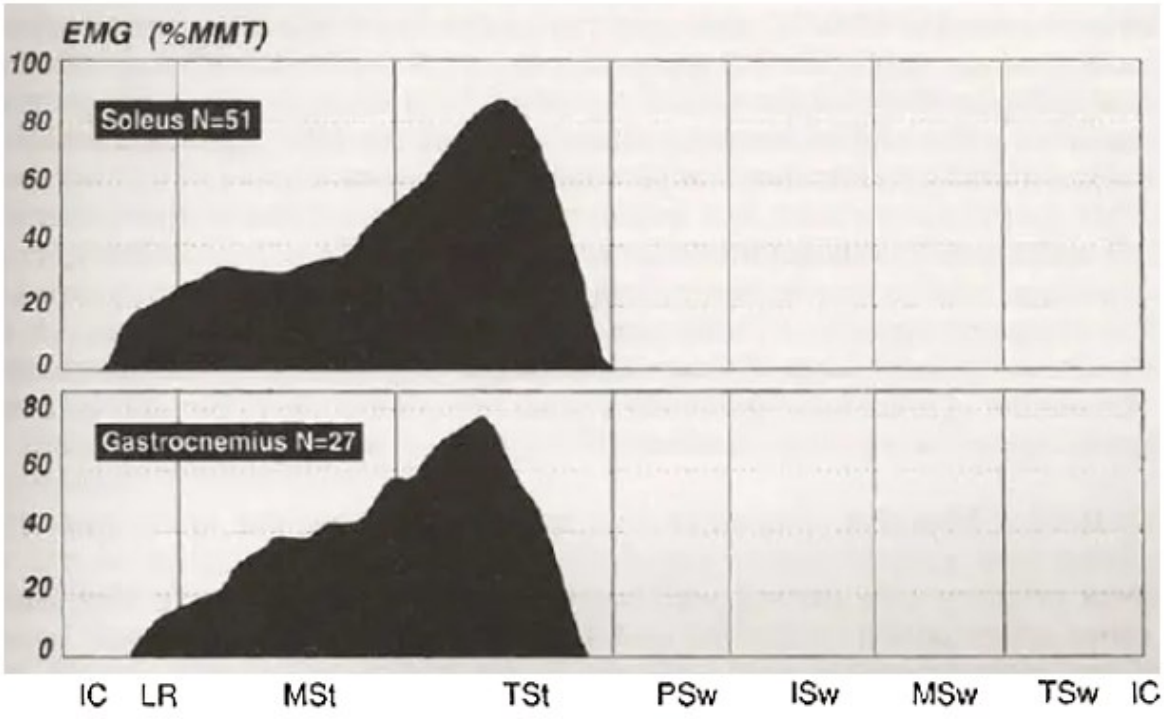

Figure 3.19 *Mean normal intensity of manual muscle test (%MMT) and activation time of the plantarflexors muscles of the tibiotarsal during free walking quantified by electromyography (Perry 1992 [80]).*

Initial contact (IC)

The tibiotarsal is at 90° (neutral position) to ensure a period of exclusive support of the calcaneus and ensure the start of rolling (Figure 3.20(a)). The support of the foot is guaranteed by the dorsal flexion thrust of the pretibial muscles.

Loading response (LR)

The tibialis anterior and long extensor pretibial muscles of the fingers intervene and decelerate the plantar flexion speed of the tibiotarsal and determine the advancement of the tibia and the contact of the foot with the ground. These two actions contribute to the progression of the limb. Also, the absorption of the impact guarantees the control of the plantar flexion of the tibiotarsal due to the ineffective action of the pretibial muscles as to control the moment of flexion requires a force greater than that used to support the foot during the swing. The result is rapid plantar flexion which serves as a short period of "free fall" of the body forward (Figure 3.20(b)).

Mid-stance (MSt)

Together with the rotation of the tibiotarsal, the soleus controls the initial increase in dorsal flexion of the tibiotarsal that follows the contact with the ground of the forefoot. The soleus reaches its peak of 25% MMT during the rotation of the tibiotarsal at 20% of the step cycle and continues its intensity until the end of the intermediate support (30% of the step cycle), while the tibiotarsal continues the dorsal flexion at a lower speed. This activity slows down the speed of advancement of the tibia. On the other hand, in the last part of the mid-stance, the gastrocnemius also acts as a flexor of the knee since it is located posterior to its axis and the demand for the quadriceps increases (Figure 3.20(c)).

Terminal stance (TSt)

With the tibiotarsal blocked by the soleus and gastrocnemius, the tibia continues to advance; this makes the forefoot the only support for the foot [Figure 3.20(d)]. There is a strong activity of the soleus and gastrocnemius (80% MMT) which is approximately equal to three times that required during mid-stance. The deceleration by the gastrocnemius and soleus of the dorsiflexor momentum determines a minimum moment of the tibiotarsal.

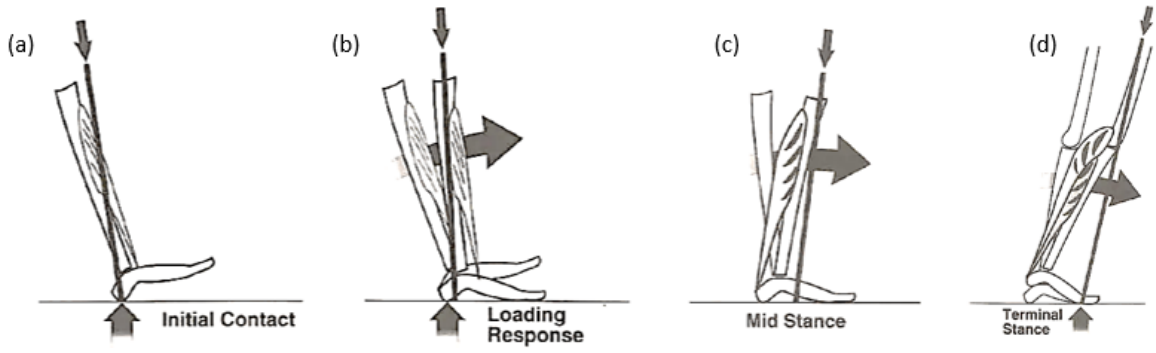

Figure 3.20 *Tibiotarsal muscles during the stance phase: (a) Initial contact, (b) Loading response, (c) Mid-stance, (d) Terminal stance.*

3.4.2 Action of the tibiotarsal muscles in the swing phase

Pre-swing (PSw)

The synergy of muscle activity and tibiotarsal movement is primarily responsible for the initiation of the swing. When the limb is discharged, the soleus and gastrocnemius rapidly reduce the intensity of their action making an important contribution to the swing and bringing the tibia anteriorly. As a result, there is rapid flexion of the knee in preparation for the swing (Figure 3.21(a)).

Initial swing (ISw)

Actions that occur during the initial oscillation are designated and facilitate progression. The pretibial muscles rapidly increase their activity (reaching 25% MMT) within 5% of the initial swing resulting in the lifting of the foot to a quasi-neutral position (Figure 3.21(b)). When the tibialis anterior and the extensor digitorum longus are active together, a dorsal flexion of the fingers is visible.

Mid-swing (MSw)

When the tibia becomes vertical, the weight of the foot determines a high moment in plantar flexion. The advancement of the limb during the mid swing still requires the action of the tibialis anterior (Figure 3.21(c)). The tibialis anterior and the extensor hallicus longus have a reduced intensity that reaches a peak of 10% MMT.

Terminal swing (TSw)

The action of the pretibial muscles optimizes contact with the ground (Figure 3.21(d)). As the tibia actively advances, the inertia of the foot is the likely cause of high muscle activity.

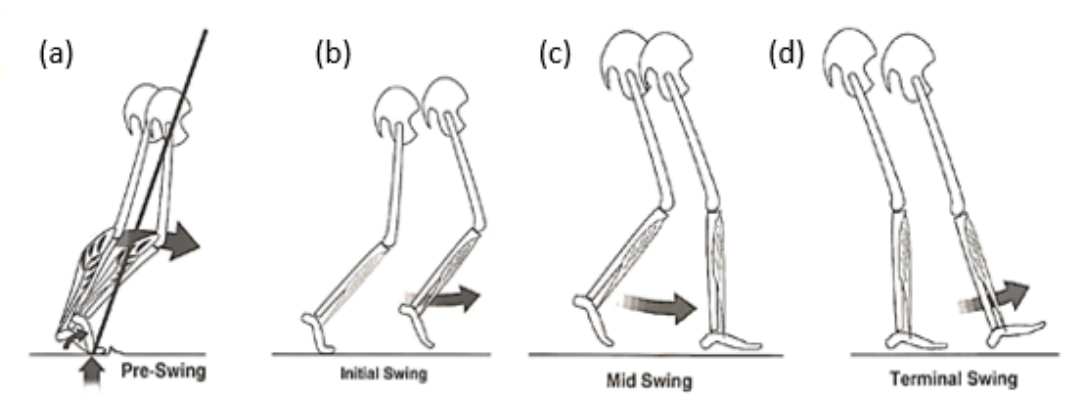

Figure 3.21 *Tibiotarsal muscles during the swing phase: (a) Pre-swing, (b) Initial swing, (c) Mid-swing, (d) Terminal swing.*

The progression effect is transferred to the thigh through the quadriceps, so that the impact with the ground is reduced. When the forefoot has contacted the ground, the tibiotarsal becomes the fulcrum to continue progression. The rate of advancement of the tibiotarsal is decelerated by the soleus muscle. This contracts to make the tibia a stable base for knee extension and to allow it to advance along with the gastrocnemius muscle**.** These flexor muscles intervene with a gradual intensity. Both the soleus and the gastrocnemius are vigorously activated to decelerate the forward speed. The flexion of the knee continues the progression of the limb: the tibiotarsal is dorsiflexed so that the vector of the body reaches the phalangeal metatarsal joints. The residual activation of the gastrosoleum muscle plantar flexes the foot through the extension of the forefoot and results in an advancement of the tibia that flexes the knee while the action of the long adductor (in the intermediate oscillation phase) flexes the hip and controls the balance on the frontal plane. The active extension of the knee in the terminal swing completes the contribution of the oscillating limb to the propulsion. The action of contraction of the muscles occurs only when the alignment of the body generates an antagonistic moment to the stability under load of the limb and trunk [80].

Chapter 4. Wavelet analysis

The Wavelet transform (WT) is a useful tool for the analysis and processing of signals and it has been used in a variety field of applications as it allows their characterization both in time and in frequency domain. In particular, the WT provides a time-scale analysis of non-stationary signals, maintaining all the signal frequency and timing information. Wavelets effectively represent the time-varying nature of real-world signals, making them a more suitable tool for signal analysis with respect to the more traditional methods [84].

4.1 Short-Time Fourier Transform Analysis (STFT)

Fourier analysis was the first method of frequency analysis which theorem states that all signals are made up of a combination of sine and cosine waves of varying frequency, amplitude and phase [85]. However, the transform is most appropriate for stationary and pseudo-stationary signals which characteristics do not vary over time. The shortcoming of the Fourier transform to describe both time and frequency characteristics of the waveform gives rise to a number of different approaches. One approach to dealing with this problem is to try to have a 'common time-frequency representation' of the signal. The traditional approach that introduces time dependence in Fourier analysis is the Short Time Fourier Transform (STFT), also called 'windowed Fourier transform', which allow to get a two-dimensional representation of the signal in a time-frequency plane (τ, *f*). The parameter *f* in the equation (1) is similar to the Fourier frequency and τ denotes the time on which the local Fourier transform is performed:

$$STFT(\tau, f) = \int x(t)\ g^*(t - \tau) e^{-2j\pi f t} dt \tag{1}$$

Of the windowed signal $x(t)\ g^*(t - \tau)$, a FT is taken, giving the frequency content of the signal in the windowed time interval [86]. This technique provides analysis of signals with time-varying information; however, the precision in the analysis resolution in time or in frequency domain is limited by the choice of window size $g(t)$. Therefore, STFT represents a sort of trade-off between the time- and frequency-based views of a signal. A short window will be able to operate locally in time by proving a precise time resolution, but it won't be able to discriminate precisely between

different frequencies. A wider window will provide a better discrimination between frequencies despite being less localized in time. Once a window has been chosen for the STFT, then the time-frequency resolution is fixed over the entire frequency-plane (Figure 4.1).

Figure 4.1 *Short time Fourier Transform (STFT): the STFT maps a signal into a two-dimensional function of time and frequency; window size is fixed regardless of time and frequency [87].*

As seen in the Figure 4.1 , in order to have a good resolution both in time and frequency domain, it would be necessary to create extremely small windows, but this is prevented by the uncertainty principle, since the product duration-band il lower bounded according to the Heisenberg inequality, which states that the product of time resolution Δt and frequency resolution Δf (bandwidth-time product) is constant as reported in the equation (2) [86]:

$$\Delta t \Delta f \geq \frac{1}{4\pi} \tag{2}$$

Once fixed a certain size, which represents the resolution over time, of the window $g(t)$, a fixed resolution in the frequencies Δf is obtained. From this principle it is clear that it is not possible to obtain good resolution in both domains, but a time-frequency trade-off has to be considered. In order to overcome the resolution limitation of the STFT, Δt or Δf can be varied in the time-frequency plane in order to obtain a multiresolution analysis (MRA).

4.2 Wavelet Transform

As an alternative to the STFT, the wavelet transform or wavelet analysis is developed to enable a multiresolution analysis using varying levels of resolution and a time-scale representation of the signal [78].The Wavelet analysis is a windowing technique similar to the STFT but with variable-sized windows (Figure 4.2): a shorter or longer window is shifted along the signal to determine the spectrum for each position of the window, to obtain a collection of time-frequency representations all with different resolutions.

Figure 4.2 *Wavelet Transform (WT): the WT allows time-frequency representation in which the width of the temporal windows is variable, so as to allow a good localization in both domains [87].*

Wavelet analysis allows the use of long-time intervals to provide precise informations about low-frequency content and shorter time intervals associated to the high-frequency content. Therefore, it provides a coverage of the time-frequency plane such that it can quantify the variations of the frequency content over time of time-varying signals without losing resolution in both time and frequency domains. Moreover, in contrast to the Fourier transform, the wavelet transform is able to keep the locality present in the signal allowing its local reconstruction [87]. To obtain a variable resolution analysis, it is necessary to ensure that the resolutions relative to Δt and Δf are constant and this requires that as the frequency *f* increases, the Δf band increases proportionally [88]. This can be achieved by constructing a set of basic functions, by means of translation and change of scale, of an initial function called mother Wavelet, ψ(t) [88]. This function is known as a wavelet, a little wave that always takes an oscillatory shape to be able to distinguish between different frequencies:

$$\psi_{a,b}(t) = \frac{1}{\sqrt{|a|}}\psi\left(\frac{t-b}{a}\right) \tag{3}$$

The CWT performs a multiresolution analysis by contraction and dilatation of the wavelet functions, where a and b are the scale and translation parameters respectively. The * indicates the operation of complex conjugation, and the normalizing factor $1/\sqrt{a}$ ensures that the energy is the same for all values of a (all values of b as well, since translations do not alter wavelet energy) [88,89]. From the definition of mother Wavelet, it is possible to describe the continuous wavelet transform (CWT) of the signal x(t):

$$CWT\ (a,b) = \frac{1}{\sqrt{a}}\int_{-\infty}^{+\infty} x(t)\psi^*\left(\frac{t-b}{a}\right)dt \tag{4}$$

The scale factor allows to compress or stretch the wavelet, instead the translation (time shifting) factor allows to translate the mother wavelet along the signal. A small value of the scale factor a indicate compressed wavelets over time, therefore containing high frequency harmonics. This implies to obtain projections that carry information on signal details related to rapidly changing phenomena. On the other hand, large values of a involve narrow-band wavelets that are slowly variable and represent the long-term behaviour of the signal (Figure 4.3).

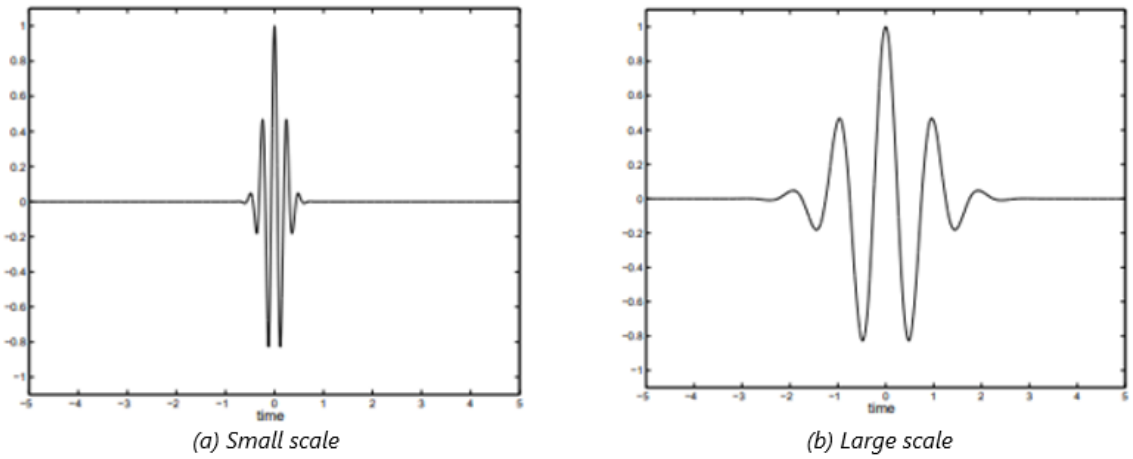

(a) Small scale (b) Large scale

Figure 4.3 *Compression (a) and stretching (b) of the mother Wavelet in function of the scale factor.*

The wavelet analysis therefore consists in making a comparison between the signal and the mother wavelet, suitably scaled and translated along it. This allows the signal to be broken down into numerous coefficients that are function of scale and position. This procedure is iterated by producing different coefficients at different scale values by different sections of the signal, so as to carry out a multi-resolution decomposition of the signal. The coefficients constitute the results of a regression of the original signal performed on the wavelets [87]. There are different types of mother wavelets and during the analysis the waveform to be used is chosen according to its similarity with the input signal. In fact, the greater is the degree of similarity, the greater will be the value of the coefficients describing the signal in the domain of the transform. Among the different Mother Wavelets shown in Figure 4.4, for this study a Daubechies of order 4 with 8 levels of decomposition was chosen, as it appears to have a form factor similar to that of the action potential of the motor unit [90].

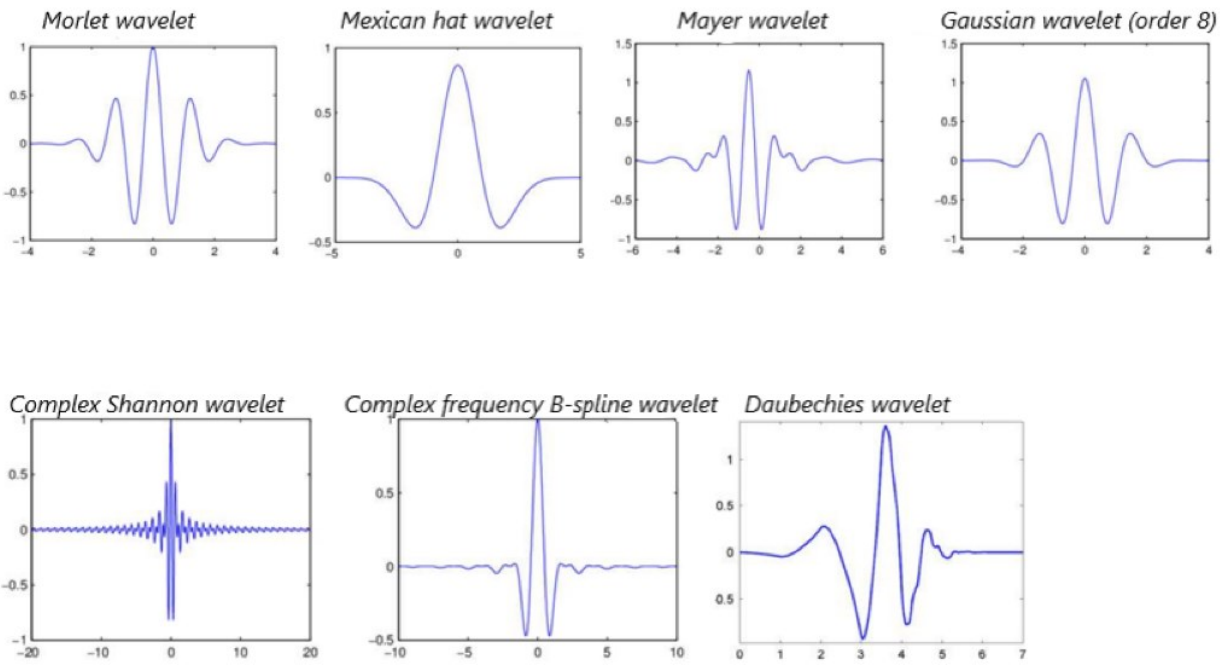

Figure 4.4 *Mother Wavelets family illustration.*

4.3 Wavelet properties

If the wavelet function, $\psi(t)$, is appropriately chosen, then it is possible to reconstruct the original waveform from the wavelet coefficients just as in the Fourier transform. Since the CWT decomposes the waveform into coefficients of two variables, a and b, a double summation (or integration) is required to recover the original signal from the coefficients [88]:

$$x(t) = \frac{1}{C}\int_{a=-\infty}^{\infty}\int_{b=-\infty}^{\infty} CWT(a,b)\psi_{a,b}(t)da\,db \tag{5}$$

Where

$$C = \int_{-\infty}^{\infty}\frac{|\psi(\omega)|^2}{|\omega|}d\omega < +\infty \tag{6}$$

in which $\psi(\omega)$ stands for the Fourier transform of $\psi(t)$. The wavelets must satisfy the conditions of admissibility and regularity: the admissibility condition implies a band-pass spectrum described by the equation (6) and the Fourier transform of $\psi(t)$ vanishes at the zero frequency ($\psi(0) = 0$) . Since the average value of the wavelet in time domain vanishes must be a wave (oscillatory) [89]. On the other hand, the regularity condition implies that the wavelet has smoothness and concentration in both time and frequency domains. Since the average value of the wavelet in time domain vanishes ψ (t) must be a wave (oscillatory). Satisfying the regularity condition means that the wavelet possesses smoothness and concentration in both time and frequency domains. Another property of the wavelet is to have a finite energy, which distribution is represented by the scalogram function. However, the CWT has the problem to be highly redundant in the reconstruction of the original signal, since many coefficients can be generated, but this is a problem that can be overcome through the use of the Discrete Wavelet Transform (DWT), which provides for the discretization of scale and translation parameters.

4.4 Scalogram and Coscalogram

The relationship between scale and frequency of the CWT is of fundamental importance to the scalogram/coscalogram representation of the local energy density of the signals considered. The

scalogram is defined as the square of the absolute value of the CWT coefficients, W_x, as represented in the equation (7):

$$P_W x(a,b) = |W_x(a,b)|^2 \tag{7}$$

where $W_x(a,b)$ is the matrix of CWT coefficients at time b and scale a:

The scalogram provides the localization of energy density, which represents the information content of the signal, in the time-frequency plane [91]. Differently from the spectrogram of the STFT, the analysis allows energy distribution of the signal with different resolutions and a localized analysis for small scales [86]. On the other hand, a local time-frequency energy density, which measures the cross-energy of two signals (that identifies their local correlation), is known as wavelet coscalogram (equation 8). The CWT coscalogram identifies the cross-correlations providing a detailed information about the interaction of the signals in the time-frequency domain [90].

$$P_W xy(a,b) = W_x(a,b) \cdot W^*{}_y(a,b) \tag{8}$$

Where x and y represents the two denoised signals and $W_x(a,b)$ and $W^*{}_y(a,b)$ are the matrices of CWT coefficients of the two signals, at scale a and time b with the operator * that represents the conjugate complex.

4.5 Multiresolution decomposition

As described in the previous sections, in the wavelet analysis a signal is decomposed into a number of multi-resolution components in accordance with the wavelet function. There are two sets of coefficients called “approximations” and “details”. The component corresponding to the highest scale factor will be considered as an approximation of the original signal, while any other component will represent the detail. This multiresolution can also be obtained using filter banks, resulting in the discrete wavelet transform (DWT). This is made through a process that is equivalent to low-pass and high passes filtering, respectively, in which the approximation coefficients represent the low frequency components, and the detail coefficients represent the high-frequency signal components. in the first step, the original signal (S) is passed through two complementary filters, a low-pass filter

and a high-pass filter, and emerges as two signals, approximations and details. The first-level approximation coefficient array (cA1) is obtained from a low-pass filter which includes down-sampling, and the first-level detail coefficient array (cD1) is passed through a high-pass filter with down-sampling [92]. Down-sampling procedure allows to reduce the number of samples of the input function without losing any information [87] However, the signal resulting from low-pass filtering may still contain details (high frequency contents), so a further filtering phase is performed, obtaining two additional signals. This process can be iterated as shown in Figure until to obtain the desired final level approximation and detail coefficients arrays. The reconstructed signal (S'), final level approximation and all level details, are true components of the original signal. This is called the perfect reconstruction. The reconstruction process is performed by up sampling each coefficient array prior to refiltering, the process of lengthening a signal component [87,92].

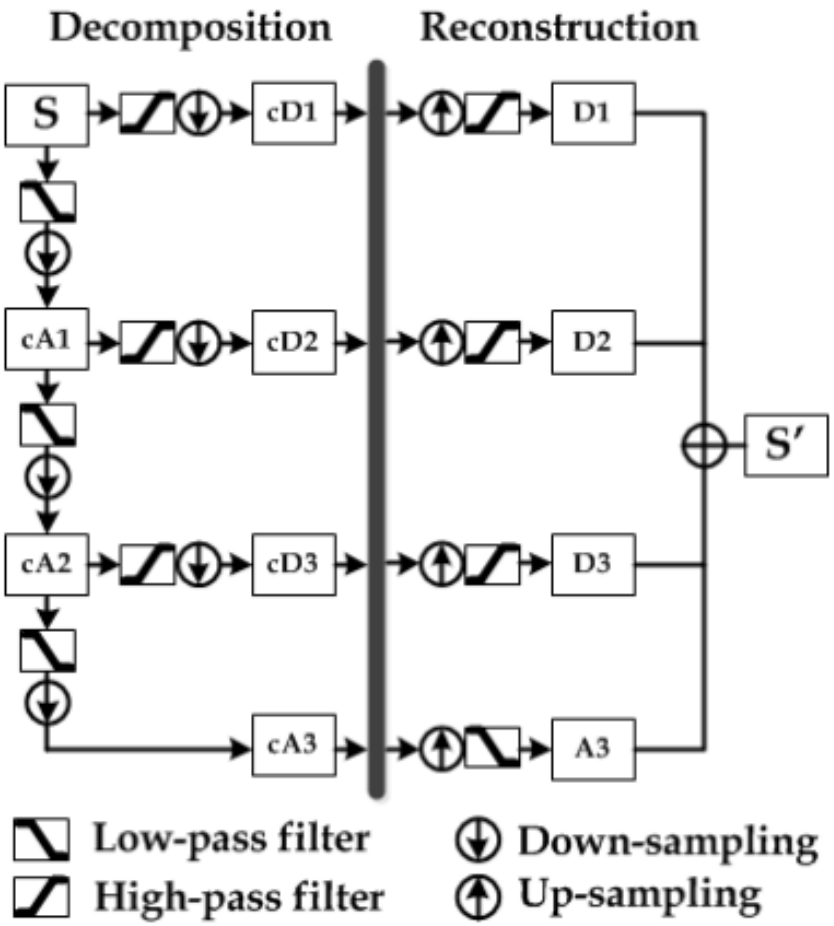

Figure 4.5 *Wavelet decomposition and reconstruction processes with 3 levels of decomposition [92].*

4.6 Denoising

Before beginning the reconstruction process, unwanted wavelet coefficients that contain random noise can be eliminated in order to obtain a cleaner signal. To achieve this result, wavelet thresholding is employed to delete or reduce some coefficients of the DWT detail sub-signals.

The first denoising technique suggested the use of thresholding in the wavelet domain. The threshold value can be divided into the soft threshold and hard threshold. The overall effectiveness of a wavelet processor for noise reduction is significantly influenced by the selection of threshold settings and thresholding functions. Wavelet-based denoising algorithm is based on the underlying model and it is basically of the following form [92]:

$$s(n) = x(n) + \sigma e(n) \tag{9}$$

where $s(n)$ is the measured or noisy signal, $x(n)$ is the original or clean signal and $e(n)$ is a Gaussian white noise N (0,1), σ is the strength of the noise, and time n is equally spaced (equation 9). The hard thresholding can be described as the process of setting to zero the elements whose absolute values are lower than the threshold and the soft thresholding is an extension of hard thresholding, first setting to zero the elements whose absolute values are lower than the threshold, and then shrinking the coefficients greater in magnitude than the threshold towards 0, differently from the hard thresholding [87].

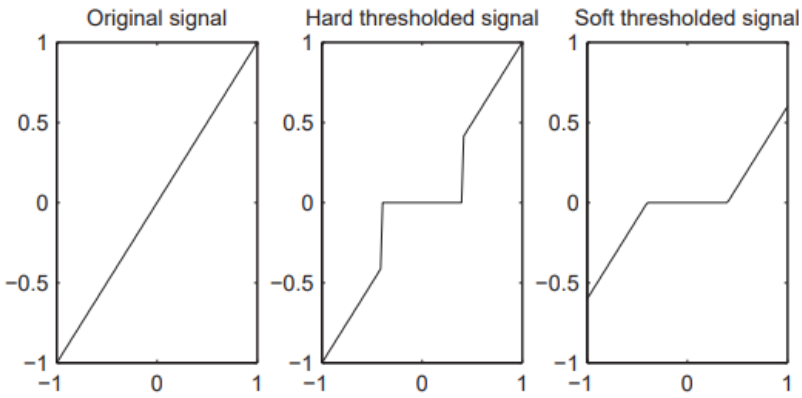

Figure 4.6 *threshold types*

The two threshold operations can be written as in the following equations:

$$HT(x) = \begin{cases} x & if\ |x| > t \\ 0 & if\ |x| \leq t \end{cases} \tag{10}$$

$$ST(x) = \begin{cases} sign(x)(|x| - t) & if\ |x| > t \\ 0 & if\ |x| \leq t \end{cases} \tag{11}$$

The 'soft' implementation requires more computations but gives better denoising performance is the most used and allows better performance as it allows the elimination of noise, with Gaussian density, because its values are concentrated around their average value (zero) [89]. At this point the signal can be reconstructed as the sum of all its components, approximations and details, having eliminated the noisy component.

Chapter 5. Materials and methods

5.1 Dataset/ Subjects

sEMG data from 19 PD patients and 10 healthy controls were analyzed from the database collected at BioMovlab Laboratory of the Department of Information Engineering at the University of Padova. Steps (about 6 strides for each population) and were collected during self-selected speed overground gait trial in a 10 meters walkaway in a forward direction. Data were collected until at least two complete gait cycle were collected bilaterally.

The mean (± standard deviation, SD) characteristics of healthy individuals were: age: 61.9 ± 6.5 years; height: 1.7 ± 0.1 cm; weight: 76.2 ± 15.7 kg; body Mass Index (BMI): 26.3 kg/m^2 and the following exclusion criteria have been adopted for the selection of healthy subjects:

- > 80 years old;
- cardiovascular, neurological, or psychiatric disease;
- severe visual or auditory impairments;
- orthopedic diseases or previous surgery at the lower extremities;
- ability to walk without walking aids;
- pregnancy.

Instead, PD individuals characteristics were: age: 64.7 ± 10.4 years; height: 1.7 ± 0.1 cm; weight: 80.2 ± 17.6 kg; Body Mass Index (BMI): 27.7 kg/m^2 with the following exclusion criteria:

- presence of significant freezing of gait;
- severe balance disorders and co-morbidities that prevent safe mobility;
- severe dysautonomia with hypotension;
- major depression and dementia;
- pregnancy;
- cardiac pacemakers and deep brain stimulation;
- poor visual activity and vestibular dysfunction.

Furthermore, people with an idiopathic form of PD were enrolled with reference to inclusion criteria like disease stage between 2 and 3 on the Hoehn and Yahr scale, no sign of dementia (Mini Mental State Evaluation > 24), ability to walk autonomously and to perform the required tasks, stable drug regimen for at least 3 months and decent response to anti-Parkinsonian treatment. The research was

undertaken in compliance with the ethical principles of the Helsinki Declaration and was approved by an institutional expert committee [93].

5.2 Signal acquisition

The stereophotogrammetric system equipped with 6-optoelectronic motion cameras (frame rate=60Hz, SMART-E, BTS Bioengineering srl, Italy) synchronized with two force platforms (frame rate=960 Hz, Bertec Corporation, USA) was used for the acquisition of biomedical and biomechanical signals and to acquire spherical retroreflective markers trajectories placed on the posterior calcaneus, according to the IOR-gait protocol. These markers were used to identify contralateral heel strikes. The stereophotogrammetric system was also synchronized with two force platforms (frame rate=960 Hz, Bertec Corporation, USA) to assess foot-floor contact and the reactive forces intensity and with an 8 channels sEMG system (frame rate=1000Hz, BTS Free 1000, BTS Bioengineering s.r.l., Italy), which collected the electrical activity of four lower limb muscles bilaterally: Tibialis Anterior (TA), Gastrocnemius Lateralis (GL), Rectus Femoris (RF) and Biceps Femoris (BF). EMG electrodes were placed following the minimal crosstalk area guidelines [94] to maximize the measured selective activity per muscle after an accurate cleansing and preparation of the skin. Sensors (Hydrogel/Ag/AgCl, Kendall Arbo H124SG, Covidien, Ireland) were 24 mm in diameter and positioned 1 cm apart. Before placing the electrodes on the subject's body, the skin was cleaned with abrasive paste and a damp cloth to decrease electrode-skin impedance [93].

5.3 Signal pre-processing

The original implementation of the algorithm involved the detection of the stride and its division into percentage through the analysis of the basographic signal. According to the different kinematics acquisition mode already mentioned, the algorithm has been modified so that the start and end frames acquired by the stereophotogrammetric system have been used to identify the duration of the single stride.

By using the two force platforms integrated in the stereophotogrammetric system, each heel strike instant was identified as the first frame where the modulus of ground reaction force was greater than 5N; toe off was obtained as the first frame where the modulus of ground reaction force was less than 5N; the consequent heel strike was selected as the minimum of the vertical component of the marker trajectory placed on the ipsilateral calcaneus.

So, in order to divide each gait cycle into stance and swing phases, the frames related to the start and end of each stride were extracted from the stereophotogrammetric system and converted into the EMG data array in order to identify the duration of the single stride. In the pre-processing phase, the raw sEMG signals acquired from the tibialis anterior and gastrocnemius lateralis muscles of both right and left leg has been sampled at 1000Hz and underwent a filtering procedure using a band-pass Butterworth filter by using "*butter*" and "*filtfilt*" MATLAB functions. The latter was composed by a second order high pass filter (HPF) with cut-off frequency of 20 Hz and a second order low pass filter (LPF) with a cut-off frequency of 450 Hz.

5.4 Signal Processing

The next step in signal processing was the analysis of the sEMG signals through CWT analysis to evaluate the co-contraction of the TA and GL muscles in the time-frequency domain. This method is able to quantify temporal changes of the frequency content of non-stationary signals maintaining the resolution of signal processing in time and frequency domains [91]. In this phase, three procedures have been defined: (*i*) denoising of TA and GL signals, (*ii*) definition of the scalogram function of GL and TA and (*iii*) the calculation of the co-scalogram function. In the study, sEMG was considered as the input signal and the CWT of the sEMG was computed as the scalar product as shown in the following equation (12):

$$\mathrm{CWT}_{\mathrm{sEMG}}(\mathrm{a},\mathrm{b},\mathrm{t}) = \int \mathrm{sEMG}(\mathrm{t})\psi^{*}_{\mathrm{a,b}}(\mathrm{t})\mathrm{dt} \qquad \mathrm{a} \neq 0 \tag{12}$$

where the basis function $\psi_{\mathrm{a,b}}(\mathrm{t})$ is the mother wavelet, a represents the scale parameter, b represents the translation (time shifting) parameter, described in the equation (13):

$$\psi_{\mathrm{a,\,b}}(t) = \frac{1}{\sqrt{a}}\psi\left(\frac{t-b}{a}\right) \tag{13}$$

$\psi_{\mathrm{a,\,b}}(t)$ must satisfy mathematical criteria such as finite energy and no zero-frequency components to be eligible. The scale is inversely proportional to the spectral components. Low scales (i.e., high

frequencies) provide more local information while high scales (i.e., low frequencies) provide more global information about the sEMG signal.

- **Denoising**:

Through the denoising procedure, the signal noise was reduced. The mother wavelet allows us to define the variability of the time-frequency resolution of the signal under analysis. For this reason, it must be chosen so that its trend is similar to that of the EMG signal and so that it can detect its variations. In the algorithm, a Daubechies Mother Wavelet was chosen to be used for the transform, of order 4 with 8 decomposition levels (db4) using by using the MATLAB function "*wdenoise*", as it is suitable for detecting signal changes, having a shape similar to the action potentials of the motor unit (MUAP) [39].

Once the Mother Wavelet has been chosen, the signal was decomposed in order to obtain different multi-resolution components (coefficients). The signal resolution is a measure of the amount of detail information present in the signal and it is determined by some filtering operations [89], so, the implementation of the wavelet transform occurs through low-pass and high-pass filter banks, in order to divide the components inherent to the high-detail characteristics of the signal (high frequencies, low scale factor) from those inherent to the approximation characteristics of the signal (low frequencies, high scale factor). To achieve this purpose, sEMG signal was decomposed into its frequency content form and then reconstructed. This procedure is followed by a *thresholding method*, which defines a threshold value by which certain coefficients are reset to zero. The aim is to identify an appropriate threshold function so that those coefficients associated with the noise component can be eliminated, while the wavelet coefficients related to useful signal are preserved. The thresholding procedure can be implemented following two approaches: hard-thresholding and soft-thresholding. For this thesis project, the soft thresholding approach proposed by Donoho was implemented. According to Donoho's theory of wavelet threshold denoising, the ideal threshold should reduce the noise while maintaining the maximum amount of signal [92]. The threshold based denoising was implemented using "*MATLAB Wavelet toolbox*". At this point, the signal is reconstructed by recombining the coefficients of approximation of the original signal with the high-detail coefficients subjected to thresholding, obtaining the signal noise-free.

- **Scalogram**

Once obtained the denoised signals, the scalogram function was reconstructed by calculating the coefficients of the wavelet by using the MATLAB function *cwt* and switching from scale to frequency axis using the *scal2frq*. Wavelet scalogram, ($P_{sEMG}\ (a, b)$), measures the local time-frequency energy

density of the sEMG signal [88] and it is defined as the square of the absolute value of CWT coefficients matrix, W_{sEMG} , as described in the equation (14):

$$P_{sEMG}\,(a,b) = |W_{sEMG}(a,b)|^2 \tag{14}$$

In this study, the $P_{sEMG}\,(a,b)$ in the time–frequency domain of denoised sEMG signal was used for measuring muscular activation by identifying both localization in time and frequency of the maximum of the muscular energy density.

The time localization of maximum energy density, performed in the present study, could be interpreted as the time-interval where the sEMG signal reached its peak value of energy, i.e., the region of GC where the muscle is mainly recruited. While the frequency localization of the maximum energy density could be interpreted as the frequency band where the sEMG signal shows the maximum frequency content. This band depends on the muscle, however a common frequency band among all lower-limb muscles could be from 70 to 160 Hz [91].

To identify muscular activations of both GL and TA with respect to the percentage of gait cycle, a thresholding method was implemented for each muscle and each stride. First, the maximum peak of the scalogram was identified. Then, a proper threshold equal to the 1% of the maximum peak was set. The activation intervals are represented by those values higher than the threshold while other values below to it are set to zero.

In addition, consecutive activation intervals whose temporal distance is lower than the 3% of the gait cycle were merged in the same activation, on the contrary they were considered separated.

Finally, those activation intervals whose temporal duration was lower than the 3% of the gait cycle were removed with also their relevant frequencies which are considered negligible.

Once having identified all time intervals, activation timing was computed for each single stride as the beginning (onset) and the end (offset) of the time-intervals previously obtained and also their relevant frequencies were extracted by using the information reported in the scalogram.

- **Coscalogram**

For this thesis project, also the CWT coscalogram was calculated as the product between the coefficients of the scalogram of the first sEMG signal (TA) and the complex conjugate of the coefficients of the scalogram of the second sEMG signal (GL).

The CWT coscalogram identifies the cross-correlations between the two signals providing a detailed information about the interaction of the signals in the time-frequency domain [91] and it measures the cross-energy density between the two signals as defined in the equation (15):

$$PW_{sEMG}(a,b) = W_{sEMG1}(a,b) \cdot W^{*}{}_{sEMG2}(a,b) \quad (15)$$

Where $sEMG1$ and $sEMG2$ represents the two denoised signals related to the two muscles in consideration and $W_{sEMG1}(a,b)$ and $W^{*}{}_{sEMG2}(a,b)$ are the matrices of CWT coefficients of the two signals, at scale a and time b, the operator * represents the conjugate complex. In this study, the coscalogram is interpreted as the representation of the co-contraction in time-frequency of the two muscles considered [29].

For the calculation of the co-contraction intervals in the time domain, the same criteria have been adopted as for the scalogram functions calculated above: when the coscalogram function exceeded 1% of the cross-energy-density peak, co-contraction timing was calculated as the start (onset) and the end (offset) of the time interval for each stride. After, the frequency range connected to the coscalogram function for that particular time interval was computed to determine the correspondent co-contraction content in the frequency domain. Thus, the maximum and minimum frequency content values were calculated for each co-contraction that was evaluated in the time domain.

Moreover, for each muscular co-contraction, the occurrence frequency (OF) was computed as defined in the following equation (16):

$$OF = \frac{Number\ of\ gait\ cycles\ where\ the\ co-contraction\ occurs}{Total\ number\ of\ gait\ cycles} \times 100 \quad (16)$$

Where the number of gait cycles with activation and the total number of gait cycles are calculated over the whole population (Controls or PD) [93].

5.5 Statistics

The significant variation of parameter distribution between PD and Controls populations were examined through the parametric and non-parametric statistical tests. The two-sample t-test is the parametric test that was employed to verify the normal distribution of each parameter, on the other hand the evaluation of non-normal distributions was done by using the non-parametric Mann-Whitney test. The level of the test significance was set at 5% (p-value).

Chapter 6. Results

This chapter shows the results related to the muscle contractions and co-contractions of TA and GL muscles, obtained by the algorithm. A statistical analysis was carried out on both Controls and PD subjects. For all 29 subjects, the activation intervals of both TA and GL (ON/OFF), their relative frequency range (MIN/MAX) and the occurrence frequency of co-contraction (OF) for 174 steps were computed and analyzed.

6.1 Control subjects

In Figure 6.1, the **raw** and **Butterworth filtered** sEMG signals of right TA (blue and orange, respectively) acquired from subject 3, step 9, were reported and compared.

It is possible to appreciate that the band-pass Butterworth signal (band width 20-450 Hz) was able to reduce the noise caused by artifacts probably due to the marker's movements on the subject skin.

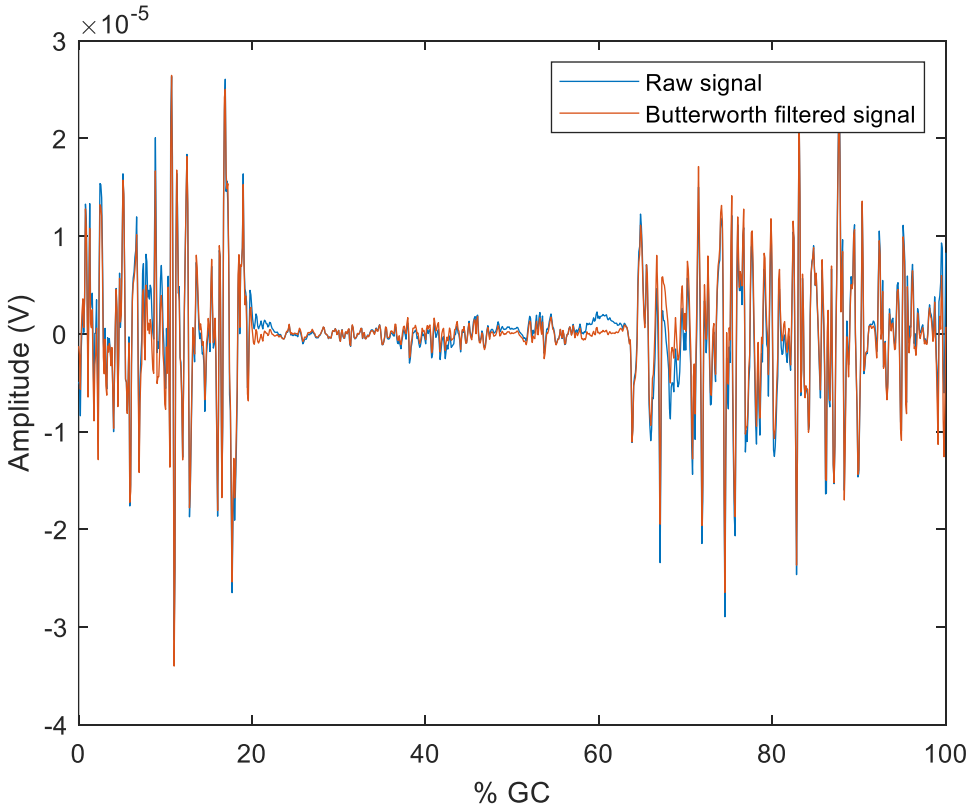

Figure 6.1 *Raw (blue) and Butterworth filtered (orange) sEMG signal of right TA for the Control subject 3, stride 9.*

sEMG of TA reported in Figure 6.1 shows an activity consistent with that described in the literature [74], with a biphasic activation, characterized by intensity peaks in the range 0-20% of the GC and in the range 60-100%.

These results confirmed that during the Initial Contact (0-2%) and Loading Response (0-10%) phases of the GC, the TA allows the correct positioning of the foot for support while during the second interval to the Swing phase (40%), the TA regulates the fall of the foot and allows its suspension.

In Figure 6.2, the **raw** and **Butterworth filtered** sEMG signals of right GL (blue and orange, respectively) acquired from subject 3, step 9, were reported and compared.

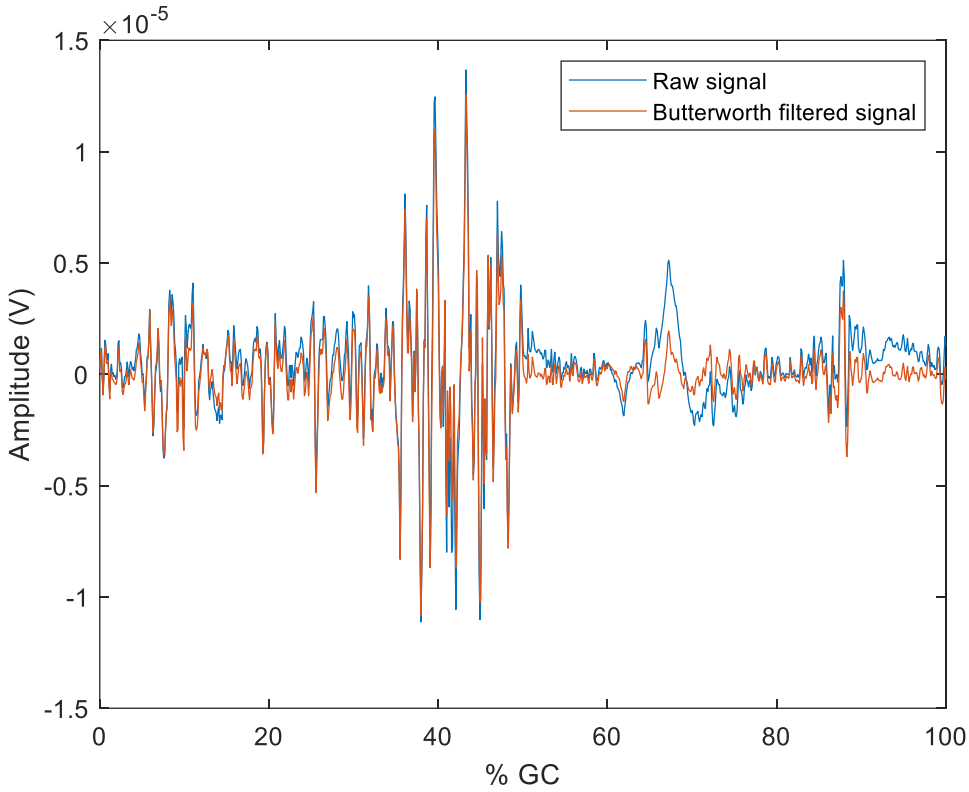

Figure 6.2 *Raw (blue) and Butterworth filtered (orange) sEMG signal of right GL for Control subject 3, stride 9.*

The raw sEMG GL signal is noisier than TA signal. As shown in Figure 6.2, a prolonged activation interval from 0% to 30% of GC is observed with a peak intensity in the range of 40-50% of GC, activations consistent with those present in the literature [80]. This activation interval was associated to the Terminal Stance phase (30-50%), where the GL plays a key role in ensuring ankle stability. A further contraction at lower intensity can also be observed in the range of 80-100% of the GC (Terminal Swing).

The rectified TA sEMG signal of the same stride (9) is shown in Figure 6.3 along with its corresponding 2D and 3D CWT scalogram functions (on the left, lower panel and right, respectively).

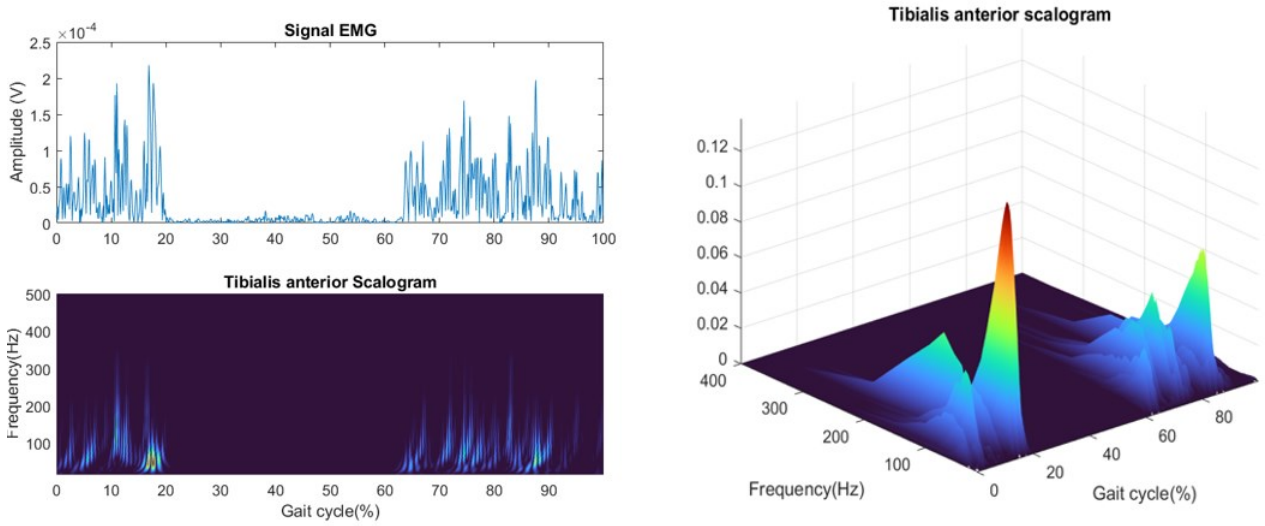

Figure 6.3 *Rectified sEMG signal (left figure, top panel) and CWT scalogram function (left figure, lower panel) of right TA muscle for Control subject 3, stride 9. On the right its corresponding 3D CWT scalogram function in which red is the condition when the percentage of energy is maximum and dark blue when the percentage of energy is minimum.*

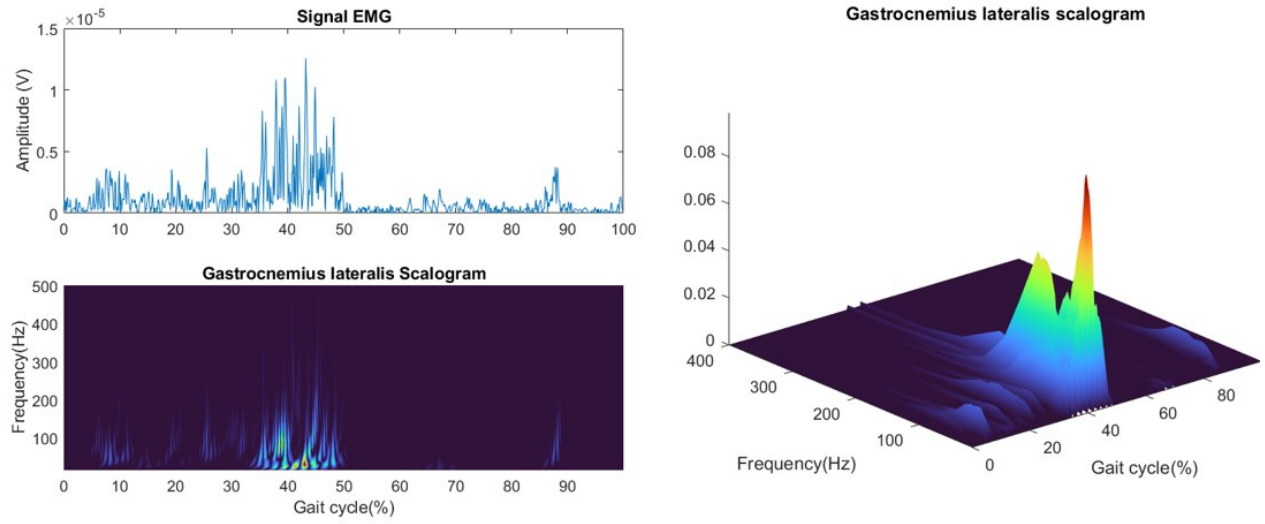

Figure 6.4 *Rectified sEMG signal (left figure, top panel) and CWT scalogram function (left figure, lower panel) of right GL muscle for Control subject 3, stride 9. On the right its corresponding 3D CWT scalogram function, in which red is the condition when the percentage of energy is maximum and dark blue when the percentage of energy is minimum.*

The rectified GL sEMG signal of the same stride (9) is shown in Figure 6.4 along with its corresponding 2D (on the left, lower panel) and 3D (on the right) CWT scalogram functions.

The 3D scalogram is very useful to have a more informative representation than the 2D one. In fact, as show in Figure 6.3 (right) and Figure 6.4 (right), the maximum of the energy density, represented by a specific colormap, represent in logarithmic scale the square of the absolute value of CWT coefficients matrix. The red color corresponds to the maximum percentage of energy density while the blue one corresponds to the minimum one.

As expected for TA, there are two evident contractions. The first one is from 0 to 20% of the GC, while the second one is from the 60% to 100% of the GC with both with a frequency range between 14 to 238 Hz. The maximum of energy was shown in the first contraction at 17% of the GC (early stance) with a frequency content equal to 47 Hz.

For GL, a considerable muscle contraction (red color) is located in the terminal stance around 43% of GC, in the transition between flat foot contact and push off phases with a frequency content of 43 Hz. The frequency range is between 14-357 Hz. The other two contractions from 63% to 72% and from 84% to 89% are characterized by a very low energy density.

The scalograms of the two denoised signals TA and GL (lower panel and middle panel, respectively) and the relative coscalogram function (upper panel) are shown in Figure 6.5.

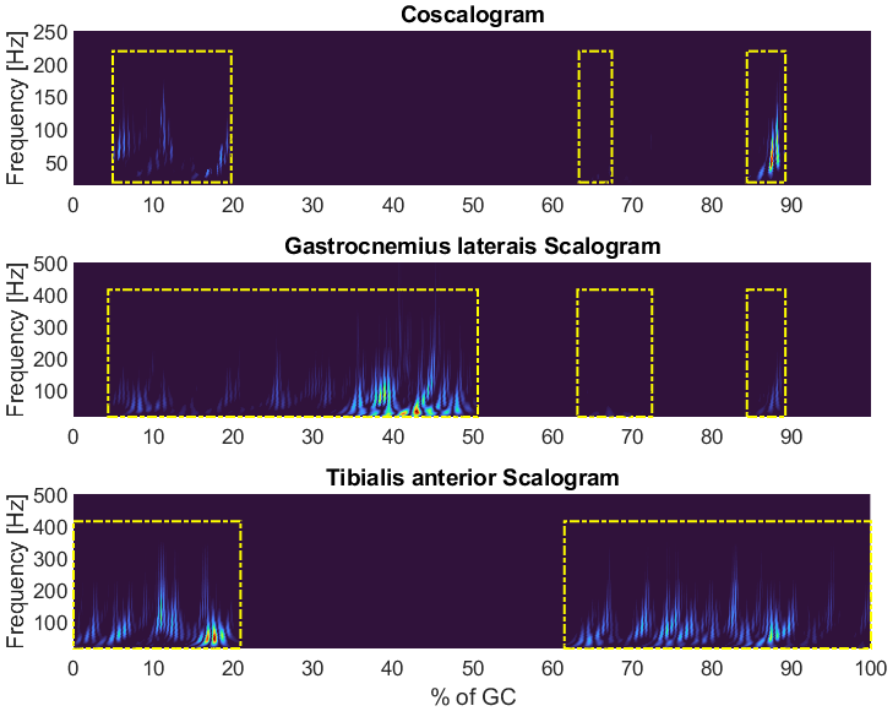

Figure 6.5 *Activation intervals (yellow boxes) highlighted in the scalogram function (lower panels) and the relative coscalogram function (upper panel) of di TA and GL muscles of the Control subject 3, stride 9, right leg.*

Yellow boxes represent activation intervals for each scalogram and co-scalogram function. More precisely, the single yellow box represents the interval during which the energy density is higher than the reference threshold (1%) of the maximum value assumed by the scalogram or co-scalogram. Additionally, all the consecutive intervals, whose temporal distance is equal or less than the 3% of GC are merged as explained in 'Material and Methods' section.

Muscular co-contractions are detected between the loading response phase and mid-stance phase (5% -19.8%), terminal swing (84.3%-89.2%). The frequency range is between 23-142.8 Hz and 20-142 Hz, respectively.

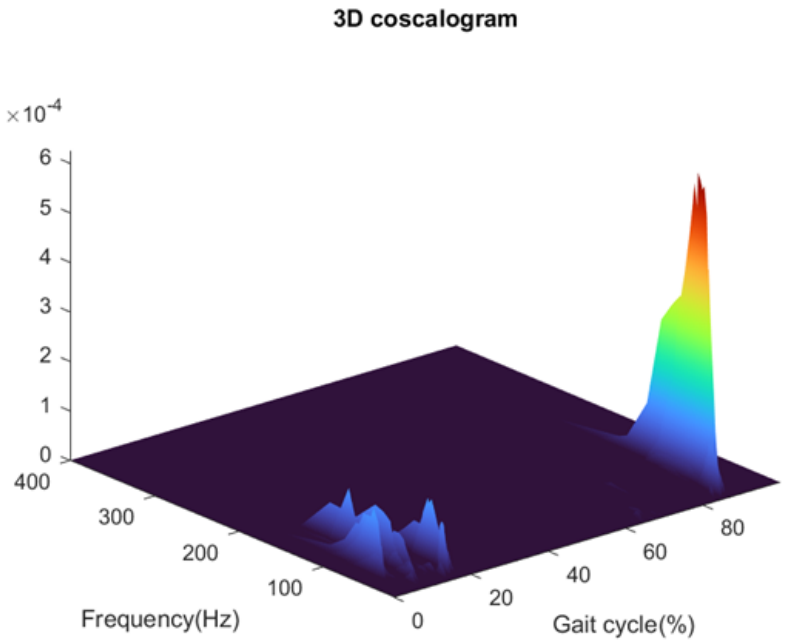

Figure 6.6 *Three-dimensional colour representation of CWT coscalogram between TA and GL for the same stride.*

A better 3D visualization of the coscalogram function is depicted in Figure 6.6. The highest energy density is detected in the terminal swing phase between 44-60 Hz.

The mean value (±SD) of the coscalogram of the minimum and maximum frequency range for all the Control subjects is 27 ± 10.3 and 130.1 ± 13.8, respectively.

6.2 Parkinson subjects

The plots obtained from the processing of the signal acquired by subject 14, step 5, right leg of the **raw** and **Butterworth filtered** sEMG signals of right TA and GL (blue and orange, respectively) were reported in Figure 6.7 and Figure 6.8. Also, in this case the raw signal for the TA is not particularly noisy than GL. The band-pass Butterworth filter (band width 20-450 Hz) was able to reduce the noise caused by artifacts.

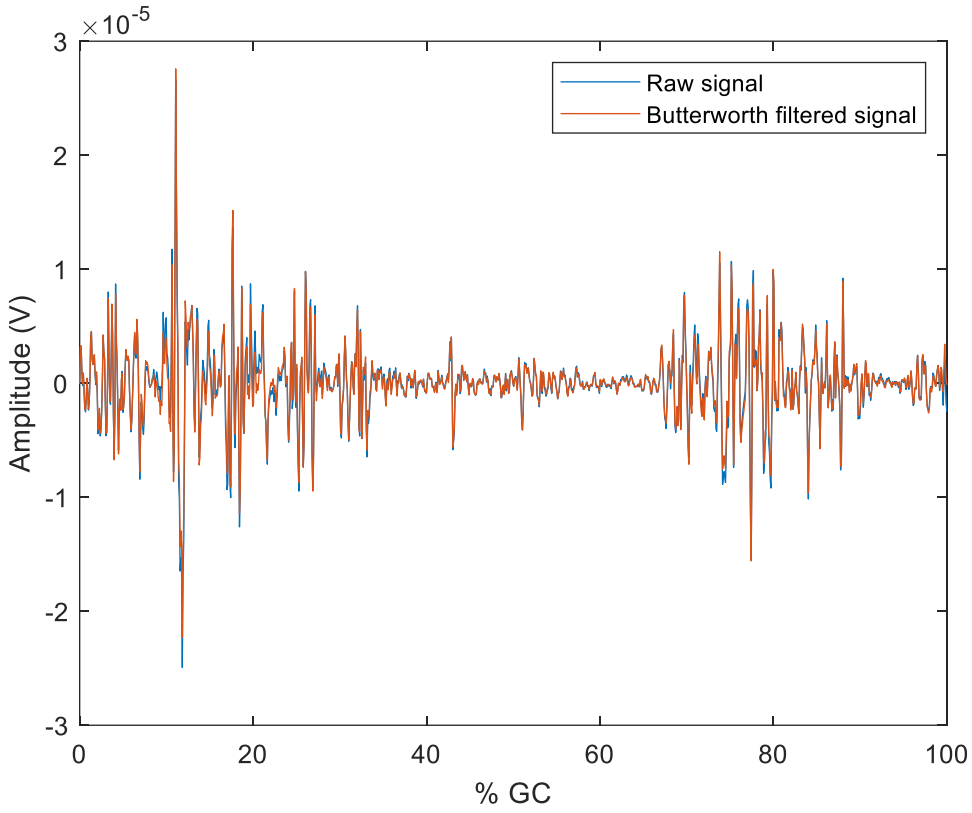

Figure 6.7 *Raw (blue) and Butterworth filtered (orange) sEMG signal of right TA for the PD subject 14, stride 5, right leg.*

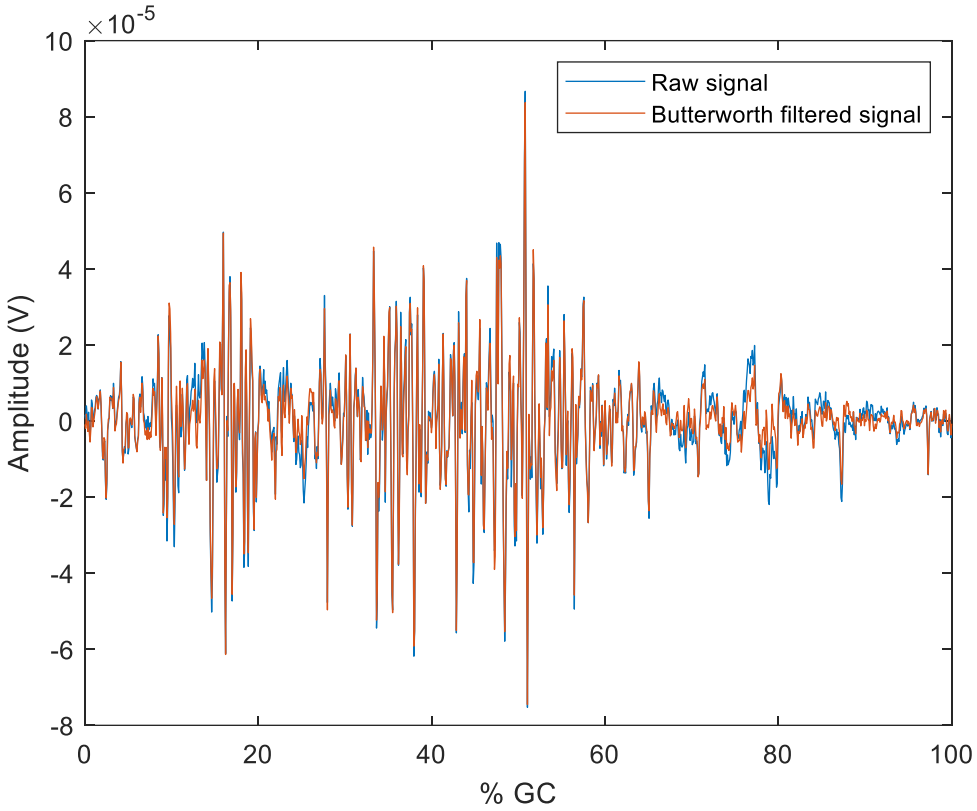

Figure 6.8 *Raw (blue) and Butterworth filtered (orange) sEMG signal of right GL for the PD subject 14, stride 5, right leg.*

As in the case of healthy subjects, the biphasic nature of the TA activations can be seen, with localization in the periods 0-32% of the GC and 65-95% of the GC with a frequency range between 14 to 238 Hz and 15.5 to 238 Hz. The maximum of energy was shown around 10% of the GC (early stance) with a frequency content equal to 54 Hz.

For GL, a considerable muscle contraction (red color) is located in the terminal stance around 50% of GC, in the transition between flat foot contact and push off phases with a frequency content of 43 Hz. The frequency range is between 14-357 Hz. The other two contractions from 63% to 72% and from 84% to 89% are characterized by a very low energy density.

The rectified TA sEMG signal and GA sEMG signal of the same stride (5) are shown in Figure 6.9 and Figure 6.10, along with their corresponding 2D and 3D CWT scalogram functions (on the left, lower panel and right, respectively).

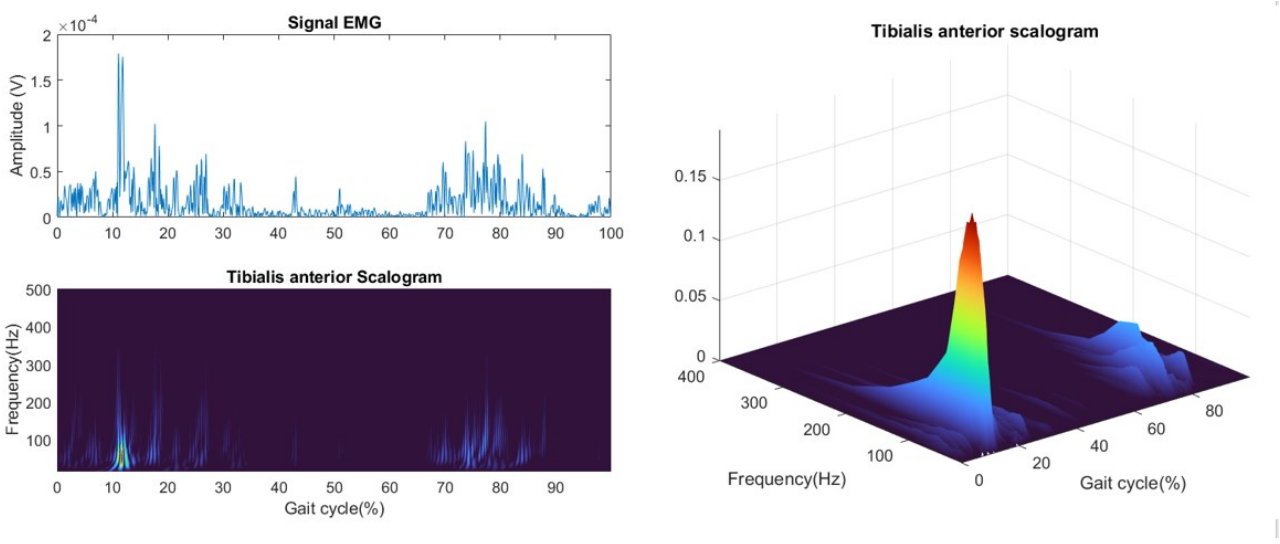

Figure 6.9 *Rectified sEMG (on top) and CWT scalogram function of TA muscle for PD subject 14, stride 5, right leg. On the right its corresponding 3D CWT scalogram function, in which red is the condition when the percentage of energy is maximum and dark blue when the percentage of energy is minimum.*

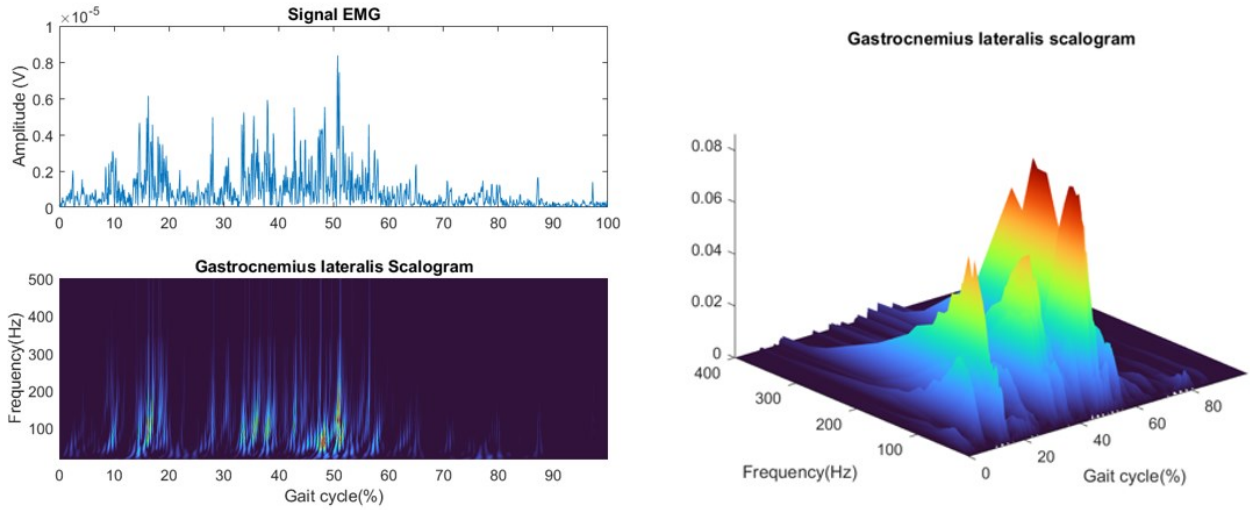

Figure 6.10 *Rectified sEMG (on top) and CWT scalogram function of GL muscle for PD subject 14, stride 5, right leg. On the right its corresponding 3D CWT scalogram function, in which red is the condition when the percentage of energy is maximum and dark blue when the percentage of energy is minimum.*

.

For GL, a considerable muscle contraction (red color) is located in the terminal stance around 43% of GC, in the transition between flat foot contact and push off phases with an energy density of 70

Hz. The frequency range is between 14-357 Hz. The other two contractions from 63% to 72% and from 84% to 89% are characterized by a very low energy density.

Figure 6.11 shows the scalograms of the two denoised signals TA and GL (lower panel and middle panel, respectively) and the relative coscalogram function (upper panel) for the PD subject. Yellow boxes represent activation intervals for each scalogram function.

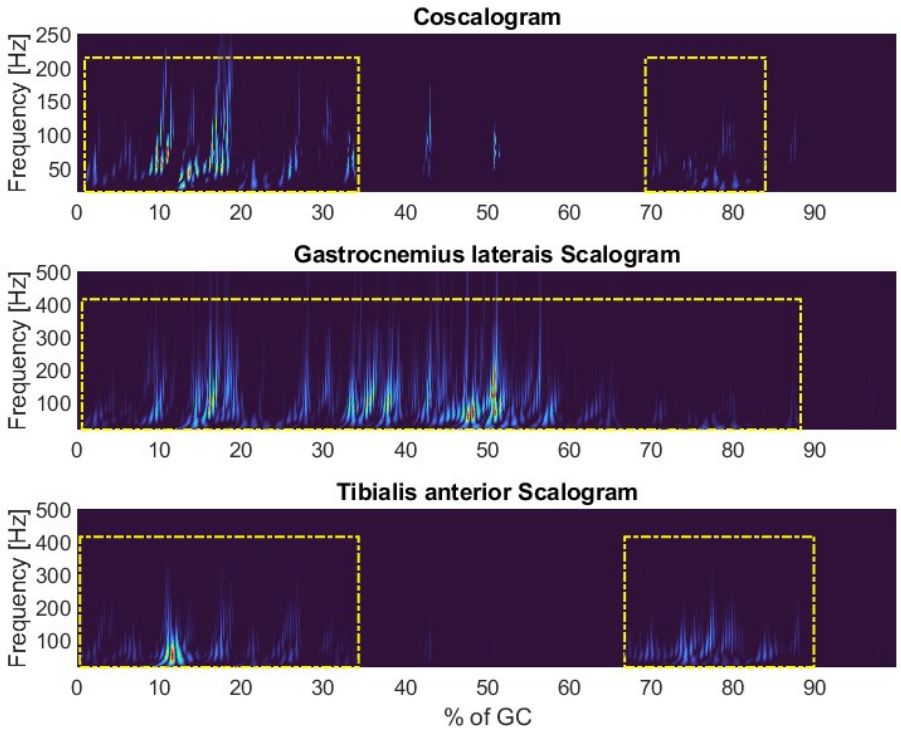

Figure 6.11 *Activation intervals (yellow boxes) highlighted in the scalogram function (lower panels) and the relative coscalogram function (upper panel) of di TA and GL muscles for PD subject 14, stride 5, right leg.*

Coscalogram frequency is in the frequency band between 14.3 -238 Hz and 15.5- 119.8 Hz and the two co-contractions are detected in the time interval between stance phase (0.9-34.4%) and early swing phase (69.3-83.9%) of the GC.

The mean value (±SD) of the coscalogram of the minimum and maximum frequency range for all the PD subjects is 22.09 ± 5.9 and 111.2 ± 31.17, respectively.

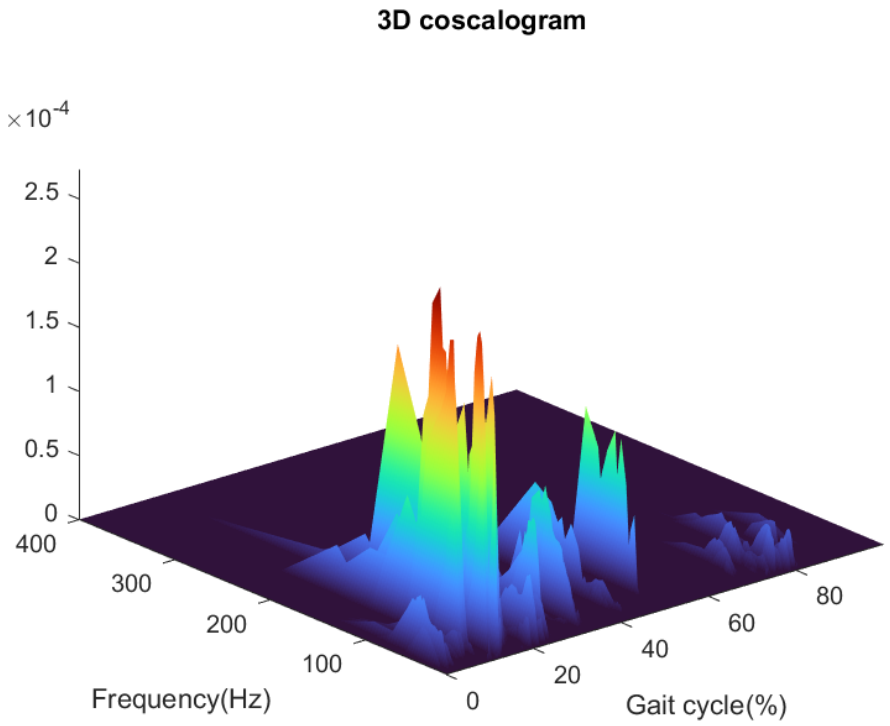

Figure 6.12 *Three-dimensional color representation of CWT coscalogram between TA and GL for the same stride.*

A better 3D visualization of the coscalogram function is depicted in Figure 6.12, higher energy density is detected in the early stance phase with values between 44-79 Hz.

6.3 Co-contractions

In this section, results relating to co-contractions were calculated such as the mean value (± SD) of the co-contraction intervals (ON/OFF), the mean (± SD) of the frequency range (MIN/MAX) and the occurrence frequency (OF) of co-contractions among the entire population and they were reported in Table 6.1 (Controls), Table 6.2 (PD), Table 6.3 (Controls), Table 6.4 (PD). Statistic values are reported in Table 6.5 and 6.6.

Beyond the GC segmentation into the two principal phases of stance (0-60%) and swing (60-100%), a further subdivision has been adopted for the co-contraction time-intervals, according to the coherent region of activation and their occurrence during the GC, in order to identify five co-contraction intervals as shown in Figure 6.13. In addition to this, the organization of the averages was performed by using visual inspection by an expert in electromyography.

The average co-contraction intervals in function of the percentage of gait cycle for both groups (Controls and PD) were shown in Figure 6.13 using a color representation according to the phase of the gait cycle when the activation occurs. Thus, the co-contractions in early stance (0-20%) mid-stance (20-40%), late stance (40-60%), early swing (60-80%), and late swing (80-100%) are represented in light yellow, yellow, orange, red, and brown, respectively.

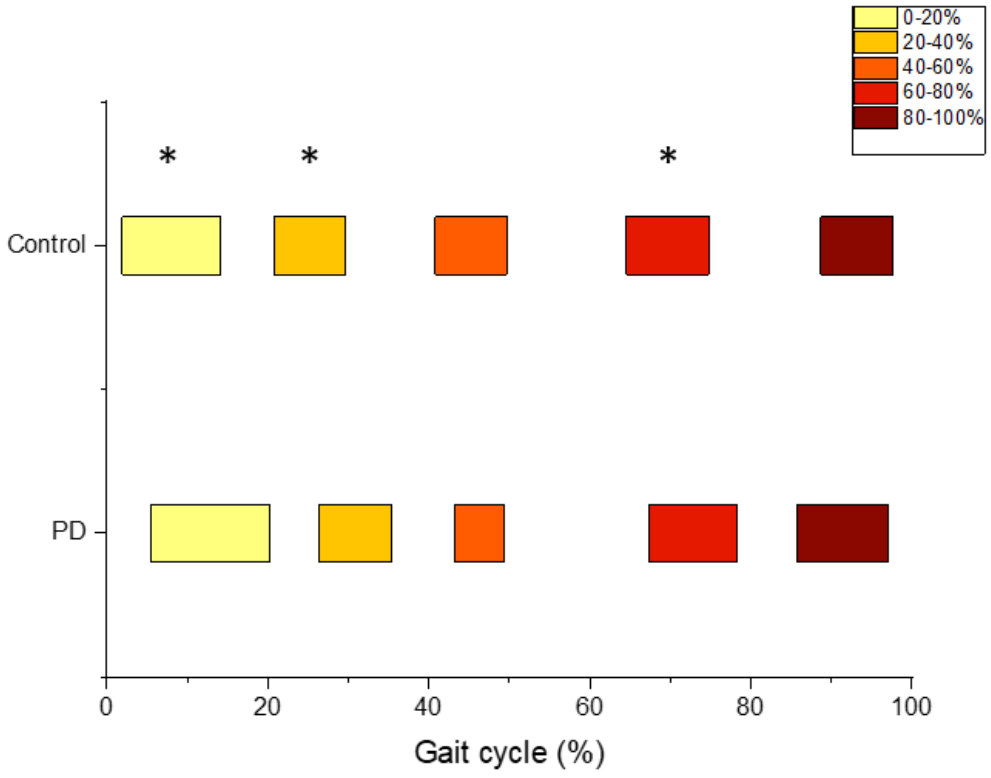

Figure 6.13 *Mean activation intervals in function of the percentage of gait cycle valued in PD patients versus Control subjects in the different phases of gait cycle: early stance (0-20%) mid-stance (20-40%), late stance (40-60%), early swing (60-80%), and late swing (80-100%) are represented in light yellow, yellow, orange, red, and brown, respectively. The * individuates the groups statistically different.*

On average, a significant delay is detected in Control compared to PD groups in both onset (1.9 ± 2.4 vs 5.5 ± 4.0, $p < 1 \cdot 10^{-3}$) and offset (14.1 ±9.0 vs 20.3± 7.6, $p < 1 \cdot 10^{-3}$) timing for the first co-contraction interval (0-20%) during early stance phase and also in the onset (20.8± 8.2% vs 26.4 ± 5.9% of GC, p=0.01) and in the offset (29.7 ± 6.7 vs 35.3 ±8.2, p=0.02) timing for the mid-stance activation interval (20-40%), respectively.

No greater significant differences in the average onset (40.8 ± 2.8 vs 43.3 ± 4.5, p=0.24) and offset (49.7± 4.8 vs 49.4 ± 4.9, p=0.98) timing of the III co-contraction interval during late stance (40-60 %) between the two groups.

Additionally, PD group shows a statistical difference in the IV co-contraction interval (60-80%, early swing) in the onset (64.5 ± 5.3 vs 67.3 ± 7.7, p=0.01) and offset (74,8 ± 5.8 vs 78.2 ± 8.0, p=0.001) timing. No significant differences are shown in the V co-contraction interval (80-100%, late swing) in the onset (88.7 ± 6.1 vs 85.8 ± 9.4, p=0.50) and offset (97.7 ± 4.1 vs 97.1 ± 3.4, p=0.14) timing.

N°of co-contraction	Muscle activation range	Mean (±SD)	Occurence frequency (%)
I co-contraction	ON1	1.9 ± 2.4	
(%GC)	OFF1	14.1 ± 9.0	78.9
II co-contraction	ON2	20.8 ± 8.2	
(%GC)	OFF2	29.7 ± 6.7	36.8
III co-contraction	ON3	40.8 ± 2.8	
(%GC)	OFF3	49.7± 4.8	8.8
IV co-contraction	ON4	64.5 ± 5.3	
(%GC)	OFF4	74.8 ± 5.8	59.6
V co-contraction	ON5	88.7 ± 6.1	
(%GC)	OFF5	97.7 ± 4.1	45.6

Table 6.1 *Mean (± SD) and occurrence frequency (OF) associated to the co-contraction intervals reported in Figure 6.13 for Control subjects.*

N°of co-contraction	Muscle activation range	Mean (±SD)	Occurence frequency (%)
I co-contraction	ON1	5.5 ± 4.0	
(%GC)	OFF1	20.3 ± 7.6	91.8
II co-contraction	ON2	26.4 ± 5.9	
(%GC)	OFF2	35.3 ± 8.2	22.4
III co-contraction	ON3	43.3 ± 4.5	
(%GC)	OFF3	49.4 ± 4.9	30.6
IV co-contraction	ON4	67.3 ± 7.7	
(%GC)	OFF4	78.2 ± 8.0	45.9
V co-contraction	ON5	85.8 ± 9.4	
(%GC)	OFF5	97.1 ± 3.4	14.3

Table 6.2 *Mean (± SD) and occurrence frequency (OF) associated to the co-contraction intervals reported in Figure 6.13 for PD subjects.*

Figure 6.14 and Figure 6.15 show a comparison between the mean value of the frequency content for each co-contraction detected in the time domain for both Controls and PD. Figure 6.14 reports the average value of the minimum frequency content of the co-contraction intervals while maximum frequency values are shown in Figure 6.15.

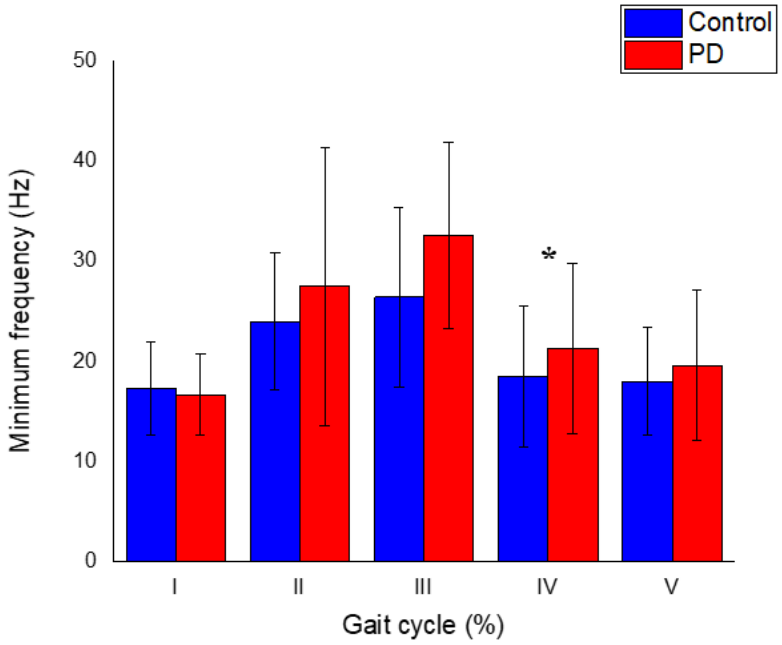

Figure 6.14 *Mean value of the minimum frequency computed in the five co-contraction intervals detected in the time-domain. The blue and red bars represent the minimum frequency content of the co-contraction for the Controls and PD subjects, respectively. The * individuates the groups statistically different.*

Non-statistical differences are reported during stance and swing phases in the I, II, III and V co-contraction intervals, conversely statistical difference is shown in Figure 6.14 during swing phase in the IV co-contraction (18.5 ± 7.1 and 21.3 ± 8.5, p=0.03, for controls and PD respectively). The highest average values for minimum frequency are shown in the III co-contraction during the stance phase for both groups.

As shown in Figure 6.15, highest maximum frequency is detected in the early stance phase (I co-contraction) for PD group, while for Controls during the late stance phase. The maximum frequency for PD is higher than controls during the early stance phase (I co-contraction) (125.0 ± 42.7 and 147.5 ± 44.3, p=0.04. respectively) and during the swing phase in the IV co-contraction interval (93.3 ± 41.2 and 113.3 ± 34.0, p=0.01).

Vice versa, in the II, III, V intervals, the maximum frequency reach higher in Controls than PD (128.3 ± 50.0 and 112.1 ± 40.4, p=0.10, 148.9 ± 31.7 and 115.7 ± 26.8, p=0.02, 128.4 ± 37.8 and 104.2 ± 49.2, p= 0.02, respectively). Statistical significances are shown in the last three co-contractions during the late stance and swing phases (p=0.02, p=0.01, p=0.02).

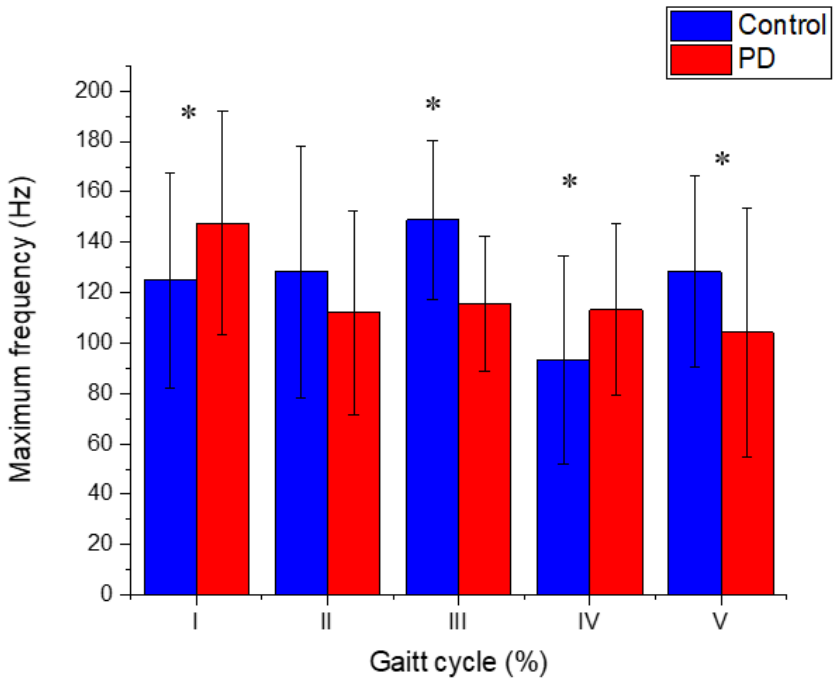

Figure 6.15 *Mean value of the maximum frequency computed in the five co-contraction intervals detected in the time-domain. The blue and red bars represent the maximum frequency content of the co-contraction for the Controls and PD subjects, respectively. The * individuates the groups statistically different.*

N°of co-contraction	Frequency	Mean (±SD)	Occurence frequency (%)
I co-contraction	MIN1	17.3 ± 4.7	
(%GC)	MAX1	125.0 ± 42.7	78.9
II co-contraction	MIN2	24.0 ± 6.8	
(%GC)	MAX2	128.3 ± 50.0	36.8
III co-contraction	MIN3	26.4 ± 9.0	
(%GC)	MAX3	148.9 ± 31.7	8.8
IV co-contraction	MIN4	18.5 ± 7.1	
(%GC)	MAX4	93.3 ± 41.2	59.6
V co-contraction	MIN5	18.0 ± 5.4	
(%GC)	MAX5	128.4 ± 37.8	45.6

Table 6.3 *Mean (± SD) and occurrence frequency (OF) associated to the co-contraction frequency content reported in Figure 6.14 and Figure 6.15 for Control subjects (blue bars).*

N°of co-contraction	Frequency	Mean (±SD)	Occurence frequency (%)
I co-contraction	MIN1	16.7 ± 4.0	
(%GC)	MAX1	147.5 ± 44.3	91.8
II co-contraction	MIN2	27.5 ± 13.9	
(%GC)	MAX2	112.1 ± 40.4	22.4
III co-contraction	MIN3	32.6 ± 9.3	
(%GC)	MAX3	115.7 ± 26.8	30.6
IV co-contraction	MIN4	21.3 ± 8.5	
(%GC)	MAX4	113.3 ± 34.0	45.9
V co-contraction	MIN5	19.6 ± 7.5	
(%GC)	MAX5	104.2 ± 49.2	14.3

Table 6.4 *Mean (± SD) and occurrence frequency (OF) associated to the co-contraction frequency content reported in Figure 6.14 and Figure 6.15 for PD subjects (red bars).*

The bar graph in Figure 6.16 reports the occurrence frequency (OF %) assessed in both PD patients and Control subjects in the different phases of gait cycle. The bars are represented in blue and red colours for Controls and PD, respectively.

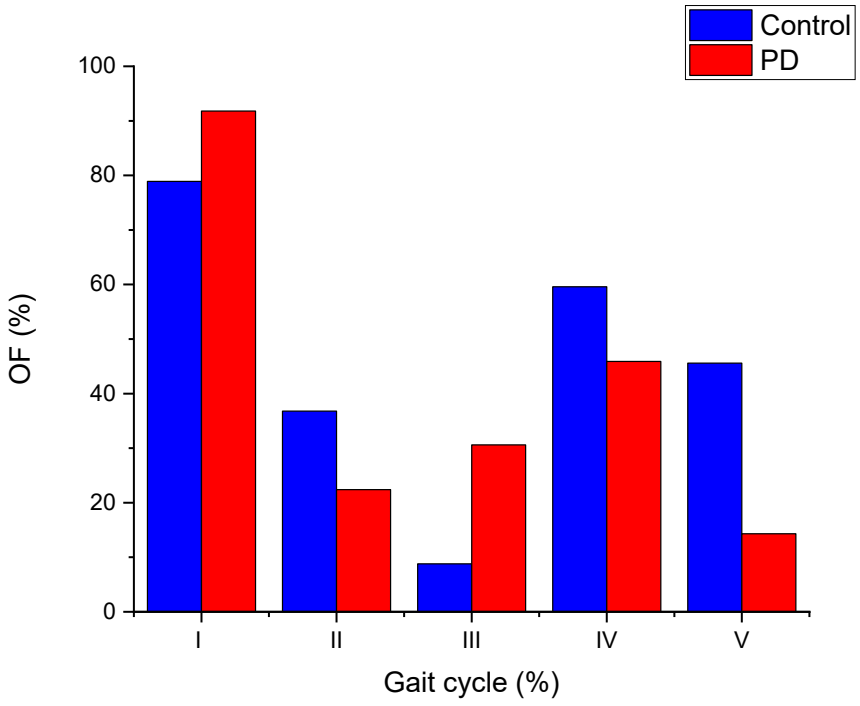

Figure 6.16 *Occurrence frequency (OF %) assessed in PD patients (red bars) versus Control subjects (blue bars) in the different phases of gait cycle.*

Since OF is a scalar quantity and not a distribution, statistical tests, used to compare onset and offset values between the two populations, cannot be adopted for OF.

The bar graph in Figure 6.16 shows large difference between the two groups in the early-stance phase related to the III co-contraction intervals and in the late swing phase regarding the V co-contraction interval. The III co-contraction shows an OF 8.8% and 30.6% for Control and PD, respectively while the V co-contraction shows an OF of 45% for Controls and 14.3% for PD.

No particular differences are detected in the IV co-contraction during swing phase (59.6% and 45.9% for Controls and PD, respectively).

In Table 6.5 and Table 6.6 are reported the statistical differences of the time activation intervals and frequency ranges between the two populations.

Subjects	Test	Mean	Median	p-value
ON1_C	M-W	1.9	0.8	$p < 1{\cdot}10^{-3}$
ON1_P		5.5	4.6	
OFF1_C	M-W	14.1	11.8	$p < 1{\cdot}10^{-3}$
OFF1_P		20.3	20.0	
ON2_C	T-T	20.8	19.5	0.01
ON2_P		26.4	28.5	
OFF2_C	T-T	29.7	30.9	0.02
OFF2_P		35.3	35.0	
ON3_C	T-T	40.8	41.4	0.24
ON3_P		43.3	44.2	
OFF3_C	M-W	49.7	51.8	0.98
OFF3_P		49.4	50.0	
ON4_C	M-W	64.5	64.2	0.01
ON4_P		67.3	68.5	
OFF4_C	M-W	74.8	75.6	0.001
OFF4_P		78.2	80.8	
ON5_C	M-W	88.7	91.0	0.50
ON5_P		85.8	88.1	
OFF5_C	M-W	97.7	99.6	0.14
OFF5_P		97.1	98.6	

Table 6.5 *Mean, median and p-value of the activation intervals between the two populations. Mann-Whitney test (M-W) and two sample t-test (T-T) are performed.*

Subjects	Test	Mean	Median	p-value
MIN1_C	M-W	17.3	14.3	0.90
MIN1_P		16.7	14.3	
MAX1_C	M-W	125.0	119.0	0.04
MAX1_P		147.5	142.8	
MIN2_C	M-W	24.0	23.0	0.87
MIN2_P		27.5	23.9	
MAX2_C	M-W	128.3	142.9	0.10
MAX2_P		112.1	119.0	
MIN3_C	M-W	26.4	24.6	0.08
MIN3_P		32.6	29.2	
MAX3_C	T-T	148.9	142.9	0.02
MAX3_P		115.7	119.0	
MIN4_C	M-W	18.5	14.7	0.03
MIN4_P		21.3	17.9	
MAX4_C	M-W	93.3	89.3	0.01
MAX4_P		113.3	119.0	
MIN5_C	M-W	18.0	15.9	1.00
MIN5_P		19.6	15.9	
MAX5_C	M-W	128.4	142.8	0.02
MAX5_P		104.2	95.6	

Table 6.6 *Mean, median and p-value of the minimum and maximum frequency ranges between the two populations. Mann-Whitney test (M-W) and two sample t-test (T-T) are performed.*

Chapter 7. Discussion and conclusion

The aim of the present study was to provide a quantitative evaluation of muscle co-contraction of the antagonist muscles of the ankle joint (TA and GL) during walking in parkinsonian subjects, compared with healthy subjects in the time-frequency domain. The co-contraction quantification was done in terms of onset and offset of co-contraction timing, minimum and maximum frequency content, and occurrence frequency of each muscle activation interval. To this aim, an algorithm based on the continuous wavelet transform (CWT) has been adopted and in particular, the use of the CWT coscalogram function allows to characterize the muscular co-contraction activity in the time–frequency domain based on the cross-energy localization of two sEMG signals. The algorithm has been tested on a pathological population and its application is adherent with what was previously seen with the normal subject [29] allowing to carry out a comparative analysis of the results between normal and pathological subjects. By confirming the reliability of the algorithm for the study of co-activation in healthy subjects, this allowed to structure an adequate term of comparison to evaluate co-contraction in Parkinson's subjects.

The application of the algorithm allowed to obtain a representation of the activity of the TA and GL consistent with that obtained from the signal subjected to denoising and specifically allows to localize the energy density of muscle contractions represented by a specific colormap as a function of time (GC (%)) and frequency (Hz) as shown in Figures 6.3,6.4,6.9,6.10, for both Controls and PD. The time localization of maximum energy density, performed in the present study, could be interpreted as the time-interval where the sEMG signal reached its peak value of energy, i.e., the percentage of GC where the muscle is mainly recruited. While the frequency localization of the maximum energy density could be interpreted as the frequency band where the sEMG signal shows the maximum frequency content [91]. From this representation, it is possible to simultaneously evaluate onset and offset timing together with the frequency content of each muscular activations and how the signal amplitude changes depending on the frequency as shown in Figures 6.5 and 6.11.

Figure 6.5 and 6.6 for Control subjects and 6.11 and 6.12 for PD patients show that the implementation of the CWT approach was able to represent the co-contraction between the TA and GL activity in the functions of time, frequency and magnitude (x-axis, y-axis, coloured scale, respectively) allowing a direct identification of co-contraction in the time domain (% of gait cycle) in a 3D visualization.

Regarding to the muscle activation’s pattern of the two muscles in healthy subjects, these are consistent with those reported in the literature [80,95].

However, PD patients show reduced activation during stance phase and increased and anticipated activation during swing phase for TA, resulted to be consistent with literature [6,24,25]. As far as GL is concerned, the activations patterns for PD are also consistent with literature [93], showing more activation in early and late stance phases.

Even so, the differences between the two groups are probably due to the fact that PD subjects put in place compensation mechanisms to increase stability by contracting muscles more.

Nevertheless, the limitation behind the algorithm implemented, is based on partitioning consecutive co-contraction intervals.

The co-contraction intervals detected in Figure 6.13, show on average delay in PD patients with respect to Controls; in particular the I and II co-contractions during stance phase in the onset (1.9 ± 2.4 vs 5.5 ± 4.0, $p < 1 \cdot 10^{-3}$) and in the offset (14.1 ± 9.0 vs 20.3 ± 7.6, $p < 1 \cdot 10^{-3}$) timing and in the onset ($20.8 \pm 8.2\%$ vs $26.4 \pm 5.9\%$ of GC, $p=0.01$) and in the offset (29.7 ± 6.7 vs 35.3 ± 8.2, $p=0.02$) timing. In general, in PD subjects, it seems to be an increase in the length of the stance phases; assuming co-contraction as a phenomenon aimed at improving subject's stability through the action on the joint by an agonist muscle and an antagonist muscle [12], a possible interpretation of the different co-contraction intervals, could be given by a greater request for stability during the movement for the foot in single support and would be justified in the prolonged recruitment of the gastrocnemius muscle in pathological. On the other hand, with respect to Controls, the V co-contraction of PD during swing phase results to be anticipated in the onset (88.7 ± 6.1 vs 85.8 ± 9.4, $p=0.50$) and offset (97.7 ± 4.1 vs 97.1 ± 3.4, $p=0.14$) timing. Instead, the IV co-contraction for PD is postponed, resulting to be statistically significant (64.5 ± 5.3 vs 67.3 ± 7.7, $p= 0.01$ and 74.8 ± 5.8 vs 78.2 ± 8.0, $p=0.001$, onset and offset timing for Control and PD, respectively).

The analysis of OF parameter provides very interesting insights in the difference between PD and Control subjects. From this point of view the behavior of PD patients is very peculiar around (before and after the heel strike (HS) event: PD patients increase the occurrence co-contraction recruitment before HC and decrease it after HC, compared to controls. This suggests that subjects of both populations need to control the joints movement to have adequate support during this delicate phase of the gait cycle, but PD patients anticipate this action before the contact with the floor.

Interestingly, the OF shows that during the late stance phase, when the subject is about to detach the tip from the ground (toe-off), the parkinsonian subject co-contracts the two muscles more frequent than a healthy subject, probably to avoid falling. Nevertheless, greater co-activation of TA and GL muscle is exhibited by PD groups compared to Controls, resulting to be consistent with literature [6,24]. The result suggests that increasing the occurrence of co-contraction could be the neuromuscular strategy adopted by PD when postural stability is at least partially compromised.

Additionally, the Figures 6.14 and 6.15, show a high variability in both minimum and maximum frequency in both Controls and PD. A reasonable explanation for this result could be found in the control roles played by the many co-contraction events that occur during the gait cycle. In particular, the minimum frequency variability assumes a higher value during the stance phase than swing, higher in PD than in Controls.

No statistical differences are detected during stance and swing phases in the I, II, III and V co-contraction intervals. Thus, although a statistical difference is shown during swing phase in the IV co-contraction), the overall picture of the minimum frequency is comparable between the two populations.

As shown in Figure 6.15, highest maximum frequency is detected in the early stance phase (I co-contraction) for PD group, while for Controls during the late stance phase. Also in this case, co-contraction event plays a functional key role. The maximum frequency for PD is higher than controls during the early stance phase (I co-contraction) (125.0 ± 42.7 and 147.5 ± 44.3, $p=0.04$. respectively) and during the swing phase in the IV co-contraction interval (93.3 ± 41.2 and 113.3 ± 34.0, $p=0.01$). Vice versa, in the II, III, V intervals, the maximum frequency reach higher value in Controls than PD (128.3 ± 50.0 and 112.1 ± 40.4, $p=0.10$, 148.9 ± 31.7 and 115.7 ± 26.8, $p=0.02$, 128.4 ± 37.8 and 104.2 ± 49.2, $p= 0.02$, respectively). At the moment, a detailed explanation of this phenomenon is hard to provide. Thus, further studies are solicited to deepen the possible usefulness of these outcomes.

In conclusion, the approach used in this study can therefore be confirmed as adequate for the time-frequency characterization of the co-contractions of the antagonist ankle muscles in healthy subjects and is equally adequate for the study of the phenomenon in parkinsonian subjects during walking. The results, in fact, detect evident alterations in the duration and number of co-contractions adopted by parkinsonian subjects during walking.

References

[1] A. Delamarre et al, “Epidemiology, environmental risk factors and genetics of Parkinson's disease”, Presse Med., vol.46, pp. 175-181, 2017, doi: 10.1016/j.lpm.2017.01.001.

[2] A. Samii et al., “Parkinson's disease”, Lancet, vol. 363, pp. 1783-93, 2004, doi: 10.1016/S0140-6736(04)16305-8

[3] A. A. Moustafa et al., “Motor symptoms in Parkinson’s disease: A unified framework,” Neurosci. Biobehav. Rev., vol. 68, pp. 727–740, 2016

[4] C. Váradi, “Clinical Features of Parkinson's Disease: The Evolution of Critical Symptoms”, Biology, vol.9, pp.1-13, 2020

[5] G. Pacini Panebianco, D. Ferrazzoli, G. Frazzitta, M. Fonsato, M. C. Bisi, S. Fantozzi and R. Stagni, “A Statistical Approach for the Assessment of Muscle Activation Patterns during Gait in Parkinson’s Disease”, Electronics, vol. 9, 2020

[6] S. M. Keloth, S. P. Arjunan, S. Raghav, et al. “Muscle activation strategies of people with early-stage Parkinson’s during walking”, J NeuroEngineering Rehabil, vol. 18, p.133, 2021

[7] M.E. Jenkins, et al. “Plantar cutaneous sensory stimulation improves single-limb support time, and EMG activation patterns among individuals with Parkinson’s disease”, Parkinsonism Relat. Disord., vol. 15, pp. 697–702, 2009

[8] A. V. Dietz, K. L. Leenders, and G. Colombo, “Leg muscle activation during gait in Parkinson’s disease: influence of body unloading”, Electroencephalogr. Clin. Neurophysiol. Suppl., vol. 105, pp. 400–405, 1997

[9] G. Albani, et al. “Differences in the EMG pattern of leg muscle activation during locomotion in Parkinson’s disease”, Funct. Neurol., vol. 18, pp. 165–170, 2003

[10] H. Mitoma, R. Hayashi, N. Yanagisawa, and H. Tsukagoshi, “Characteristics of parkinsonian and ataxic gaits: a study using surface electromyograms, angular displacements and floor reaction forces”, J. Neurol. Sci., vol. 174, pp. 22–39, 2000

[11] M. Cioni, C. L. Richards, F. Malouin, P. J. Bedard, and R. Lemieux, “Characteristics of the electromyographic patterns of lower limb muscles during gait in patients with Parkinson’s disease when OFF and ON L-Dopa treatment”. Ital. J. Neurological Sci., vol. 18, pp. 195–208, 1997

[12] K. Falconer and D. A. Winter, “Quantitative assessment of cocontraction at the ankle joint in walking”, Electromyogr. Clin. Neurophysiol., vol. 25, pp. 135–149, 1985

[13] P. Le, T.M. Best, S.N. Khan, E. Mendel, W.S. Marras, “A review of methods to assess coactivation in the spine”, J Electromyogr Kinesiol, vol. 32, pp. 51-60, 2017

[14] M. Darainy & D. J. Ostry, (2008). “Muscle cocontraction following dynamics learning”, Experimental Brain Research, vol.190, pp 153–163, 2008

[15] M. L. Latash, “Muscle coactivation: definitions, mechanisms, and functions”, Review Progress in Motor Control, Journal of Neurophysiology”, vol.120, pp. 88-104, 2018

[16] A. Lamontagne, C. Richards and F. Malouin, “Coactivation during gait as an adaptive behavior after stroke”, Journal of Electromyography and Kinesiology, vol.10, pp. 407–415, 2000

[17] B. A. Knarr, J. A. Zeni, J.S. Higginson,” Comparison of electromyography and joint moment as indicators of co-contraction”, J Electromyogr Kinesiol, vol.22, pp.607-11, 2012

[18] V. B. Unnithan, J. J. Dowling, G. Frost, B. Volpe Ayub, O. Bar-Or, “Cocontraction and phasic activity during GAIT in children with cerebral palsy”, Electromyogr Clin Neurophysiol., vol. 36, pp. 487-94, 1996

[19] M. E. Busse, C. M. Wiles, and R. W. M. Van Deursen, “Muscle co-activation in neurological conditions”, Physical therapy reviews, vol. 10, pp. 247-253, 2005

[20] F. Di Nardo, A. Strazza, A. Mengarelli, S. Ercolani, N. Morgoni, L. Burattini, S. Fioretti, “Surface EMG patterns for quantification of thigh muscle co-contraction in school-age children: Normative data during walking”, Gait & Posture, vol. 61, pp. 25–33, 2018

[21] F. Di Nardo, A. Mengarelli, E. Maranesi, L. Burattini, S. Fioretti, “Assessment of the ankle muscle co-contraction during normal gait: a surface electromyography study”, J. Electromyogr Kinesiol., vol.25, pp. 347-54, 2015

[22] F. Di Nardo, A. Strazza, A. Mengarelli, S. Cardarelli, A. Tigrini, F. Verdini, A. Nascimbeni, V. Agostini, M. Knaflitz, S. Fioretti, “EMG-Based Characterization of Walking Asymmetry in Children with Mild Hemiplegic Cerebral Palsy”, Biosensors (Basel), vol.9, p.82, 2019

[23] V. Dietz, W. Ziiistra, T. Prokop, and W. Berger, “Leg muscle activation during gair in Parkinson’s disease: adaptation and interlimb coordination”, Electroencephalogram, Clin. Neurophysiol/Electromyogr. Mot. Control, vol. 97, pp. 408-415, 1995

[24] O. Bello, G. Marquez and M. Fernandez del Olmo, “Effect of treadmill walking on leg muscle activation in Parkinson’s disease”, Rejuvenation Res., vol. 22, pp. 71–78, 2018

[25] K. C. Lang, M. E. Hackney, L. H. Ting, J. L. McKay, “Antagonist muscle activity during reactive balance responses is elevated in Parkinson’s disease and in balance impairment”, PLoS ONE., vol.14, pp. e0211137–e0211137, 2019

[26] P. Arias, N. Espinosa, V. Robles-García, R. Cao and J. Cudeiro, “Antagonist muscle co-activation during straight walking and its relation to kinematics: Insight from young, elderly and Parkinson’s disease”, Brain Research, vol.1455, pp.124–131, 2012

[27] G. De Michele, S. Sello, M.C. Carboncini, B. Rossi, S. K. Strambi, “Cross-correlation time-frequency analysis for multiple EMG signals in Parkinson's disease: a wavelet approach”, Med Eng Phys., vol.25, pp.361-9, 2003.

[28] P. J. Sparto, M. Panianpour, E. A. Barria, J. M. Jagadeesh, “Wavelet analysis of electromyography for back muscle fatigue detection during isokinetic constant torque exertions”, Spine, vol. 24, pp. 1791–8, 1999

[29] F. Di Nardo, M. Morano, A. Strazza, S. Fioretti, “Muscle Co-Contraction Detection in the Time–Frequency Domain”, Sensors, vol. 22, p. 4886, 2022

[30] F. Di Nardo, T. Basili, S. Meletani and D. Scaradozzi, "Wavelet-Based Assessment of the Muscle-Activation Frequency Range by EMG Analysis”, IEEE Access, vol. 10, pp. 9793-9805, 2022

[31] V. F. Froelicher and J. Myers, “The Physiologic Response to the Exercise Test”, Manual of Exercise Testing, pp. 1–15, 2007

[32] L. A. Frey-Law, K.G. Avin, “Muscle coactivation: a generalized or localized motor control strategy?”, Muscle Nerve. vol. 48, pp. 578-85, 2013

[33] C. McCuller, R. Jessu, A.L. Callahan, “Physiology, Skeletal Muscle”, Treasure Island (FL), 2023

[34] B. Lindsay, et al., “Anatomy & Physiology”, Oregon State Open Educational Resources, 2019

[35] W. R. Frontera, J. Ochala, “Skeletal muscle: a brief review of structure and function”, Calcif Tissue Int., vol.96, pp.183-95, 2015

[36] S. Pham, Y. Puckett, “Physiology, Skeletal Muscle Contraction,” Treasure Island (FL), 2022

[37] J. C. Calderón, P. Bolaños, C. Caputo, “The excitation-contraction coupling mechanism in skeletal muscle”, Biophys Rev., vol.6, pp.133-160, 2014

[38] C. J. De Luca, “Electromyography. Encyclopedia of Medical Devices and Instrumentation”, (John G. Webster, Ed.) John Wiley Publisher, pp. 98-109, 2006

[39] M. B. Raez, M.S. Hussain, F. Mohd-Yasin, “Techniques of EMG signal analysis: detection, processing, classification and applications,” Biol Proced Online, vol.8, pp. 11-35, 2006

[40] R. H Chowdhury, M. B. Reaz, M. A. Ali, A. A Bakar, K. Chellappan, T.G. Chang,” Surface electromyography signal processing and classification techniques”, Sensors (Basel)., vol.13, pp. 12431-66, 2013

[41] L. McManus, G. De Vito and M. M Lowery, “Analysis and Biophysics of Surface EMG for Physiotherapists and Kinesiologists: Toward a Common Language with Rehabilitation Engineers”, Frontiers in Neurology, vol. 11, p. 576729, 2020

[42] R. Merletti, A. Botter, C. Cescon, M. A. Minetto, & T. M. M. Vieira, “Advances in Surface EMG: Recent Progress in Clinical Research Applications. Critical Reviews in Biomedical Engineering”, vol.38, pp. 347–379, 2010

[43] B. Gerdle, S. Karlsson, M. S. Day, Djupsjöbacka, Acquisition, Processing and Analysis of the Surface Electromyogram”, In: Windhorst, U., Johansson, H. (eds) Modern Techniques in Neuroscience Research. Springer, Berlin, Heidelberg, 1999

[44] A. Merlo, I. Campanini, “Technical aspects of surface electromyography for clinicians”, The open rehabilitation journal, vol. 3, pp.98-109, 2010

[45] P. Konard, "The ABC of EMG: A Practical Introduction to Kinesiological Electromyography", Noraxon Inc., USA, 2005

[46] C. J. De Luca, "Physiology and Mathematics of Myoelectric Signals", in IEEE Transactions on Biomedical Engineering, vol. 26, pp. 313-325, 1979

[47] G. Kamen, and D. A. Gabriel, “Essentials of electromyography. Leeds: Human Kinetics”, pp. 72-4, 2010

[48] W. Rose, “Electromyogram analysis”, Mathematics and Signal Processing for Biomechanics, 2019

[49] P. Bonato, T. D’Alessio and M. Knaflitz, “A statistical method for the measurement of muscle activation intervals from surface myoelectric signal during gait”, IEEE Trans. on Biomedical Engineering, vol. 45, pp. 287-299, 1998

[50] A. Merlo, D. Farina, R. Merletti, “A fast and reliable technique for muscle activity detection from surface EMG signals” IEEE Trans Biomed Eng., vol.50, pp.316-23, 2003

[51] S. Solnik, P. Rider, K. Steinweg, P. DeVita, T. Hortobágyi, “Teager-Kaiser energy operator signal conditioning improves EMG onset detection”, Eur J Appl Physiol., vol. 110, pp. 489-98, 2010

[52] F. Di Nardo, A. Nocera, A. Cucchiarelli, S. Fioretti, C. Morbidoni, “Machine Learning for Detection of Muscular Activity from Surface EMG Signals”, Sensors, vol.22, p.3393, 2022

[53] I. González, A. Malanda, E. Gorostiaga, M. Izquierdo, “Electromyographic Models to assess muscle fatigue”, vol. 22, pp. 501-512, 2012

[54] G. Milton and H. Kabat, “Cocontraction and Reciprocal Innervation in Voluntary Movement in Man”, Science, New Series, vol. 116, pp. 115-118, 1952

[55] J. B. Nielsen, “Human Spinal Motor Control”, Annual Review of Neuroscience,vol. 39, pp. 81–101, 2016

[56] B. Antohe, M. Rata, G. Rata, “The role of muscle activation index in motor control-A theoretical presentation”, Physical Education, Sport and Kinetotherapy Journal, vol.59, pp. 26-34, 2020

[57] M. L. Latash, “Muscle coactivation: definitions, mechanisms, and functions”, Review Progress in Motor Control, Journal of Neurophysiology”, vol.120, pp. 88-104, 2018

[58] P. Le, T.M. Best, S.N. Khan, E. Mendel, W.S. Marras, “A review of methods to assess coactivation in the spine”, J Electromyogr Kinesiol, vol. 32, pp. 51-60, 2017

[59] M. Darainy & D. J. Ostry, (2008). “Muscle cocontraction following dynamics learning”, Experimental Brain Research, vol.190, pp 153–163, 2008

[60] C. L. Banks, H. J. Huang, V. L. Little, C. Patten, “Electromyography Exposes Heterogeneity in Muscle Co-Contraction following Stroke”, Front Neurol., vol.8, p.699, 2017

[61] K. S. Rudolph, et al., “Dynamic stability after ACL injury: Who can hop? Knee Surg Sports Traumatol”, Arthrosc. vol.8, pp. 262-269, 2000

[62] H. Souissi, R. Zory, J. Bredin, P. Gerus, “Comparison of methodologies to assess muscle co-contraction during gait”, J. Biomech., vol. 24, pp. 141–145, 2017

[63] C. Marras et al., “Prevalence of Parkinson’s disease across North America,” npj Parkinson’s Disease, vol.4, pp. 1-7, 2018

[64] J. C. Bridi et al., “Mechanisms of α-Synuclein Induced Synaptopathy in Parkinson’s Disease”, Front. Neurosci., vol 12, pp.1-18, 2018, doi: 10.3389/fnins.2018.00080

[65] T. B. Stoker et al., “Parkinson’s Disease: Pathogenesis and Clinical Aspects”, Brisbane (AU): Codon Publications, pp. 11-12, 2018, PMID: 30702835

[66] S. Sgroi, R. Tonini, “Opioidergic Modulation of Striatal Circuits, Implications in Parkinson's Disease and Levodopa Induced Dyskinesia”, Front Neurol., vol. 9, pp. 524, 2018

[67] C. W. Olanow et al., “Safinamide – A New Therapeutic Option to Address Motor Symptoms and Motor Complications in Mid- to Late-stage Parkinson’s Disease,” European Neurological Review, vol. 11, no.2, pp. 2-15, 2016

[68] M. J. ArmstronG, M.S. Okun, “Diagnosis and Treatment of Parkinson Disease: A Review,” JAMA, vol.323, pp.548-560, 2020

[69] J. Jankovic, “Parkinson’s disease: Clinical features and diagnosis”, J. Neurol. Neurosurg. Psychiatry, vol. 79, pp. 368–376, 2008

[70] K. Kimmell, et al., “Postural instability in Parkinson Disease: To step or not to step”, J. Neurol. Sci., vol. 357, pp. 146–151, 2015

[71] Y. Okuma, “Freezing of gait in Parkinson's disease”, J Neurol., vol. 253, pp. 27-32, 2006

[72] A. Park, M. A. Stacy, “Non-motor symptoms in Parkinson’ s disease”, J Neurol. vol. 256, pp. 293–298, 2009

[73] R. Doty, “Olfactory dysfunction in Parkinson disease”, Nat Rev Neurol, vol. 8, pp. 329–339, 2012

[74] W. Poewe, “Non-motor symptoms in Parkinson’s disease”, European Journal of Neurology, vol. pp. 14–20, 2008

[75] B. S. Connolly, et al., “Pharmacological treatment of Parkinson disease: a review”, Jama, vol. 311, pp. 1670-83, 2014

[76] C. A. Davie, “A review of Parkinson's disease,” Br Med Bull., vol. 86, pp. 109-27, 2008

[77] S. J. Groiss, L. Wojtecki, M. Südmeyer, A. Schnitzler, “Deep brain stimulation in Parkinson's disease,” Ther Adv Neurol Disord., vol. 2, pp. 20-8, 2009

[78] C. G. Goetz et al., “Movement Disorder Society-Sponsored Revision of the Unified Parkinson’s Disease Rating Scale (MDS-UPDRS): Scale presentation and clinimetric testing results,” Mov. Disord., vol. 23, pp. 2129–2170, 2008

[79] V. Agostini, M. Ghislieri, S. Rosati, G. Balestra, and M. Knaflitz, “Surface Electromyography Applied to Gait Analysis: How to Improve Its Impact in Clinics?” Front. Neurol., vol. 11, no. September, pp. 1–13, Sep. 2020, doi: 10.3389/fneur.2020.00994

[80] J. Perry, “Gait Analysis: Normal and Pathological Function”, Slack Inc.: Thorofare, pp 9-130, NJ, USA, 1992

[81] A. D. Kuo, “The six determinants of gait and the inverted pendulum analogy: A dynamic walking perspective”, Hum Mov Sci., vol.26, pp. 617-56, 2007

[82] M. Malanga, MD, J. Delisa, A.Joel, “Gait analysis in the science of rehabilitation”, Diane Publishing, vol.2 pp. 1-4 , 1998

[83] C. L. Brockett, G. J. Chapman, “Biomechanics of the ankle”, Orthopaedics and Trauma, vol. 30, pp. 232-238, 2016

[84] N. E. Miner, “An Introduction to Wavelet Theory and Analysis”, United States: pp. 1-28, 1998. Web. doi:10.2172/1896

[85] S. Mallat, “A wavelet tour of a signal processing”, Accademic press, First edition, pp.557, 1998

[86] O. Rioul, M. Vetterli, “Wavelets and signal processing”, IEEE Signal Processing Magazine, vol.8, pp. 14-38, 1991

[87] M. Misiti, Y. Misiti, G. Oppenheim, and J-M Poggi, “Wavelets Toolbox Users Guide”, The MathWorks, 2000

[88] N. M. Sobahi "Denoising of EMG signals based on wavelet transform", Asian Transactions on Engineering, vol. 5, pp.17-23, 2011

[89] X. Zhang, Y. Wang, & R. P. Han, “Wavelet transform theory and its application in EMG signal processing”, Seventh International Conference on Fuzzy Systems and Knowledge Discovery, vol. 5, pp. 2234-2238, 2010

[90] P. Sukiennik, J.T. Białasiewicz, “Cross-correlation of bio-signals using continuous wavelet transform and genetic algorithm”, J Neurosci Methods., vol.247, pp. 13-22, 2015

[91] A. Strazza, F. Verdini, L. Burattini, S. Fioretti, F. Di Nardo, “Time-frequency analysis of surface EMG signals for maximum energy localization during gait”, Elsevier B.V.,Gait & Posture 57S, pp. 1-40, 2017

[92] A. Phinyomark, P. Phukpattaranont & C. Limsakul “The Usefulness of Wavelet Transform to Reduce Noise in the SEMG Signal. EMG Methods for Evaluating Muscle and Nerve Function”, 2012, doi:10.5772/25757

[93] M. Romanato, F. Spolaor, D. Volpe, S. Fioretti, Z. Sawacha and F. Di Nardo, "Recruitment of Gastrocnemius Lateralis during walking in Parkinson's Disease assessed by EMG analysis,” IEEE International Symposium on Medical Measurements and Applications (MeMeA), Messina, Italy, pp. 1-6, 2022

[94] Y. Blanc e U. Dimanico, “Electrode Placement in Surface Electromyography (sEMG)” Minimal Crosstalk Area “(MCA)”, Open Rehabil. J., vol. 3, pp. 110–126, 2010

[95] F. Di Nardo, G. Ghetti, S. Fioretti, “Assessment of the activation modalities of gastrocnemius lateralis and tibialis anterior during gait: a statistical analysis”, J Electromyogr Kinesiol., vol. 23, pp. 1428-33, 2013